HYDROPHOBIC FORCES IN FREE THIN FILMS OF WATER IN THE PRESENCE AND ABSENCE OF SURFACTANTS

by

Bayram Suha Aksoy

Dissertation submitted to the Faculty of the Virginia Polytechnic Institute and State University in partial fulfillment of the requirements for the degree of

DOCTOR OF PHILOSOPHY

in

Mining and Minerals Engineering

APPROVED:

_____

Dr. Roe-Hoan Yoon (chairmen)

_____ _____

Dr. M.E. Karmis, Department Head Dr. James P. Wightman

_____ _____

Dr. Richey M. Davis Dr. Gerald H. Luttrell

May, 1997

Blacksburg, Virginia

HYDROPHOBIC FORCES IN FREE THIN FILMS OF WATER IN THE PRESENCE AND ABSENCE OF SURFACTANTS

by

Bayram Suha Aksoy

Chairman: Dr. Roe-Hoan Yoon

Mining and Minerals Engineering

ABSTRACT

In this study, two different system were studied to investigate the forces interacting in thin liquid films. In the former, direct force measurements were conducted with bitumen-coated mica surfaces using a Mark IV surface force analyzer. Besides long-range electrostatic repulsive forces at separation distances above approximately 70 nm, unexpectedly strong repulsive forces were measured at shorter separation distances. These non-DLVO forces may be attributed to the steric repulsion between asphaltenes extracted on the bitumen surface. The steric forces increased with pH and temperature, which may be explained by the increased solubilization of asphaltenes in water. The steric force also increased with electrolyte concentration, possibly due to a decrease in the mobility of the tails of the asphaltenes on the surface.

The kinetics of coalescence of bitumen droplets was studied by measuring the induction time. There was a general agreement between the force data and the kinetic information, suggesting that bitumen suspensions are stabilized by asphaltene. The steric forces identified by

the direct force measurements may have profound implications on the hot water processing of Alberta Tar Sands.

In the later, a thin film balance (TFB) of Scheludko and Exerowa-type was used to determine equilibrium film thicknesses of dodecylammonium chloride and sodium dodecyl sulfate solutions. The hydrophobic force as a third component of the extended DLVO theory was represented as a power law. The results showed that at low surfactant concentrations, the hydrophobicity parameter, K_{232} is positive and decreases with increasing surfactant concentration. By extrapolating this data for the zero surfactant concentration, K_{232} was found about 10^{-17} J, which is approximately 270 times larger than the Hamaker constant, A_{232}. These results suggest that air bubbles are hydrophobic and the hydrophobicity decreases with increasing surfactant concentration..

The disjoining pressure isotherm for both surfactant systems in the presence of inorganic electrolyte (*NaCl*) were also obtained. The results indicated that the K_{232} values estimated from the equilibrium film thickness measurements can be used to fit the experimentally obtained disjoining pressure isotherm. Consideration of hydrophobic force predicted a rupture thickness larger than predicted using the DLVO theory, but is substantially smaller than the experimental result. This discrepancy may be ascribed to the hydrodynamic force operating in the film thinning process.

To compare the hydrophobicity of air bubbles and solid surfaces, an air bubble was simulated by using a hydrophobic solid surfaces. The equilibrium contact angle of aqueous surfactant solutions on hydrophobic surfaces was measured using a contact angle goniometer. The results indicated that the nature of both the air-water interface and the solid-water interface is

altered gradually from hydrophobic to hydrophilic with increasing surfactant concentration. The results also suggested that the hydrophobicity of both systems are comparable, i.e., K_{232} is about 10^{-17} J, which is estimated using the extended DLVO theory, and K_{131} is in the order of 10^{-16} J, which is obtained by direct force measurements between the hydrophobic surfaces. It was showed that hydrophobic forces much higher than the London-van der Waals forces for both systems need to be included when the stability of foams and colloids is considered.

ACKNOWLEDGMENTS

First and foremost I acknowledge my thesis advisor, Dr. Roe-Hoan Yoon. His pursuit of excellence and total commitment as an educator made this work possible. I also thank my other committee members Dr. M.E. Karmis , Dr. James P. Wightman, Dr. Rickey M. Davis, Dr. Gerald H. Luttrell, and for reviewing this thesis and their constructive comments. Special thanks to Dr. David. A. Guzonas and Dr. Yakov I. Rabinovich , and Vivik Subramanian for helpful discussions and teaching me SFA and AFM. Special thanks to Dr. D. Exerowa for supplying a thin film balance (TFB) and Dr. Robert J. Puge for teaching me the force measurement technique using TFB.

Special appreciation is given to surface force group Dr. Darrin H. Flinn, Vivik Subramanian, Dr. Ravishankar S.A. and Dr. Cesar Basilio for their valuable discussions, assistance, friendship and support. I also wish to thank to Roy Hill for teaching me the image analyzer technique and Alisa Alls, Barbara Owens, and Keith Kutz for being extremely supportive and helpful, and Wayne Slusser, Jim Overfelt for their technical assistance. I would like to thank to all other graduate students at Holden Hall and Plantation road laboratory for their friendship and company when I work during the late hours.

Finally, I wish to thank the two most important people, first, my mother, Hatice for her understanding, unconditional love and support from miles and miles away. Second, my best friend, Charles Paige who is an instrumentation specialist at the power plant, for not only his friendship and brotherhood but also his technical assistance while I set up my experimental apparatus.

Acknowledgments

TABLE OF CONTENTS

Table of Contents

LIST OF FIGURES

List of Figures

List of Figures

List of Figures

List of Figures

List of Figures

List of Figures

List of Figures

LIST OF TABLES

CHAPTER 1

INTRODUCTION

1.1 General

The stability of thin liquid films is a major subject of surface and colloid science. Many industrial processes and products rely on fundamental interfacial interactions which occur in the thin-film region. For example, ore flotation and oil recovery operations basically depend on control and manipulation of liquid films for the various phases involved. The stability of foams, particle dispersions, and emulsions also depend on the stability (lifetime) of the intervening films within these disperse systems. In order to stabilize these intervening films, organic and/or inorganic substances (impurities) must exist in the continuous phase (liquid).

It has been known that the pure liquids cannot foam unless these impurities are present. For instance, the waves in the oceans create bubbles and foams when they break at the top of the waves because of the presence of these substances in the oceans. On the other hand, the lakes and rivers cannot foam since the most of them contain none or fairly low concentrations of these impurities. Another example would be when gas bubbles are introduced below the surface of a pure liquid, they rise upward through the liquid due to the buoyancy force and burst spontaneously as soon as they reach the air-liquid interface. However, in the presence of surfactants, the air-liquid interface is in equilibrium with the adsorbed surfactant molecules, appearing as a reduced surface tension of the solution. As soon as the bubbles approach the air-liquid interface, the air bubbles cause an expansion of the air-liquid interface, and disturb the equilibrium at the interface. Then the forces re-establish the equilibrium at the air-liquid interface.

The forces acting in the film formed between the air-liquid interface and the gas bubbles causes this phenomena so that the film most likely does not rupture spontaneously.

In foams that are in contact with the atmosphere, the whole volume (or height) of the foam diminishes with time. This process takes place simultaneously with the internal foam collapse, which does not change the foam volume. The time for complete distraction takes longer and is a parameter widely used as a characteristic of foam stability.

The properties of thin liquid films separating the bubbles, i.e., rate of thinning, equilibrium thickness, permeability, elasticity, stability, etc., have a decisive influence on all processes in a foam and its stability. The study of the various physicochemical properties of thin films in foams is very difficult or even impossible in most cases.

It has been emphasized that the mechanical-dynamical properties of the foams, i.e., surface elasticity and surface viscosity, are important to the kinetic stability of foams and films. These properties are experimentally measurable. Basically, surface viscosity reflects the speed of the relaxation process which restores equilibrium in the system after imposing stress on it. It is also a measure of the energy dissipation in the surface layer. On the other hand, the surface elasticity is a measure of the energy stored in the surface layer as a result of an external stress.

The earliest theories to explain the stability of the foams and films are Gibbs elasticity (E) and the Marangoni effect. The former suggests that during the stretching of a film, a local increase in surface tension occurs due to the depletion of the surfactant in the stretched area so that the elasticity of the thin film changes. Gibbs defined a coefficient of surface elasticity (E) as the increase in surface tension resulting from an increase in the area of the film. This theory only applies to a static system where there is insufficient surfactant in the film to diffuse to the surface

and lower the surface tension. Under the dynamic conditions the Marangoni effect operates on both expanding and contracting film and provides a restoring force. This effect depends on both the lowering of the surface tension and the rate of re-establishing the equilibrium over the film surface. The extension of the film surface reduces the concentration of the surfactant in the surface layer. This provides a slow diffusion from the bulk of the solution to the surface region. Then the film can rapidly heal itself by the flow of surfactant from solution under a surface pressure gradient. There is no technique to measure the magnitude of this effect and the theoretical treatment is incomplete.

The stability of thin metastable films could not be explained by these mechanical-dynamical theories. In these cases, the metastable films become so thin that surface forces are involved. These forces in a thin film were measured and the concept of positive disjoining pressure (Π) was introduced by Derjaguin (1,4).

Derjaguin (4) recognized that there are at least three types of forces in thin films which contribute to the disjoining pressure (Π). They are the electrostatic double layer interaction, long range van der Waals forces and short range steric repulsive interactions.

Following this introduction of the disjoining pressure concept, great progress in understanding the essence of the different processes and phenomena that take place in foam films was achieved on the basis of investigations of free films, especially microscopic films. These microscopic films have been used as an adequate model of the film structure in polyhedral foams. Then the forces interacting in these free microscopic films have been measured successfully by using a force measurement technique of Derjaguin and Titievskaya (20,21), a capillary tube technique of Scheludka and Exerowa (22), and a porous ring technique of Mysels (45).

Chapter 1 Introduction

In addition to these three forces, most recent studies (46,47) on the stability of thin films showed that the hydrophobic forces may be responsible for the film rupture. Puge and Yoon (46) conducted the critical film thickness measurements on nonionic surfactants. Based on their experimental results they attempted to calculate the magnitude of the hydrophobic forces using a single exponential force law. Later, Tchaliovska, et al. (47), measured equilibrium film thickness of dodecylammonium chloride (RNH_3Cl) using the thin film balance (TFB). Their attempt was to calculate the potential at the air-water interface by means of the DLVO theory, which considers only electrostatic and dispersion forces. Then the potential was calculated using the Gibbs adsorption isotherm based on the surface tension data. It was shown that there is a large difference between the potential calculated from two different techniques. The discrepancy is attributed to an additional attractive force.

These are the pioneering studies conducted to emphasize that the hydrophobic force plays an important role in explaining the spontaneous rupture of the air bubbles in pure water. The interfacial tension at the air-water interface is among the highest those at the hydrophobic solid-water interfaces. Even though the hydrophobic forces were measured between the hydrophobic solid surfaces and various theories have been proposed to quantify these attractive forces, their origin is not well understood.

The primary purpose of present research is to gain a better understanding of the intermolecular forces, especially hydrophobic and steric forces which basically control the stability of these thin films. In this fundamental study of foam stability, the direct force measurements will be conducted using TFB and SFA to determine the magnitude of hydrophobic and steric forces for the various systems. Then, the results will be reported in the form of disjoining pressure

isotherms ($\Pi(h)$). It is believed that all these information can then be used to design chemical systems, e.g. surfactants, electrolytes, etc. that will meet the needs of the numerous industries, i.e., mining, chemical, biology, oil, etc.

1.2 Literature Review

1.2.1 Disjoining Pressure

A thin interfacial region (a so called transition region) exists at the vicinity of every interface. The thermodynamic properties of this region deviate from the properties of the two neighboring bulk phases. As crossing the phase boundary, these transition regions result from the changes in the molecular interaction. If two interfaces approach one another, these changes signify themselves as macroscopic surface forces. This situation occurs when two phases such as two air bubbles approach each other or an air bubble approaches an air-liquid interface while an intervening third (water) phase separating the air bubbles grows thinner. When the thickness of the water phase becomes comparable to the thickness of the interfacial regions (overlapping of interfaces) the properties of the bulk water phase no longer exist in the interlayer (film). At this point, further decreases in film thickness require additional work which originates from repulsive or attractive forces generated by the overlapping interfaces. After the overlapping occurs, an external pressure is needed to maintain a constant film thickness. The process described above can be summarized with the similar analogy when two magnets approach one another. If the two positive or negative poles are opposing one another, an external force (pressure) needs to be applied in order to bring them closer. This situation is also true for a positive and a negative pole which approach one another to maintain the distance separating them. As in the case of foams

and emulsions, the intervening solution in a thin aqueous film drains and the interfaces (e.g., two air-liquid interfaces) approach one another. Then the phases (in this case, air and air) separated by the solution interact. This net interaction (positive or negative) between the phases can be expressed as an excess pressure versus separation distance (film thickness, h), and so called "disjoining pressure isotherm" by definition. The disjoining pressure (Π) is assumed to be positive when it resists film thinning. In an equilibrium film, therefore, Π is equal to the hydrostatic pressure in the vertical films or the capillary pressure at the Plateau-Gibbs border of the film.

In 1936, the concept of the disjoining pressure for thin liquid films was formulated and its existence was verified for the first time by Derjaguin and Obuchov (1). Derjaguin and Churaev (2) later gave the more general definition of the disjoining pressure, which is " In mechanical equilibrium the disjoining pressure, $\Pi(h)$, is equal to the difference existing between the component P_{zz} of the pressure tensor in the interlayer and the pressure, P_B, set up in the bulk of the phase from which it has been formed by thinning out:

$$\Pi(h) = P_{zz} - P_B = P_N - P_B, \qquad [1.1]$$

where P_N is the pressure normal to the surface of a thin plane-parallel interface and directions are defined by the coordinate system pictured in Figure 1.1. In the simplest case of a one-component liquid phase, mechanical equilibrium under isothermic conditions implies thermodynamic equilibrium. In that case the disjoining pressure is a single-valued function of the interface thickness, h, …"

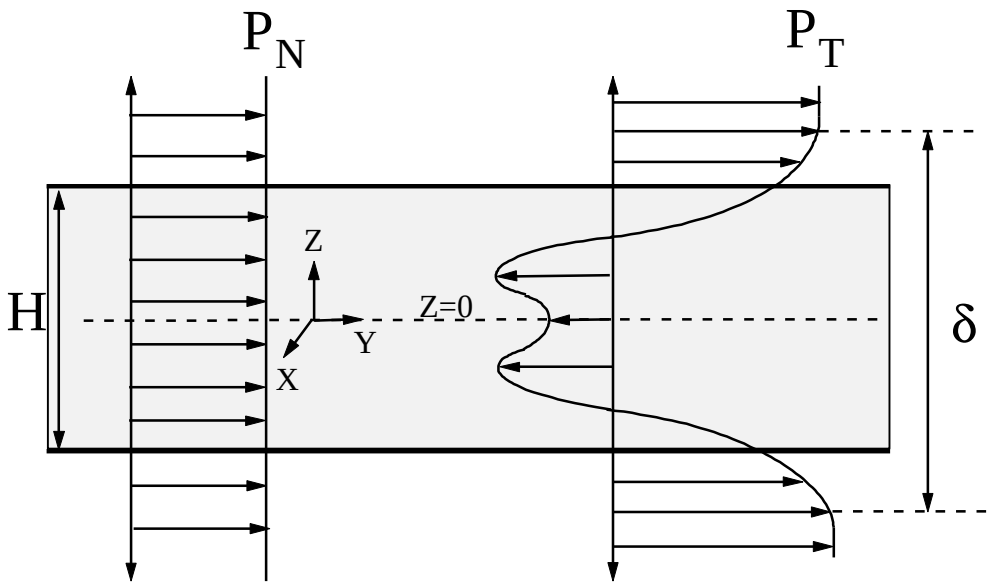

Figure 1.1 Typical distribution of the pressure tensor components P_N and P_T in a thin liquid film (after Derjaguin and Churaev (2))

In 1988 and 1990, Kralchevsky and Ivanov (3) extended Equ. [1.1] and gave a general vectorial expression for the disjoining pressure,

$$\Pi = n \bullet \left(\tilde{P} - P_R \tilde{U} \right)_{r=r_o} \qquad [1.2]$$

where $\tilde{U}$ is the three-dimensional idemfactor, $\tilde{P}$ is the total pressure tensor, and n is an outer unit normal to the reference surface. r_o corresponds to a reference surface dividing the film into two halves and P_R is a reference pressure.

1.2.2 Thermodynamic Definition

Derjaguin et al. (4) and Erikson and Toshev (5) defined alternatively the disjoining pressure in terms of thermodynamic variables. The work required to change the film thickness at constant temperature (T), total pressure (P), area of the film (A), and the number of moles (N_i), can be formulated by Gibbs free energy chance in the film,

$$\Pi(h) = -\left(\frac{\partial G}{\partial h} \right)_{T,P,A,N_i} \qquad [1.3]$$

Using Equ.[1.3], Erikson and Toshev (5) and de Feijter, et al.(6), generated the following form of the well known Gibbs-Duhem equation for the film,

$$2d\gamma + S^f dT + \Pi dh + 2\sum_i \Gamma_i^f d\mu_i = 0 \qquad [1.4]$$

in which γ is the film surface tension, S^f is the excess entropy of the film surface, and Γ_i^f and μ_i are the surface excess (from Gibbs adsorption) and chemical potential of i^{th} component. At constant potential and temperature, they reduced the Equ. [1.4] to the following form,

$$\Pi = -2\left(\frac{d\,g}{dh}\right)_{T,m_i} . \qquad [1.5]$$

Then they integrated Equ.[1.5] to obtain the relationship between the surface tension of the film interfaces and the disjoining pressure isotherm as follows,

$$2\,g(h) = 2\,g(h=\infty) - \int_{\infty}^{h} \Pi dh \qquad [1.6]$$

where $2\gamma(h=\infty)$ is the surface tension of bulk solution. As an equivalent expression Toshev and Ivanov (7) derived an equation for the film tension, γ^f, as a membrane model,

$$g^f = 2\,g(h=\infty) - \int_{\infty}^{h} \Pi dh + \Pi h = 2\,g(h=\infty) + \int_{\Pi(h=\infty)}^{\Pi(h)} h d\Pi . \qquad [1.7]$$

They could use this equation when film properties were ascribed to a single, two-dimensional plane.

Rowlinson and Widom (8) combined the thermodynamic and mechanical approaches to the definition of the disjoining pressure by using the Bakker equation (9) for the definition of surface tension at each interface of a symmetrical film,

$$g(h) = \int_{z=0}^{h_0/2} (P_N - P_T) dz \qquad [1.8]$$

in which P_N and P_T are the normal and tangential components of the pressure tensor, respectively, and z is the coordinate perpendicular to the interface. Figure 1.1 shows the distributions $P_N(z)$ and $P_T(z)$ in a liquid interlayer 3 of thickness, h, bounded by two identical phases 1 and 2 (liquid or gaseous). This situation shown in Figure 1.1 can be visualized easily to understand the limits of integration. The upper limit, $\delta/2$, represents the normal distance from the film interface far enough away from the interface zone to guarantee an isotropic bulk pressure, i.e., $P_N = P_T = P_B$.

The lower limit at z=0 corresponds to the center of the film. As the film thickness approaches infinity, $\gamma(h) \rightarrow \gamma(h = \infty)$ in Equ. [1.8], the bulk surface tension can be recovered (Figure 1.1). Substitution of Equ. [1.8] into Equ.[1.5] relates the thermodynamic description of the disjoining pressure to its mechanical origins (anisotropy of the pressure tensor within the film),

$$\Pi = -\frac{\partial\left(2\int_{z=0}^{d/2}(P_N - P_T)dz\right)}{\partial h}. \qquad [1.9]$$

Rowlins and Widom (7) used Equ. [1.9] to relate the disjoining pressure to intermolecular potentials through standard statistical mechanic expressions from P_N and P_T. In a similar context Kuni and Rusanov (9) applied the statistical mechanic approach to calculate the distribution functions and the pressure tensor for films of simple liquids.

Figure 1.1 also shows how the pressure distributions P_N and P_T change in the thin film region. The length of the horizontal arrows represent the magnitude of the pressure components while the direction (right or left) signifies the sign (positive or negative, respectively). For plane parallel films in equilibrium the normal component of the pressure tensor cannot change and remain constant through the film. Conversely, the tangential component can change in both sign and magnitude. However, beyond the transition zone defined by δ in Figure 1.1, $P_N = P_T$, the pressure is isotropic and equal to the bulk pressure of the contiguous phases. Erikson and Toshev (5) showed a more detailed picture for a soap film stabilized by ionic surfactants.

1.2.3 Thin Film Structure and Types

It has been well known that a minimum surfactant concentration is required to obtain a stable film, and its stability and characteristic properties depend on the concentration of the surfactants or electrolytes. The thickness and characteristic properties of each type of thin film differ substantially. Based on the thickness and the characteristic properties, the thin liquid film has been classified in the following types:

1) common thin films (CF),
2) common black films (CBF), and
3) Newton black films (NBF) (14).

Usually CFs occur in regions of low electrolyte concentration where the electrostatic pressure (Π_E) dominates over dispersion pressure (Π_D), which are the components of the total disjoining pressure and will be discussed in detail in section 1.2.3.

The measured film thicknesses of CF are in the range of 30 nm. Since the Π_D is relatively small, Π_E is equal to the capillary pressure of the meniscus (P_C) (20-22). The thin liquid films rupture when the film thickness reaches a critical value (H_C). In the low electrolyte concentration region, most of the thin film experiments were conducted systematically on film equilibrium to determine the values of ψ_O and σ_O (21,23). In 1959, Scheludko and Exerowa (22) studied the equilibrium in films obtained using $5x10^{-5}$ % saponine solutions in which the dispersion force was small that the electrical component of disjoining pressure was calculated only knowing the capillary pressure of the meniscus. In the range of thicknesses 50-120 nm, the measured equilibrium thicknesses corresponded well to those theoretically calculated with ψ_o = 90 mV, and P_c =73 N/m^2. In another work of Scheludko and Exerowa (23) in 1960, the equilibrium in thinner

films (25-55 nm) obtained at high electrolyte concentration was studied. In that case the electrostatic (Π_E) and dispersion (Π_D) components of the disjoining pressure were comparable. From the comparison of the calculated thicknesses and the thicknesses obtained in the experiment the molecular interaction (Π_D) was estimated.

The CBFs were observed during the thinning process when the conditions for the equilibrium are not fulfilled. Two different phenomenon were observed during this thinning process on addition of surfactants: the film either reached a semi-equilibrium state before it ruptured or suddenly transited to a thinner stable state which occurred through formation of black spots. This thinnest film with a thickness of 4-5 nm was called an NBF.

Pioneer studies of Exerowa (25) demonstrated that the critical electrolyte concentration (C_{Cr}) corresponding to the transition for CBFs to NBFs depends on the type of surfactants and is usually higher for ionic surfactants than for nonionic surfactants.

The conditions for equilibrium and transitions from CBFs and NBFs were interpreted qualitatively by means of the disjoining pressure ($\Pi(h)$) isotherm. Figure 1.2 shows such an isotherm. Equilibrium in films at thicknesses larger than H_{max} corresponds to the DLVO theory. On the other hand, for NBFs an additional component of disjoining pressure, so called the adsorption (steric) component of the disjoining pressure was included in order to explain the stability of the NBFs. This additional force was attributed as a repulsion force and arises when the polar groups of the adsorbed surfactant molecules come into contact. In the region $H_{max} > H > H_2$ (Figure 1.2), the films are unstable (H_2 being NBF thickness). At smaller thicknesses NBFs form above $\Pi (h) = 0$.

In 1992, Bergeron and Radge (37) and Bergeron (38) extensively studied thin aqueous films obtained from sodium dodecyl sulfate (SDS) in the absence and presence of supporting inorganic electrolytes (NaCl). In their studies, the disjoining pressure isotherms were obtained at low ($9x10^{-3}$ M) and high (10^{-1} M) surfactant concentrations. The low surfactant concentration was chosen since it is quite near the CMC ($8x10^{-3}$ M). The thickness of the stable films was found in the range from 20-11.6 nm. At approximately 13 nm a strong repulsive branch in the isotherm stabilized the film to pressure greater than 70 kPa. Films observed in this thickness region were referred to as CBF. Their stability was attributed to electrostatic repulsive forces generated by overlapping double layers in the interfacial region (4).

At the low concentration, the disjoining pressure measurements were also performed at high ionic strength of the solution which was increased by adding NaCl ($1.8x10^{-1}$ M) to a fresh $1x10^{-3}$ M SDS solution. A good agreement was found among the data obtained by Mysels and Jones (39), and by Exerowa et al. (40). At higher ionic strengths the CBF was encountered at much smaller thicknesses, e.g., approximately 8 versus 11 nm, and the slope of the isotherm in this region increased. It was shown that both effects, reduced thickness and increased slope, result from the increased electrostatic screening caused by the addition of electrolytes consistent with DLVO theory.

It was also shown that there exists an abrupt transition in thickness from 7 to 4.5 nm in the presence of NaCl which results in the forming of an NBF (38). The transition between the CBF and the NBF was explained by hydration, steric undulation, and protrusion forces (41,42) and was discrete because films at the intervening film thickness are thermodynamically unstable. de Vries

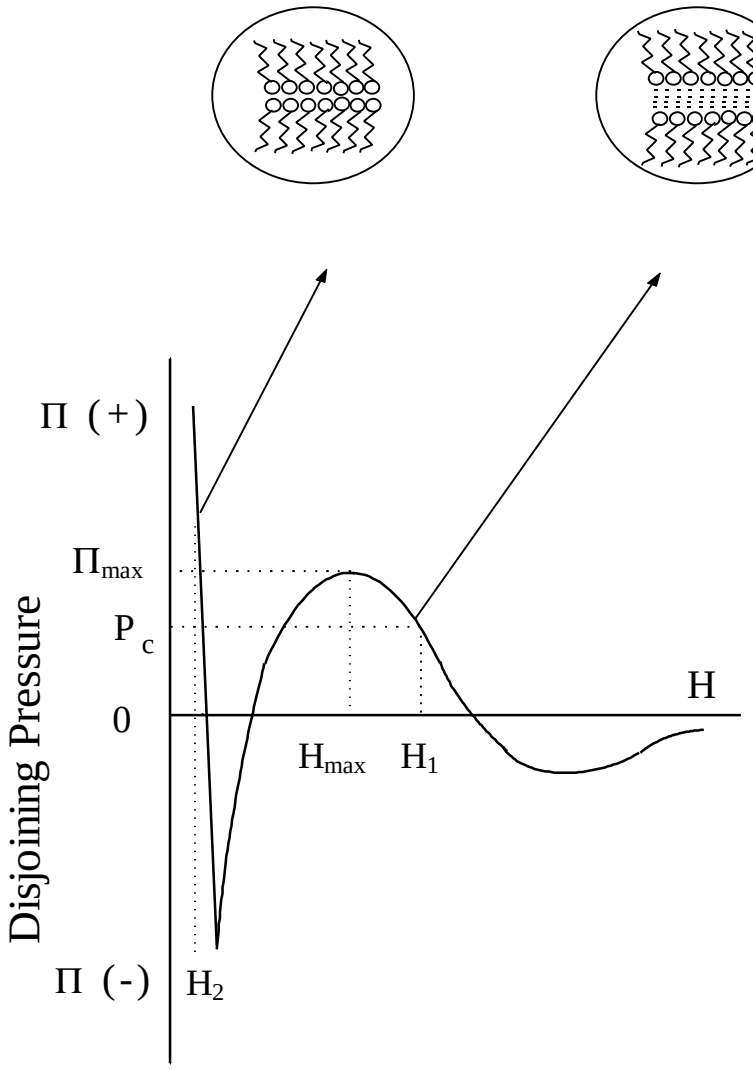

Figure1.2 A disjoining pressure isotherm in 0.01-0.1 M electrolyte. Π is disjoining pressure, P_c is the capillary pressure and H is the film thickness. H corresponds to a CF, H_1 to a CBF and H_2 to a NBF. The isotherm shape depends on the type and concentration of surfactant and indifferent electrolyte (23).

(43) established that free films are unstable whenever the slope of the disjoining pressure isotherm is positive.

1.2.4 Charging Mechanism at the Air-Water Interface

According to McTaggart (26), the first attempt was made by Quincke in 1861 to measure the potentials at the air-solution interface using a spinning cylinder technique. Alty (27) and McTaggart (26) continued this investigation using the same technique. In these investigations the major findings were that air bubbles acquire different charges depending on the solution (containing surfactants and/or electrolytes) composition, and that air bubbles exhibit negative charges in pure water (27, 28).

Currie and Alty (28) proposed a charging mechanism for the bubbles in distilled water. This mechanism presumes that the water dipoles orient themselves such that negative OH^- ions are attached to the interface. In 1986, another charging mechanism was proposed by Yoon and Yordan (29). According to the mechanism, there is a large difference in the hydration energies of OH^- (-446.8 kJ/mole), and H^+ ions (-1104 kJ/mole). As a result, the concentration of H^+ ions is higher than that of OH^- ions in the bulk water phase. Therefore, the negative charge of bubbles and hydrocarbon droplets should be expected. This proposed mechanism suggested further that the charge arises due to the intrinsic property of water rather than to the nature of the interface as long as the second phase, e.g., hydrocarbon (30) and air, does not have a significant acid-base property.

The effect of pH on the charges of air bubbles and hydrocarbon droplets in pure water was also investigated (29). It was presumed that, at a low pH, some of the H^+ ions should move back to the interface due to the increased chemical potential, while, at a high pH, more of the OH^- ions should be present at the interface for the same reason. McShea and Callaghan (31) reported that the zeta potential of air bubbles in pure water is -74.2 ±60 mV at pH 7, -22.5 ±7.7 mV at pH 6, and -0.6 ±0.1 mV at pH 4. These results were a supporting evidence for the mechanism proposed by Yoon and Yordon (29).

The experimental results showed that anionic surfactants produce negatively charged bubbles, while cationic surfactants produce positively charged bubbles. On the other hand, the sign of the charged bubble is pH dependent in the solutions of nonionic surfactants. The negatively charged bubbles are produced in the alkaline pH range while the positively charged bubbles are produced in the acidic pH range. The pH of the solution also plays an important role in the charging mechanism of bubbles produced with some of the ionic surfactants.

In 1974, Dibbs, et al. (32), carried out the experiments using a streaming current technique to determine the signs and the changes in magnitude of bubble charges in the presence of dodecylammonium hydrochloride. It was shown that bubbles give positive current which increased with increasing surfactant concentration. This indicates that the bubbles are positively charged in this condition.

Usui and Sasaki (33) investigated the potential of air bubbles using the Dorn potential technique which was essentially the same as the streaming current technique. They reported their results in terms of zeta potential using the equation commonly employed for calculating zeta potential from sedimentation potential. The sign of the potential is basically determined by the

sign of the polar head of the surfactant; cationic surfactants produce positively charged bubbles and anionic surfactants produced negatively charged bubbles. It was shown that the bubbles produced with nonionic surfactants exhibited negative zeta potential and the magnitude of which did not change significantly with surfactant concentration. It was also reported that the zeta potential of a bubble varies with its sign (24).

By using an electrophoretic flat cell technique, Collons, et al. (34), Fukui and Yuu (35), and Kabuta, et al. (36), measured the electrophoretic mobilities of small gas bubbles that were generated by either electrolysis or a dissolved air technique at the bottom of a flat cell. Their findings showed that when the anionic surfactants were used the negative zeta potential increased with increasing concentration until it reached a constant value near the critical micelle concentration (CMC).

In 1983, McShea and Callaghan (31) conducted experiments using a spinning cylinder to measure the mobilities of air bubbles. They demonstrated that bubbles are negatively charged both in distilled water and in the solutions containing 10^{-4} M KCl at pH 7. Their findings also agreed with those obtained by Usui and Sasaki (33) about the potentials created by the surfactants at the air-water interface.

Yoon and Yordan (29) also carried out the electrophoretic mobilities of microbubbles from which the zeta potentials were calculated in the presence of anionic (sodium dodecyl sulfate and sodium oleat), cationic (dodecyl amine hydrochloride and cetypyridinium chloride), and nonionic (polypropylene glycol, polyoxyethylene methyle ether, and polyoxyethylene dodecyl ether) surfactants. They also reached a similar conclusion about the charges of the bubbles in aqueous solutions as discussed above. In addition, they showed that for the case of ionic

surfactants, the magnitude of the zeta potentials is reduced when the pH approaches the value of pK_a or the pH of precipitation. They also showed that the higher the oxygen-to-carbon ratio in the surfactant molecules, the higher the isoelectric point (i.e.p) value and the more negative the zeta potential.

1.2.5 Components of Disjoining Pressure

The various components of the disjoining pressure have received considerable attention in recent years, and three main types of intermolecular forces are recognized as operating in the film (10-12). The first is a relatively long-range electrostatic force, $\Pi_E(h)$, which results from the repulsion of the similarly charged surfaces of the film core as the diffuse parts of their respective double layers overlap during thinning (13, 14). The second is the London-van der Waals attraction, $\Pi_D(h)$, which is a negative contribution because it acts to thin the film, therefore reducing the total disjoining effect. The third type of force has been called structural forces, $\Pi_S(h)$, which are named as short range steric repulsion forces, $\Pi_S(h)$, hydration forces, $\Pi_{Hyd}(h)$, and hydrophobic forces, $\Pi_H(h)$. In general, based on the theoretical assumptions, their contributions to the total disjoining pressures, $\Pi_T(h)$, are additive, e.g.,

$$\Pi_T(h) = \Pi_E(h) + \Pi_D(h) + \Pi_S(h) \; . \qquad [1.10]$$

In earlier approximations, only the electrical and dispersion forces in the equation [1.10] were combined to explain the stability of the colloid particles interacting with each other in a medium, so called the DLVO theory. On the other hand, the studies on direct force

measurements show that the structural forces exist and their contributions are important for colloid science to describe interaction between the bodies.

In the following sections, each of the components of the disjoining pressure (Equ.10) will be discussed individually for the purpose of explaining the origin of the disjoining pressure isotherm.

1.2.5.1 Electrostatic Forces

The most extensively studied component of the disjoining pressure for colloids and foams is the electrostatic forces between the charged surfaces or interfaces. These interactions occur when the two charged interfaces or their electrical double layers overlap at the interfaces. Figure 1.3 represents the charged surfaces for solid plates and interfaces with the absorbed hydrocarbon molecules. When the separation distance between them comes near twice the characteristic Debye length of the diffuse layer, an additional external force is needed to keep them in the constant separation distance. According to the classical

Debye-Hucel theory (15), the Debye length, $1/\kappa$ is given for the univalent electrolytes as follows:

$$\frac{1}{k} = \sqrt{\frac{ekT}{8pn_o e^2}} \approx \sqrt{\frac{1}{C}} \qquad [1.11]$$

in which ε is the dielectric constant of the medium, k is the Boltzmann constant, T is temperature, n_o is the number density of ions, e is the elementary charge, and C is the concentration of electrolyte (mole/l). This equation indicates that $1/\kappa$ decreases as the electrolyte concentration

increases. This means that interactions between surfaces become shorter range because of ionic screening.

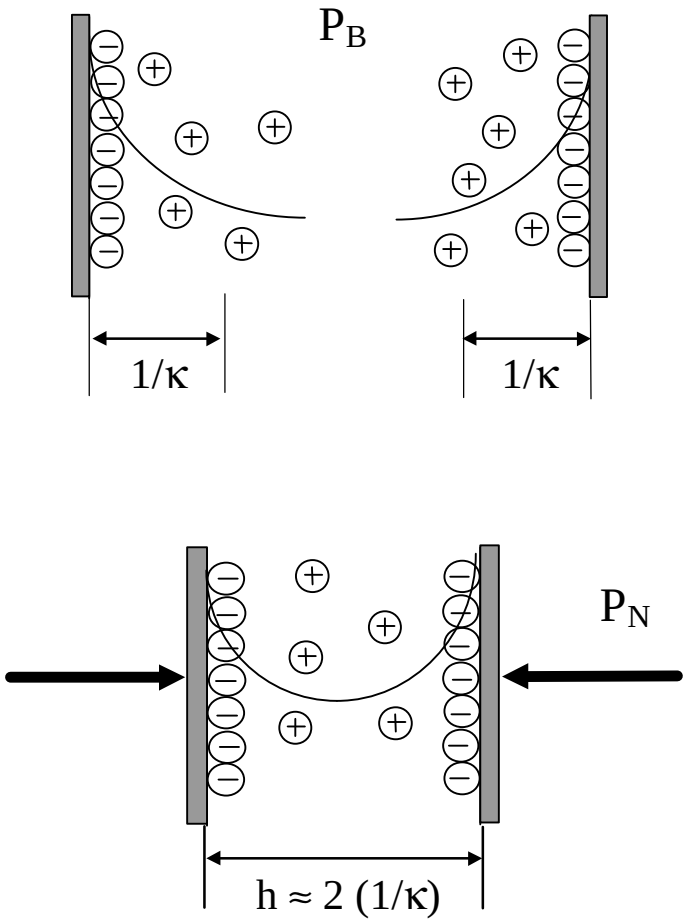

Figure 1.3 Two charged surfaces will interact in their ionic atmospheres when the separation distance approaches twice Debye length, 1/k.

The Poison-Boltzmann equation is commonly used to calculate the electrical repulsion pressure (Π_E) under a variety of different boundary conditions (13-17). In general, two approximations for calculation of Π_E are required. These approximations are valid for small surface charges if the distribution equation is linear. Under these condition and assuming univalent electrolytes, the electrical force is calculated with constant surface potential (4, 17) and/or constant surface charge (4, 18, 19) models and given as follows, respectively:

$$\Pi_E = \frac{ey_o^2}{8p}\left(\sec h^2(kh)\right) \qquad [1.12]$$

and

$$\Pi_E = \frac{2ps_o^2}{e}\left(\frac{1+\sec h\left(\frac{kh}{2}\right)}{\tanh\left(\frac{kh}{2}\right)}\right)^2 \qquad [1.13]$$

in which ψ_o is the potential and σ_o is the charge density at the interface. Hunter (16) further simplified the constant potential model (Equ.1.12) for large separation distances and small potentials to obtain the following commonly used form,

$$\Pi_E = 64n_o kT\,g^2 \exp(-kh)) \qquad [1.14]$$

where $$g = \left(\frac{\exp\left(\frac{ey_o}{2kT}\right)-1}{\exp\left(\frac{ey_o}{2kT}\right)+1}\right).$$

Hunter [16] also pointed out that Equ.[1.14] is also used for constant charge systems since the little discharges occur if the degree of the double layer overlap is small**.** Chan, et.al.(23,24),

proposed another model for the electrostatic component of the disjoining pressure which includes charge regulation boundary conditions at the surface, while Attard, et. al. (13,14), included the effects due to ionic correlation and image forces in their model.

1.2.5.2 Dispersion Forces

Besides electrostatic forces, London-van der Waals dispersion forces have been recognized not only for the particles but also as being important in thin-liquid films. The theoretical treatment of these forces has been undertaken from two basic viewpoints: i) the *microscopic* approach of de Boer(48) and Hamaker (49), based on the summation of the pair wise interactions between atoms of separated particles; ii) the *macroscopic* approach of Liftshitz (50) which treats the interacting phases as being continuous and the interaction as occurring through a continuous medium. The force of interaction between two plain parallel surfaces or interfaces separated by a liquid phase generally given (49)

$$\Pi_D = -\frac{A_{232}}{6pH^3} \qquad [1.15]$$

where A_{232} is the Hamaker constant for the air(2)-water(3)-air(2) system. H is the separation distance (film thickness for aqueous foam films).

1.2.5.3 Structural Forces

The steric (entropic) forces as a third component have been included to compensate for the contributions to the disjoining pressure which are responsible for the stability of the Newton black soap films (film thickness, H<5 nm). Steric repulsion forces (Π_{steric}) arise when the

adsorbed molecular layers overlap (4). Based on the physical origin of these forces and the various modes by which they operate, they are generally classified as headgroup overlap, peristaltic, undulation, and protrusion forces (44). Figure 1.4 shows a schematic representation of a disjoining pressure isotherm that includes contributions from van der Waals, electrostatic, and steric pressures.

On the other hand, solvation forces also become very important in extremely thin films (13). They are called hydration forces when water is the solvent. These forces are observed as the molecules order themselves at the interface. This ordering is disturbed when the interfaces approach one another and cause attractive and repulsive forces. These forces are recognized as short-range interaction forces and mostly depend on the molecular structure at surfaces or interfaces. Generally the force curves obtained for the liquids show an oscillatory interaction (13). However, water has strong dipoles that can lead to hydrogen bonding and long-range dipole polarization. As a result, repulsive hydration or attractive hydrophobic interactions are generated in addition to the short-range oscillatory interaction.

It is now well established that the additional attractive forces operate between hydrophobic surfaces immersed in water and aqueous solutions (51). These forces can be much stronger than those predicted on the basis of van der Waals interactions and are called the hydrophobic forces.

The first hydrophobic force measurement was performed between mica surfaces in cetyltrimethylammonium bromide (CTAB) solutions by Israelachvili and Pashley (51,52) using surface force apparatus (SFA). Their results indicated that there exists a short range (0-10 nm)

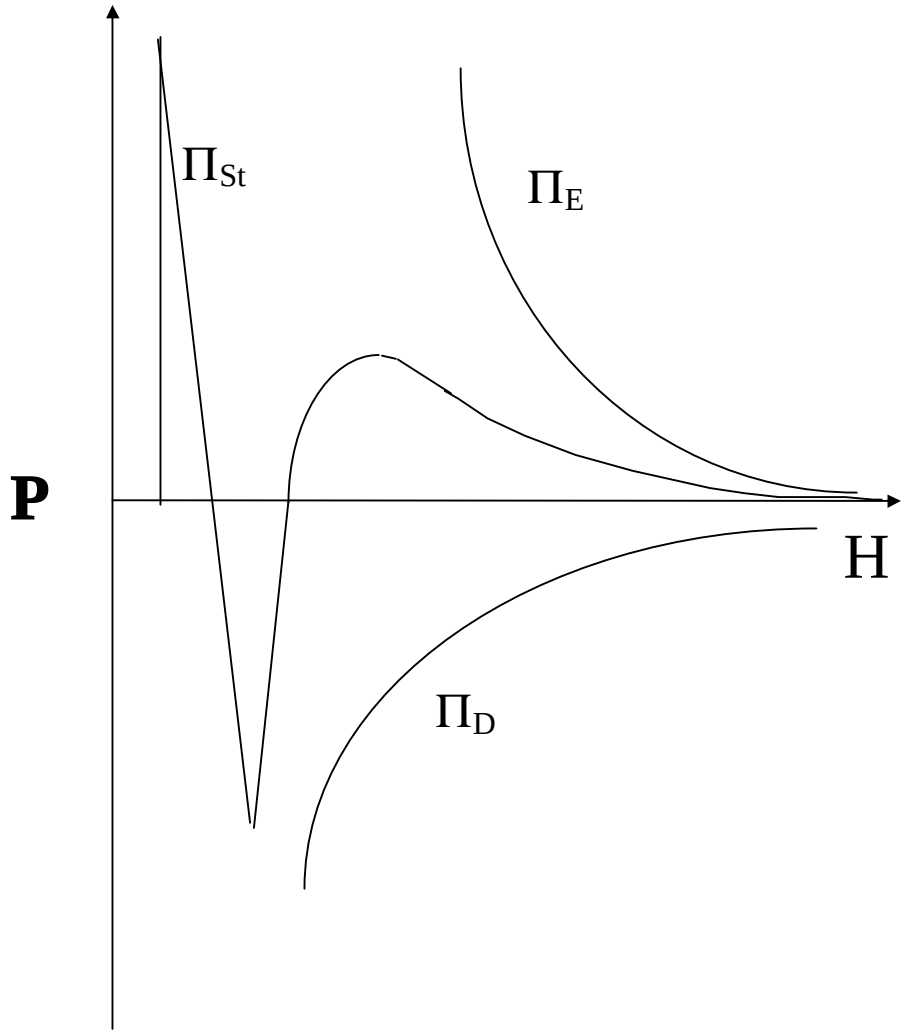

Figure 1.4 A disjoining pressure isotherm introduced by Derjaguin (1) includes the contributions of electrostatic (Π_E), dispersion (Π_D), and steric pressures (Π_{St}).

hydrophobic force between the mica surfaces hydrophobized by adsorption of CTA^+ ions at the mica surface. This hydrophobic force (F) was much stronger than the van der Waals force and decayed exponentially with the distance (H) as follows:

$$\frac{F}{R} = C_o \exp\left(-\frac{H}{D_o}\right), \qquad [1.16]$$

where R is the radius of curvature of the mica surfaces, C_o is a constant (-140 mN/m), and D_o is the decay length (1.0 nm). Later the comparable decay length values (1.0-2.5 nm) were obtained when the force measurements were conducted between mica surfaces in the surfactant solutions (53-56).

The long range hydrophobic force has been measured when the mica surfaces hydrophobized with dioctadecyldimethylammonium bromide (DDOAB) (57-60) and trimethylchlorosilane (TMCS) (57,62) and octadecyltrichlorosilane (ODTCS) (57,62). These results have shown that the hydrophobic force becomes up to four orders of magnitude stronger that those previously measured. In this case, the force curves are fitted with the experimental data using a double exponential force law and given as follows:

$$\frac{F}{R} = -C_1 \exp\left(-\frac{H}{D_1}\right) - C_2 \exp\left(-\frac{H}{D_2}\right), \qquad [1.17]$$

in which the first term represents the short-range while the second term represents the long-range hydrophobic force.

The hydrophobic force has also been described by a power law (63, 64),

$$\frac{F}{R} = -\frac{K}{6H^2}, \qquad [1.18]$$

in which K is the hydrophobic force constant. Using this law, the K values can be calculated and compared directly to the Hamaker constant (A) for the van der Waals forces. It was reported that this K value can be as high as 10^{-6} J for the very hydrophobic surfaces silanated with ODTCS and decreases with decreasing the hydrophobicity of the surface (61,62,64).

Regarding the origin of hydrophobic force, many theories have been proposed including entropic force due to configurational orientation and rearrangement of water molecules when two hydrophobic surfaces approach each other(48-51), capillary force due to cavitation in the vicinity of hydrophobic surfaces (26), subcritical density fluctuation (54), and correlation of dipoles on hydrophobic domains (55,56). However, there is no comprehensive theory or understanding of the origin of hydrophobic force.

Recently, Yoon and Aksoy (65) showed that the hydrophobic force as a third component of disjoining pressure has to be included when the stability of thin aqueous films are studied at low surfactant concentrations in the presence of ionic surfactants, i.e., dodecylammonium chloride and sodium dodecyl sulfate. The disjoining pressure obtained in their study is shown schematically is Figure 1.5, which includes the contributions from the van der Waals, electrostatic, and hydrophobic forces.

The hydrophobic component of the disjoining pressure was represented by using the power law to fit the data. The form of the power law was as follows for thin aqueous films:

$$\Pi_H = -\frac{K_{232}}{6pH^3} \qquad [1.19]$$

in which K_{232} is the hydrophobic force constant for the air(2)-water-air(2) system. Detailed results and discussions about the origin of hydrophobic force will be given in Chapter 3 and 4.

1.3 Research Objectives

The research objective of this investigation is to evaluate the structural (steric, hydration, and most importantly, hydrophobic) forces which become a major stabilizing or destabilizing factor in free water films.

The specific goals of this research are:

1) conduct direct force measurements with bitumen- and asphaltene-coated mica surfaces in the absence and presence of inorganic electrolytes at different pHs and different temperatures,
2) measure the equilibrium film thickness (H_e) of thin water films as a function of anionic and cationic surfactants concentration,
3) conduct direct force measurements using TFB to obtain the disjoining pressure isotherm,
4) determine the contribution from structural forces (steric, hydrophobic) using the extended DLVO theory,
5) discuss the origin of hydrophobic forces on the basis of the data obtained in the present study, and
6) investigate the role of hydrophobic force in thin aqueous films.

It is hoped that the results obtained in the present investigation are useful in estimating the hydrophobic force parameters that can be used for modeling bubble-particle interaction in flotation and tar sand processes.

The results of the present work are presented in a sequence of independent chapters. In Chapter 2, the surface force apparatus (SFA) used for measuring interaction forces between bitumen- and asphaltene- coated mica surfaces and an apparatus built for measuring coalescence

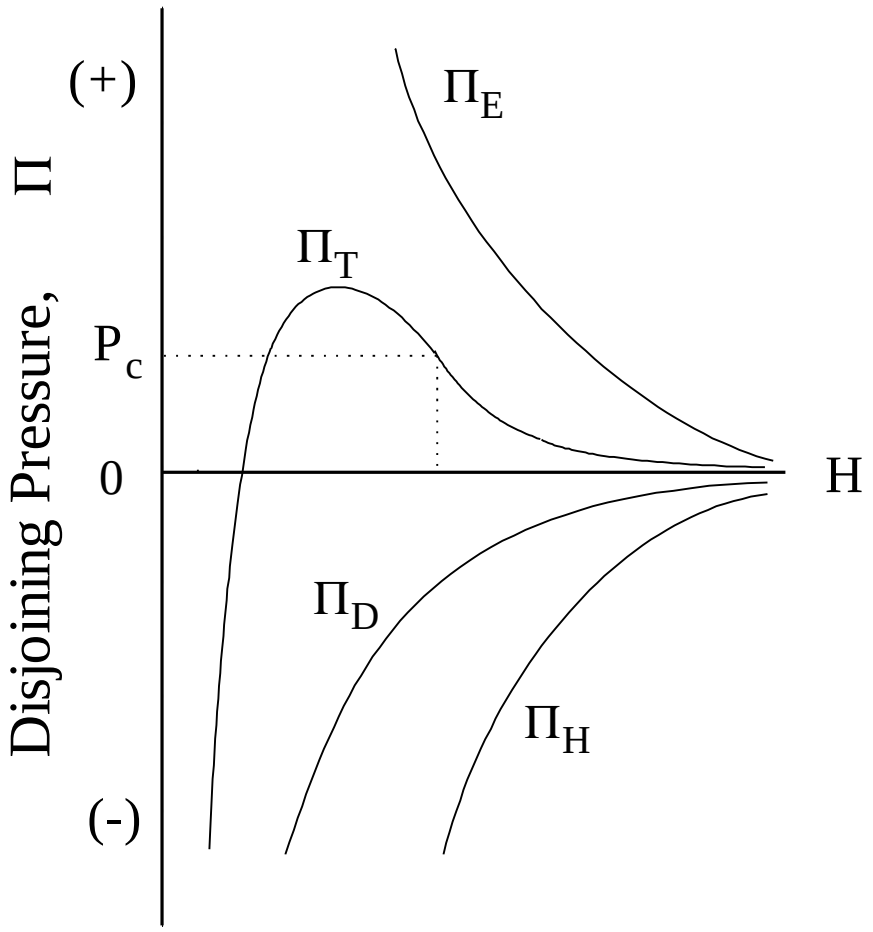

Figure 1.5 A disjoining pressure isotherm for the low surfactant and electrolyte concentrations. Π_E is electrostatic, Π_D is van der Waals, and Π_H is hydrophobic components of the total disjoining pressure, Π_T.

times between bitumen and asphaltene droplets are described. Then the results obtained for different temperature, pHs, and inorganic salts are represented. In Chapter 3, a model was developed to calculate the potential at the air-water interface, and a power law was used to estimate the magnitude of the hydrophobic force in thin water films in the presence of dodecylammonium chloride (RNH_3Cl). Not only equilibrium film thicknesses were measured but also the disjoining pressure isotherm was obtained where the hydrophobic forces dominate the stability of the films. In Chapter 4, the same methods developed in Chapter 3 were employed for sodium dodecyl sulfate (SDS) systems to calculate the potentials at the air-water interface. Then the results of the equilibrium film thickness and disjoining pressure measurements have been represented. In Chapter 5, a PTFE was used as a model of an air bubble in water, and contact angle measurements were performed in surfactant solutions. The purpose was to compare the hydrophobicity of the air bubbles with the hydrophobic surfaces. In Chapter 6, the overall conclusions reached in this study (Chapter 2 throughout Chapter 5) have been summarized. In Chapter 7, the recommendations for future research have been discussed.

Since the topics covered in these chapters are different and independent of each other, they have been written with self-contained formats; each chapter has its own introduction, experimental, result, discussion and conclusion sections. The author hopes that this organization will allow the reader to select topics that are most relevant without reading the entire document.

Chapter 1 Introduction

1.4 REFERENCES

1. Derjaguin, B., and Obuchov, E., *Acta Physic.* U.R.S.S., 5, No.1, 1-22 (1936).
2. Derjaguin, B.V., and Churaev, N.V., *J. Colloid Interface Sci*., **66**, No.3, 389-398 (1978).
3. Kralchevsky, P.A., and Ivanov, I.B., *J. Colloid Interface Sci*., **137**, No.1, 234-252 (1990).
4. Derjaguin, B.V., Churaev, N.V., and Muller, V.M., *Surface Forces*, Kichener, J.A. ed., Consaltants Bureau, New York (1987).
5. Erikson, J.C., and Toshev B.V., *Colloids and Surfaces*, **5**, 241-264 (1982).
6. De Feijter, J.A., Rijnbout, J.B., and Vrij, A., *J. Colloid Interface Sci.*, **64**, No.2, 258-268 (1978).
7. Rowlinson, J.S., and Widom, B., *Molecular Theory of Capillarity*, Oxford Press, New York, Chapter 1-4, 1989.
8. Bakker, G., *Kappillaritat und Oberflachensannung, Handbuch der Experimental Physik*, Bd6, Leipzig (1928).
9. Kuni, F.M., and Rusanov, A.I., *The Modern Theory of Capillary*, Goodrich, F.C., and Rusanov A.I. ed., Akademie-Verlag, Berlin, 107-140 (1981).
10. Lyklema, J., *Pontificiae Acad. Sci. Script. Varia*, **31**, 221 (1967).
11. Derjaguin, B.V., Titiyevskaya, A.S., Abricossova, I.I., and Malkina, A.D., *Discussions Faraday Sci*. **18**, 24 (1954).
12. Bikerman, J.J., *Foams: Theory and Industrial Applications*, Rainhold, New York, 1973.
13. Israelachvili, J.N., *Intermolecular and Surface Forces with Applications to Colloid and Biological Systems*, Academic Press, Orlando, Fl., (1985).

14. Derjaguin, B.V., *Theory of Stability of Colloids and Thin Films*, Translated by R.K. Johnson, Consultants Bureau, New York, (1989).

15. Chu, B., Molecular Forces, Based on the Baker Lectures of Peter J.W. Debye, Interscience Publishers-John Wiley and Sons, New York, (1967).

16. Hunter, R.J., *Foundation of Colloid Science*, Clarendon Press, Oxford Vol. 1 (1987).

17. Usui, S., and Hachisu, S., *Electrical Phenomena at Interfaces: Fundamentals, Measurements, and Applications*, Kitahara, A., and Marcel Dekker Inc., Surfactant Science Series, Vol. **15**, 47-98 (1980).

18. Ohshima, H., *Colloid and Polymer Sci*, **252**, 158-164 (1974).

19. Ohshima, H., *Colloid and Polymer Sci*, **252**, 257-267 (1974).

20. Derjaguin, B.V., and Titievskaya, A.S., *Kolloid. Zh.*, **15**, 416 (1953).

21. Derjaguin, B.V., and Titievskaya, A.S., *Discuss. Faraday Soc.*, **18**, 27 (1954).

22. Scheludko, A., and Exerowa, D., *Kolloid Zh.*, **165**, 148 (1959).

23. Pugh, R.J., and Manev, E., *Innovations in Flotation Technology*, P. Mavros and K.A. Matis (eds.), Kluwer Academic Publishers, 1-24 (1992).

24. Usui, S., Sasaki, H., and Matsukawa, H., *J. Colloid Interface Sci*. **81**, 80 (1981).

25. Exerowa, D., *Commun. Dept. Chem., Bulg. Acad. Sci*. **11**, 739-763 (1978).

26. McTaggart, M.A., *Philos. Mag*, **44**, 386 (1922).

27. Alty, T., *Proc. R. Soc. London Ser*. A, **106**, 315 (1924).

28. Currie, B. W., and Alty, TV., *Proc. R. Soc. London Ser*. A, **120**, 622 (1930).

29. Yoon, R-H. and Yordan, J. L., *J. Colloid Interface Sci*., **113**, 430 (1986).

Chapter 1 Introduction

30. Fowkes, F.M., in "*Physicochemical Aspects of Polymer Surface*" (K.L. Mittal, Ed.), Vol. 2, Plenum, New York (1983).

31. McShea, J.A., and Callaghan, I.C., *Colloid Poly. Sci*. **261**, 757 (1983).

32. Dibbs, H.P., Sirois, L.L. and Bredin, R., *Canad. Metall. Quart*. **13**, 395 (1974).

33. Usui, S., and Sasaki, H., *J. Colloid Interface Sci*., **65**, 36 (1978).

34. Collons, G.L., Motarjemi, M., and Jameson, G.L., *J. Colloid Interface Sci*. **63**, 69 (1978).

35. Fukui, Y., and Yuu, S., *AICHE J*. **28**(5) (1982).

36. Kubota, K., Hayashi, S., and Inoaka, M., *J. Colloid Interface Sci*. **95**, 362 (1983).

37. Bergeron, V., and Radke, C.J., *Langmuir*, **8**, 3020-3026 (1992).

38. Bergeron. V., Ph.D. thesis, University of California, Berkeley (1993).

39. Mysels, K.J., and Jones, M.N., *Discuss. Faraday Soc*., **42**, 42-50 (1966).

40. Exerowa, D., Kolarov, T., and Khistov, KHR., *Colloids and Surfaces*, **22**, 171-185 (1987).

41. Ninham, B.W., *Chemica Scripta*, **25**, 3-6 (1985).

42. Israelachvili, J.W., and Wennerstom, H., *Langmuir*, **6**, 873-876 (1990).

43. de Vries, A.J., *Recueil*, **77**, 441-461 (1958).

44. Israelachvili, J.W., and Wennerstom, H., *J. Phys Chem*, **96**, 520-531 (1992).

45. Mysels, K.J., *J. Phys. Chem.*, **68**, 3441 (1964).

46. Pugh, R.J., and Yoon, R-H., *J. Colloid Interface Sci*., **163**, 169 (1994).

47. Tchaliovska, S., Manev, E. Radoev, B., Erikson, J.C., and Cleasson, P.M., *J. Colloid Interface Sci*., **168**, 190 (1994).

48. de Boer, J.H, *Trans. Faraday Soc*., **32**, 10 (1936).

Chapter 1 Introduction

49. Hamaker, H.C., "The London-van der Waals Attraction between Spherical Particles," *Physica*, **4**, No.10, 1058-1072 (1937).

50. Lifshitz, E.M., *Zhur. eksp. teor. Fiz*., **29**, 94 (1955).

51. Israelachvili, J.N., and Pashley, R., *Nature*, **300**, 341-342 (1982).

52. Israelachvili, J.N., and Pashley, R., *J. Colloid Interface Sci*., **98**, 500 (1984).

53. Kekicheff, P., Chistenson, H.K., and Ninham, B.W., *Colloids Surf*., 40, 31 (1989).

54. Herder, P.C., *J. Colloid Interface Sci*., **134**, 346 (1990).

55. Yoon, R-H., and Ravishankar, S.A., *J. Colloid Interface Sci*., **166**, 215 (1994).

56. Pashley, R.M., McGuiggan, P.M., Ninham, B.W., and Evens, D.F., *Science*, **229**, 1088 (1985).

57. Christenson, H.K., Fang, J., Ninham, B.W., and Parker, J.L, *J. Phys. Chem*., **94**, 8004 (1990).

58. Tsao, Y., Yang, S.X., Evens, D.F., and Wennerstrom, H., *Langmuir*, **7,** 3154 (1991).

59. Claeson, P.M., Blom, C.E., Herder, P.C., and Ninham, B.W., *J. Colloid Interface Sci*., **114**, 234 (1994).

60. Christenson, H.K., Claeson, P.M., Berg, J., and Herder, P.C., *J. Phys. Chem*., **93**, 1472 (1989).

61. Rabinovich, Y.I., and Yoon, R-H., *Langmuir*, **10**, 1903 (1994).

62. Rabinovich, Y.I., and Yoon, R-H., *Colloids Surfaces*, **93**, 263 (1994).

63. Claesson, P.M., and Christenson, H.K., *J. Phys. Chem*., **92**, 1650 (1988).

64. Darrin, H. Flinn, Ph.D. dissertation, Mining Eng. Virginia Tech. Blacksburg, Virginia, 1996.

65. Yoon. R-H., and Aksoy, B.S. submitted to *J. Colloid Interface Sci*. (1996).

Chapter 1 Introduction

CHAPTER 2

ROLE OF SURFACE FORCES IN TAR SAND PROCESSING

ABSTRACT

Direct force measurements were conducted with bitumen-coated mica surfaces using a Mark IV surface force analyzer. Long-range electrostatic repulsive forces were observed at separation distances above approximately 70 nm; however, unexpectedly strong repulsive forces were measured at shorter separation distances. These non-DLVO forces may be attributed to the steric repulsion between asphaltenes extracted on the bitumen surface, which was substantiated by the force measurements conducted using asphaltene-coated mica surfaces. The steric forces increased with pH and temperature, which may be explained by the increased solubilization of asphaltenes in water. The steric force also increased with electrolyte concentration, possibly due to a decrease in the mobility of the tails of the asphaltenes on the surface.

The kinetics of coalescence of bitumen droplets was studied by measuring the induction time. There was a general agreement between the force data and the kinetic information, suggesting that bitumen suspensions are stabilized by asphaltene. The steric forces identified by the direct force measurements may have profound implications on the hot water processing of Alberta Tar sands.

2.1 INTRODUCTION

The tar sands deposits in Alberta are found in four major areas, *i.e.*, Athabasca, Wabasca, Peace River and Cold Lake. Only the high-grade tar sands are mined today using the hot water extraction process developed by Clark in the 1920's. Two companies, *i.e.*, Syncrude and Suncor, are producing approximately 100 million barrels of "synthetic crude" per year using this process. The four deposits in Alberta represent 1.7 trillion barrels of oil reserve, which is five-times larger than that in Saudi Arabia.

The ore is composed mostly of silica sand and some clay minerals (mostly kaolinite) impregnated with bitumen. The feeds to the hot water process contains typically 10% bitumen by weight, while the median size of the silica sands is about 150 μm. The ore is fed to a 18x100 feet rotating drum (tumbler), where hot water (steam) is injected along with caustic soda to raise the pH to 8.0-8.5 and the temperature to about 80^{o}C. The ore disintegrates in the tumbler to produce an oil-in-water emulsion. It is generally believed that the emulsion is stabilized by the surfactants, *e.g.*, naphtenate. The surfactants also stabilize air bubbles to produce bubbles in the range of 100-600 μm. Under the turbulent conditions imparted by the tumbler, air bubbles are engulfed by the bitumen droplets. The ore slurry is discharged over a vibrating screen to remove lumpy materials (rocks). The screen underflow, combined with a middlings stream, enters a large separation vessel (44x24 feet), where the bitumen droplets enlightened by the engulfed air bubbles float to the top, while the sand and clay are discharged to the bottom. The froth product typically contains 60% bitumen, 30% water and 10% solids. The reject stream is sent to a bank of mechanically agitated flotation machines, where the slurry is aerated to scavenge bitumen droplets not recovered in the primary separation vessel. The overall bitumen recovery in the hot water

process exceeds 93%. The froth products obtained by the hot water process are deaerated, diluted in naphtha, and centrifuged to remove solids. The bitumen is upgraded further by a combination of thermal cracking and catalytic hydrocracking processes to obtain synthetic crude oil.

Although the hot water process is conceptually simple, the mechanisms involved in different steps are not fully understood. For example, the interaction between bitumen droplets (coalescence) and between bitumen and air bubbles (flotation) are not well understood. One observation made in the plant operation is that the bitumen lost to the tailings is in the form of finely dispersed, unaerated droplets. It is not certain what controls the droplet size distributions and what controls the engulfment of air bubbles by the bitumen droplets.

It was, therefore, the objective of the present investigation to study the basic mechanisms involved in the coalescence of bitumen droplets. A surface force apparatus (SFA) was used to directly measure the surface forces between bitumen-coated mica surfaces. The force data are compared with kinetics of bitumen coalescence. The results will be useful for understanding the mechanisms for controlling bitumen size distribution and the flotation process.

2.2 EXPERIMENTAL

2.2.1 Materials

A high-purity Atabasca bitumen was obtained from Syncrude Research. Analytical grade toluene and chloroform from Fisher Scientific were used to solubilize the bitumen. The pH of the solution was adjusted using reagent grade NaOH and HCl. Analytical grade KCl, NaCl, $MgSO_4$,

borax, $NaHCO_3$ were used for induction time measurements. All of the reagent solutions were prepared using Nanopure water.

2.2.2 Procedure

2.2.2.1 Surface Force Measurements

A schematic diagram of the Mark IV surface force apparatus is shown in Figure 2.1. This apparatus has been described in detail in the literature (1). Two mica sheets were cleaved to obtain molecularly smooth surfaces. The back sides were silvered to a thickness of about 27 nm and glued, using Epon 1004, onto silica lenses. One of the silica lenses was mounted onto a piezoelectric crystal, while the other silica lens was mounted onto a cantilever spring. This leaf spring was driven by two motors; the coarse motor drives the leaf spring over large distances, while the fine motor drove with an accuracy of 0.2 nm. The closest separation distance between the two mica surfaces were determined by multiple beam interferometry using the method of Fringes of Equal Chromatic Order (FECO) (2). The surface force apparatus was mounted in a closed wooden chamber, which was designed to provide a temperature control in the range of 10-50^{o}C.

Mica surfaces were coated with bitumen using a Langmuir-Bloggett trough. A bitumen-in-chloroform solution (120 mg/ml) was spread over the water in the trough. The film appeared visibly patchy, indicating that they were not truly homogeneous monolayer films. Nevertheless,

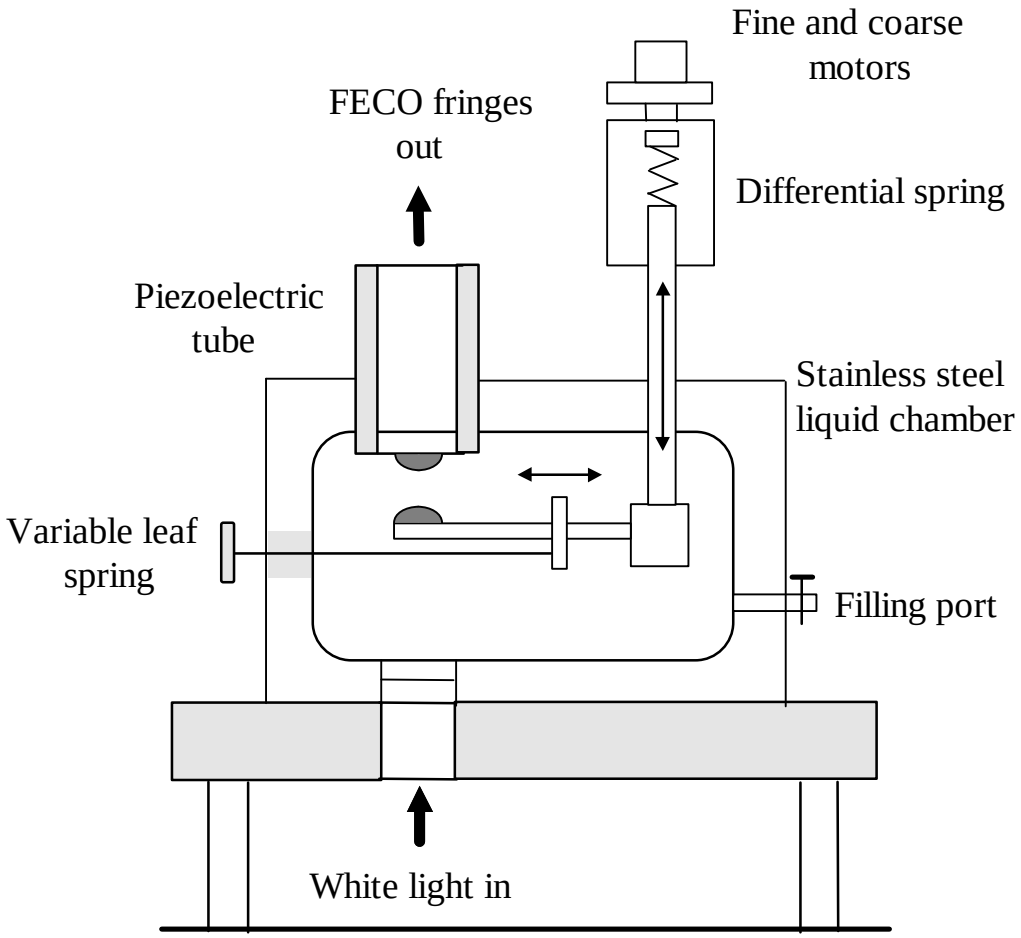

Figure 2.1. A schematic representation of the Mark IV surface force apparatus. Mica surfaces are glued on the silica discs mounted on the leaf spring and the Piezoelectric tube.

the film was transferred to the silvered mica sheet by slowly withdrawing it through the water/air interface. The coating was done at a surface pressure of approximately 25 mN/m. The IR spectrum of the L-B deposited films closely resembled that of bulk bitumen. Water contact angles on the films deposited in this manner were in the range of 45-55°.

The bitumen-coated mica sheets were allowed to dry in a laminar flow cabinet for 15 minutes and then mounted in the SFA. The solution chamber inside the SFA was flushed with dry nitrogen for 30 minutes, after which the surfaces were brought into contact. The contact position measured under dry nitrogen atmosphere was taken as the zero-position for all subsequent measurements conducted using the same mica surfaces.

After establishing the zero-position, the apparatus was filled with Nanopure water, and deaerated for several hours under vacuum to avoid possible formation of air bubbles on the mica surfaces.

The force measurements were also conducted using asphaltene-coated mica surfaces. The asphaltene was precipitated by contacting a concentrated bitumen-in-toluene solution with a large amount of n-pentane (3). The asphaltene fraction was dried, dissolved in chloroform (120 mg/ml), and used for coating mica surfaces in the same manner as described for bitumen.

2.2.2.2 Induction Time Measurements

Induction time is defined as the minimum time required for two bitumen droplets coalesce with each other. Figure 2.2 shows the device used in the present work to measure the induction time. Initially, two bitumen droplets were formed in an aqueous solution on the 1 mm holes located at the bottoms of two spherical bitumen holders by applying a positive pressure. The

lower droplet was brought to a position directly under the upper droplet by means of a micro-mover, which was capable of moving the droplet in x-, y- and z-directions. The upper droplet was then moved toward the lower droplet by means of a Nanomover (Encoder Mike Controller, Model 18011, Oriel Corporation), which was capable of moving the droplet along the z-direction at speeds in the range of 1-200 nm/sec. The process was monitored by means of a high-speed video system (Kodak/Spin Physics), which was capable of recording events at a speed of 60-2,000 frames/sec. The apparatus shown in Figure 2.2 was immersed in a water bath for temperature control.

It was difficult to create bitumen droplets using simple capillary tubes. When a gas (nitrogen) pressure was exerted on the bitumen inside a capillary tubing, a gas bubble was often formed at the end of the capillary because of the high viscosity of bitumen. This problem was overcome by using the spherical bitumen holders shown in Figure 2.2. The spherical droplet holders worked well even at room temperature.

All the glassware used for the induction time measurements were cleaned in chloroform between experiments. It was then washed by a detergent solution and rinsed with water before being cleaned further in boiling nitric acid solutions for 3-4 hours. The glassware was rinsed with copious amounts of Nanopure water before use. The droplet holders were dried with N_2 gas before introducing 10-20 grams of bitumen. The induction time was measured as the time between the moment of contact and the moment of coalescence. Under a given experimental condition, a set of 15-20 measurements were made and averaged.

Chapter 2: Role of Surface Forces in Tar Sand Processing

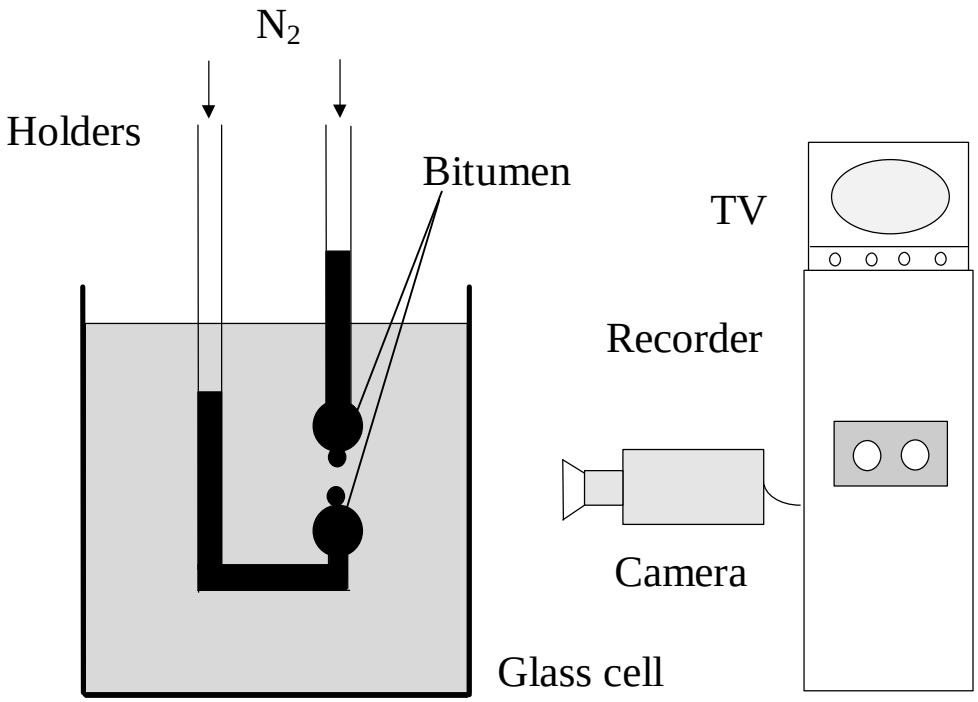

Figure 2.2 A schematic representation of the induction timer used for determining coalescence kinetics for bitumen droplets (1-1.5 mm diameter).

2.3 RESULTS

Figure 2.3 shows the force vs. distance curves obtained with bitumen-coated mica surfaces in Nanopure water at pH 5.8. A repulsive force begins to appear at a surface separation (H) of about 110 nm. The repulsive force rises steeply at H≈30 nm until the fine motor is no longer able to compress the mica surfaces further. This finding suggests that in the presence of water a polymeric substance comes out of the bitumen and deposit on the surface. The substance is difficult to compress below the thickness of approximately 15 nm using the fine motor. Using the coarse motor, it was possible to further compress the surfaces to H≈3 nm; however, no force measurement was possible using this motor. When the two bitumen-coated mica surfaces are separated from each other, the force measurements exhibit a hysterisis. Initially, the repulsive force decreases steeply and becomes attractive. At H≅70 nm, the two surfaces jump out from each other and detached. Attempts have been made to fit the force curves obtained during the approach cycle to the DLVO theory to no avail. Therefore, a simple model has been developed to account for the result obtained in the present work. As shown in Figure 2.4a, the L-B deposited film of bitumen lies collapsed on the mica surface under dry nitrogen atmosphere. In the presence of water, however, some of the more polar fractions, such as asphaltene, is extracted from the bitumen and deposited on the surface. The polar groups and tails of the asphaltene are exposed toward the aqueous phase as suggested in Figure 2.4b. On the other hand, the aromatic cores of the asphaltene molecules (or larger molecular weight asphaltenes) would stay closer to the bitumen surface, and may account for the hard-to-compress adsorbed layer on the surface. The polar groups of asphaltene, which may be mostly anionic, constitutes the charge plane.

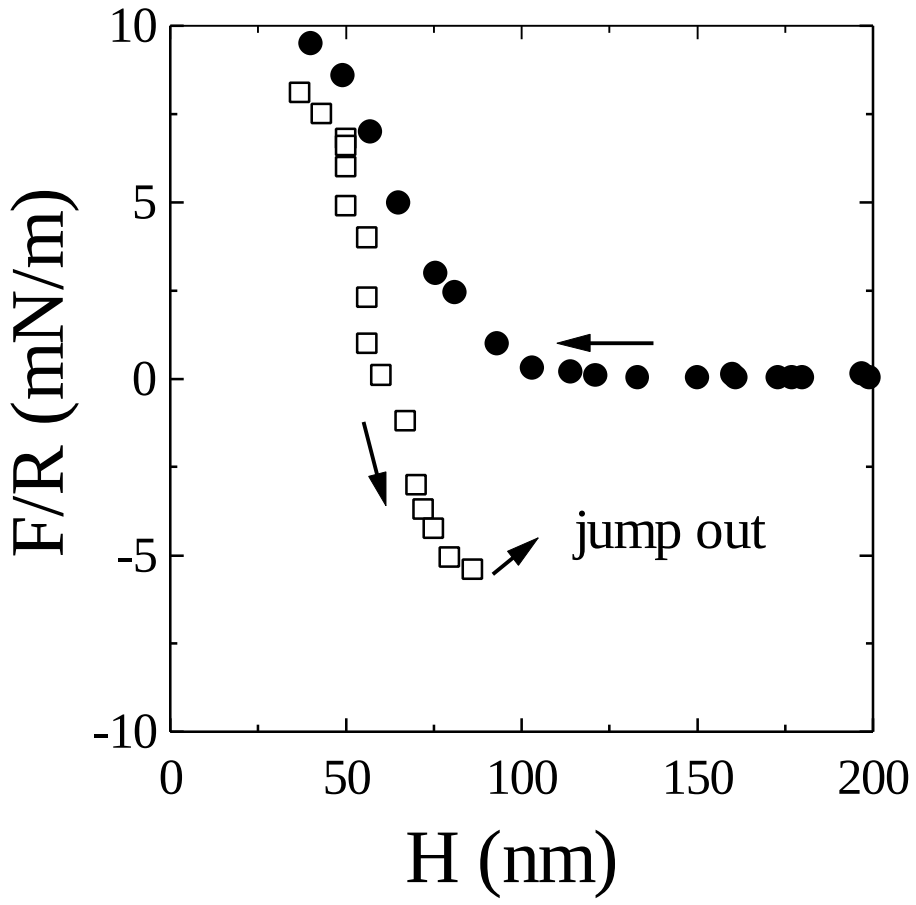

Figure 2.3 The force *vs.* distance curves measured between two bitumen- coated mica surfaces in Nanopure water at pH 5.8. The circlesrepresent data points obtained during the approach cycle and the squares represent those obtained during the separation cycle.

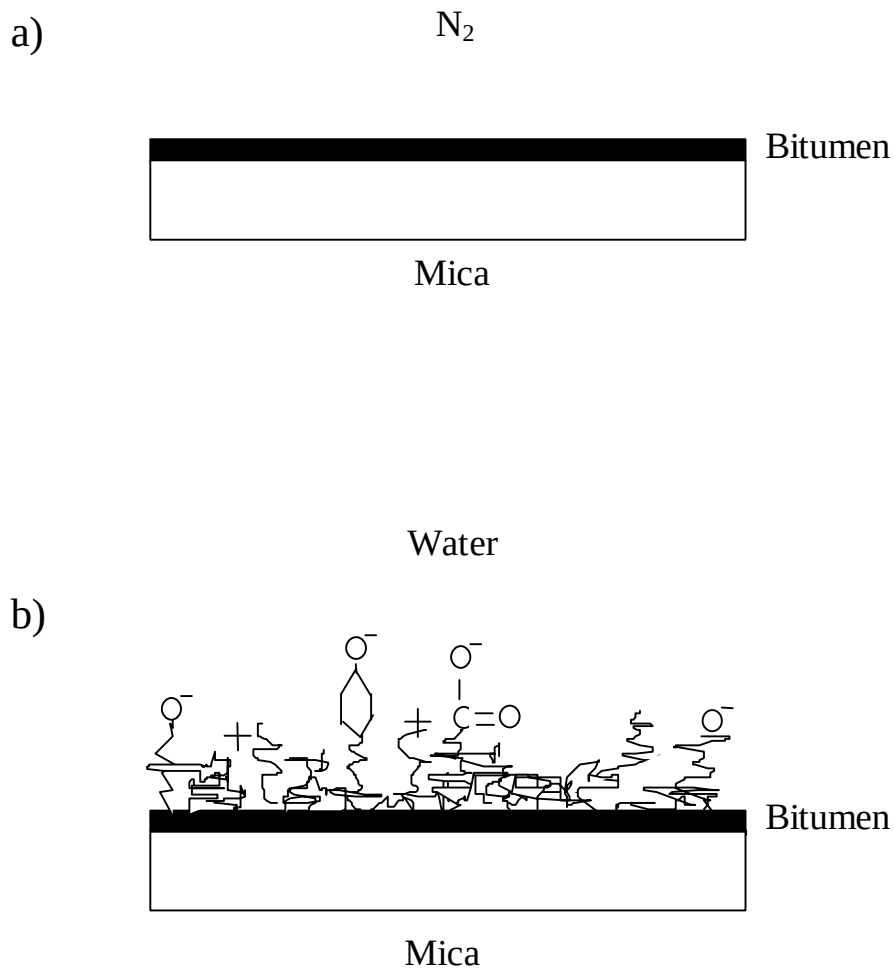

Figure 2.4 A proposed model for a) bitumen/air interface, and b) bitumen/water interface.

Thus, any attempt to fit the measured force curve to the DLVO theory with the charge plane situated at the zero-position established in nitrogen will fail. If the charge plane is shifted away from the zero position by approximately 35 nm, as suggested by the model, it would be possible to fit the tails of the measured force curve to the DLVO theory.

The data shown in Figure 2.3 can be used to verify the proposed model. The solid line shown in Figure 2.5 represents the electrostatic force curve of the DLVO theory. It has been assumed that the charge resides at a plane located at a distance of36.5 nm away from each surface. In calculating the DLVO force, the van der Waals force has been neglected on the ground that the mica surfaces are far from the separation distances under consideration, and that the asphaltene layer is not a dense-pase. Therefore, the force data obtained at H>73 nm can be fitted to the constant potential model of the DLVO theory as follows (4):

$$\frac{F}{R} = 2\pi(4.82x10^{-5})\,C^{1/2}\,\gamma^{2}\exp(-\kappa H) \qquad [2.1]$$

in which *F/R* is the force, in units of mN/m, normalized by the radius of the curvature of the mica surfaces, *C* the electrolyte concentration in moles/l, κ the reciprocal Debye length, *H* the separation distance, and

$$\gamma = \tanh\left(\frac{e\psi_{\circ}}{4kT}\right) \qquad [2.2]$$

where *e* is the electronic charge, ψ_0 the surface potential, *k* the Boltzman constant and *T* is the absolute temperature. One obtains ψ_0 = -97 mV at C = 5 x 10^{-4} M. The value of ψ_0 agrees reasonably well with the zeta (ζ) potential values measured for pure bitumen, as will be shown later. Interestingly, the location of the plane of charge at 36.5 nm corresponds to the observed

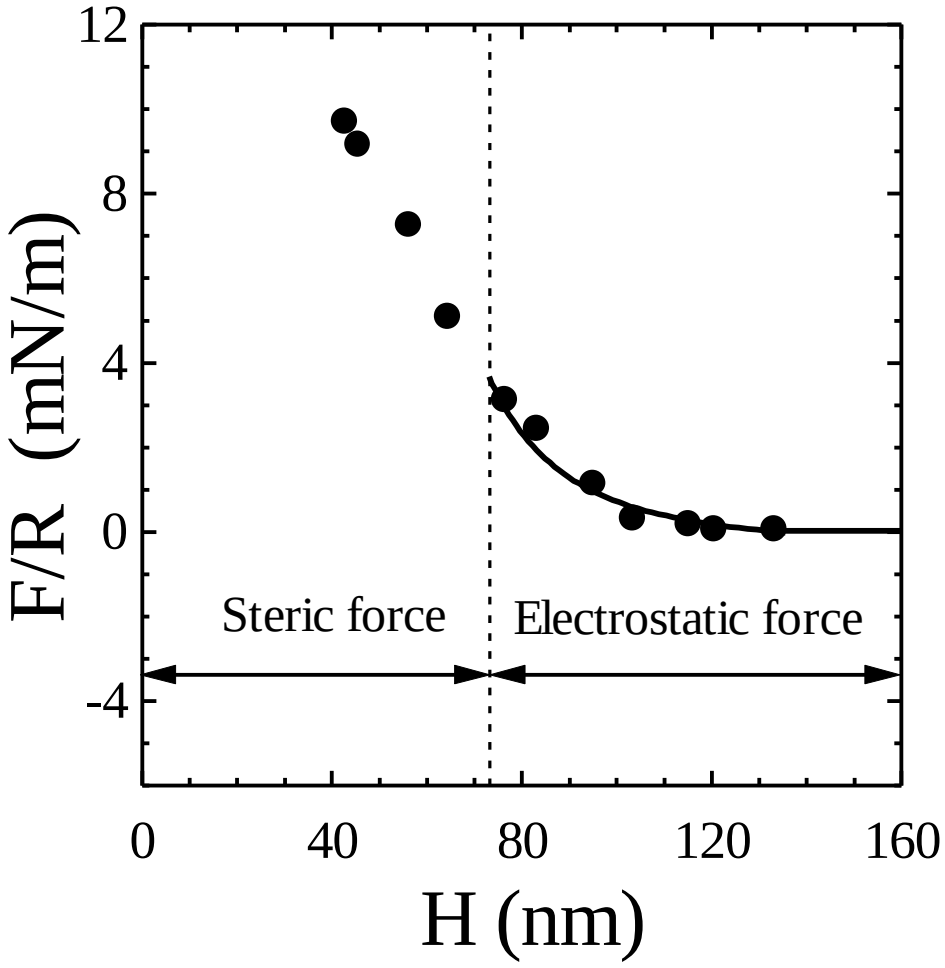

Figure 2.5 A DLVO fit of the force curve obtained with bitumen-coated mica surfaces in Nanopure water (pH 5.8) using Eq. (1); Ψ_o=-97 mV and $C = 5 \times 10^{-4}$ M. Contributions from dispersion force has been ignored. The solid line represents the DLVO fit. The data obtained at H<70nm cannot be fitted by Eq. (1).

distance (H=70 nm) at which the two mica surfaces are separated from each other (Figure 2.3), providing further evidence that the thickness of the asphaltene layer exposed on the bitumen surface is about 35 nm on each surface.

According to the model proposed in the present work, the repulsive force observed at 40<H<73 nm are due to steric repulsion between the tails of asphaltenes. The repulsive steric force arises from the resistance of the tails to a decrease in entropy when they are tangled with each other.

The proposed model is consistent with the general knowledge of bitumen. Approximately 17% of the Atabasca bitumen is asphaltene (3), and its number-mean molecular weight is 3,600. However, more than 50% of the asphaltene has a molecular weight greater than 13,000 (5). NMR studies showed that the asphaltenes consist of aromatic cores surrounded by n-alkyl chains of various lengths (6). It has been suggested that asphaltenes are responsible for the stability of water-in-oil emulsions (7-9). In a study conducted with Norwegian crude oil, Borve *et al.* isolated the interfacially active, emulsion-stabilizing fractions, which were found to be polydispersed, low molecular weight polymers with a mean molecular weight of 950-1450 $gmol^{-1}$ (9).

Figure 2.6 compares the force-distance curves obtained with bitumen-coated mica surfaces in Nanopure water at pH 5.8 and 8.5. The change in pH has little effect on the forces measured at H<70 nm, indicating the steric force is relatively insensitive to pH at ambient temperature. At longer separation distances, however, the repulsive forces measured at pH 8.5 are slightly larger. Assuming that the charge plane is 36 nm away from the mica surface,

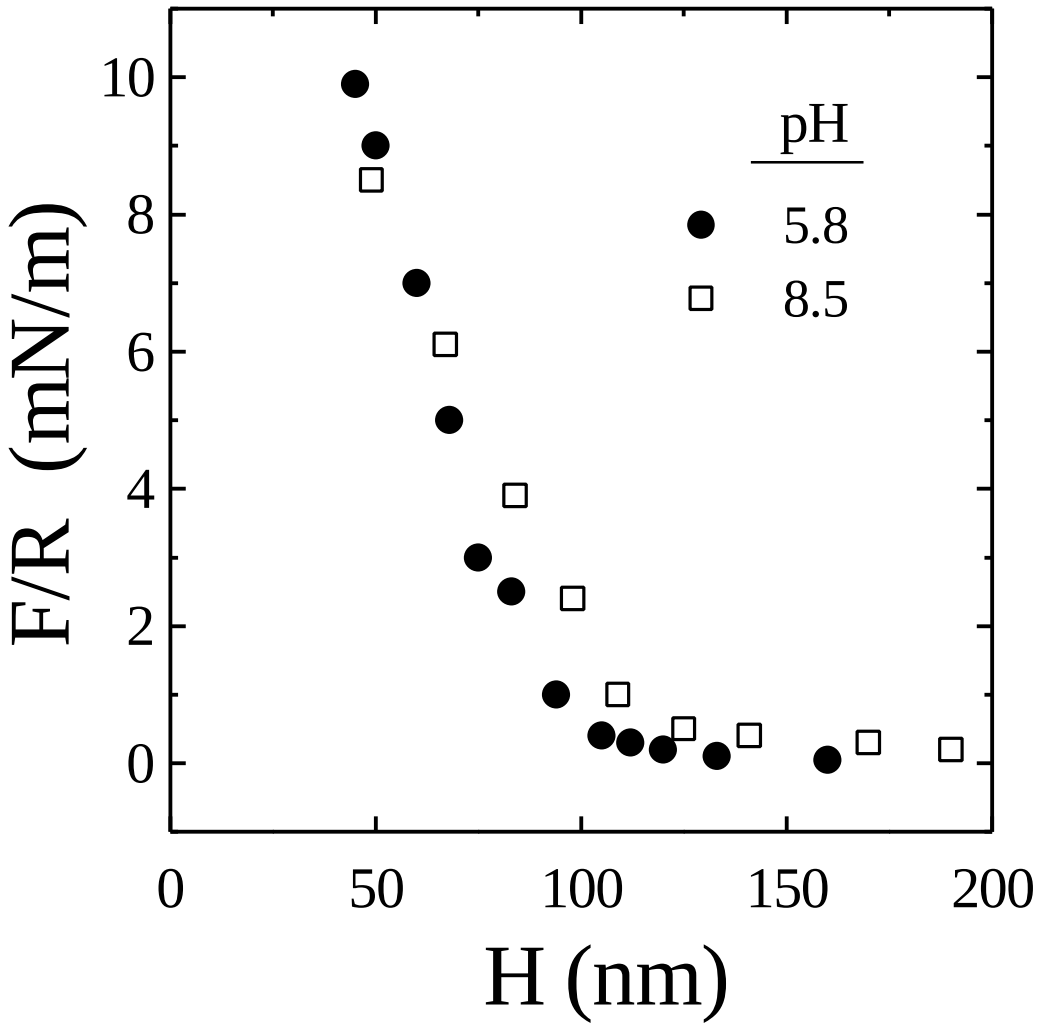

Figure 2.6 Effects of pH on the force *vs.* distance curves obtained with bitumen-coated mica surfaces.

the force data can be fitted with ψ_0=-150 mV. That this value is substantially higher than that (ψ_0=-97 mV) obtained at pH the asphaltene are more fully ionized at the higher pH.

Figure 2.7 shows the force curves obtained in 10^{-4} and 10^{-2} M KCl solutions at pH 8.5. At H>75 nm, the repulsive force is reduced at higher electrolyte concentration, indicating that the double layer is compressed by the electrolyte. The opposite is true at H<75 nm. Apparently, the steric force increases at higher electrolyte concentration.

The next set of force measurements were conducted using mica surfaces coated with the asphaltene extracted from bitumen. Figure 2.8 shows the data obtained at 25°C. The force curve obtained during the approach cycle was similar to that observed between the bitumen-coated mica surfaces in that large repulsive force that cannot be explained by the DLVO theory was observed. Unlike the case with bitumen-coated mica surfaces, it was possible to bring the surfaces to H≈0 using the coarse motor. Apparently, some of the hard-to-compress asphaltenes were not extracted by the process employed in the present work. The force curve obtained during the return cycle exhibited strong hysterisis, indicating that the asphaltene molecules are irrevesively-compressed. However, when the force measurements were repeated several hours after the return cycle, the strong repulsive force could again be measured.

Figure 2.9 compares the force curves obtained with asphaltene-coated mica surfaces at 25 and 45°C. There are very little changes in the force curves at H>60 nm; however, the long-range repulsive force appears to be slightly larger at the higher temperature, which is consistent with the double layer theory. At H<40 nm, the repulsive force increase substantially, suggesting that the steric repulsion, which is entropic in origin, increases with temperature. This increase is due to an

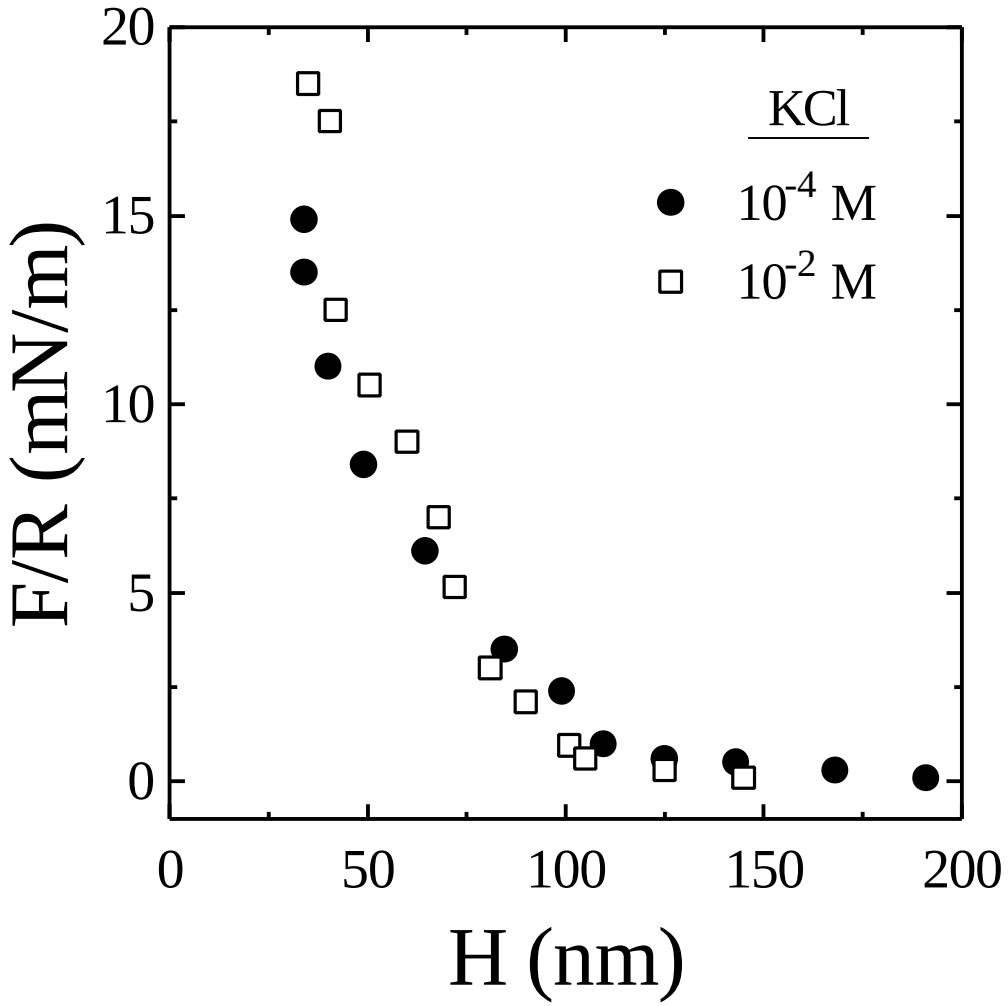

Figure 2.7 Effect of KCl concentration on the force *vs.* distance curves obtained with bitumen-coated mica surfaces at pH 8.5.

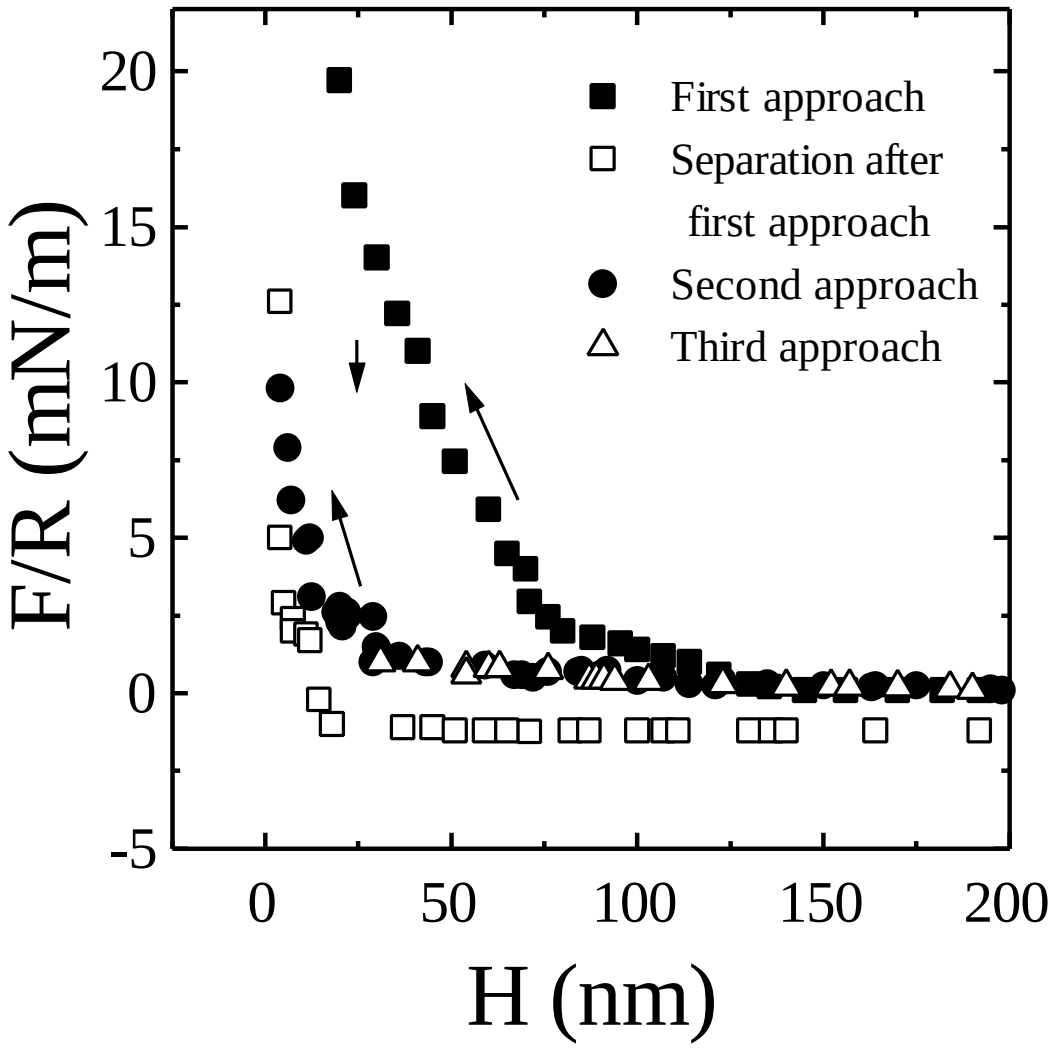

Figure 2.8 The force vs. distance curves between two asphaltene-coated mica surfaces at pH 5.8.

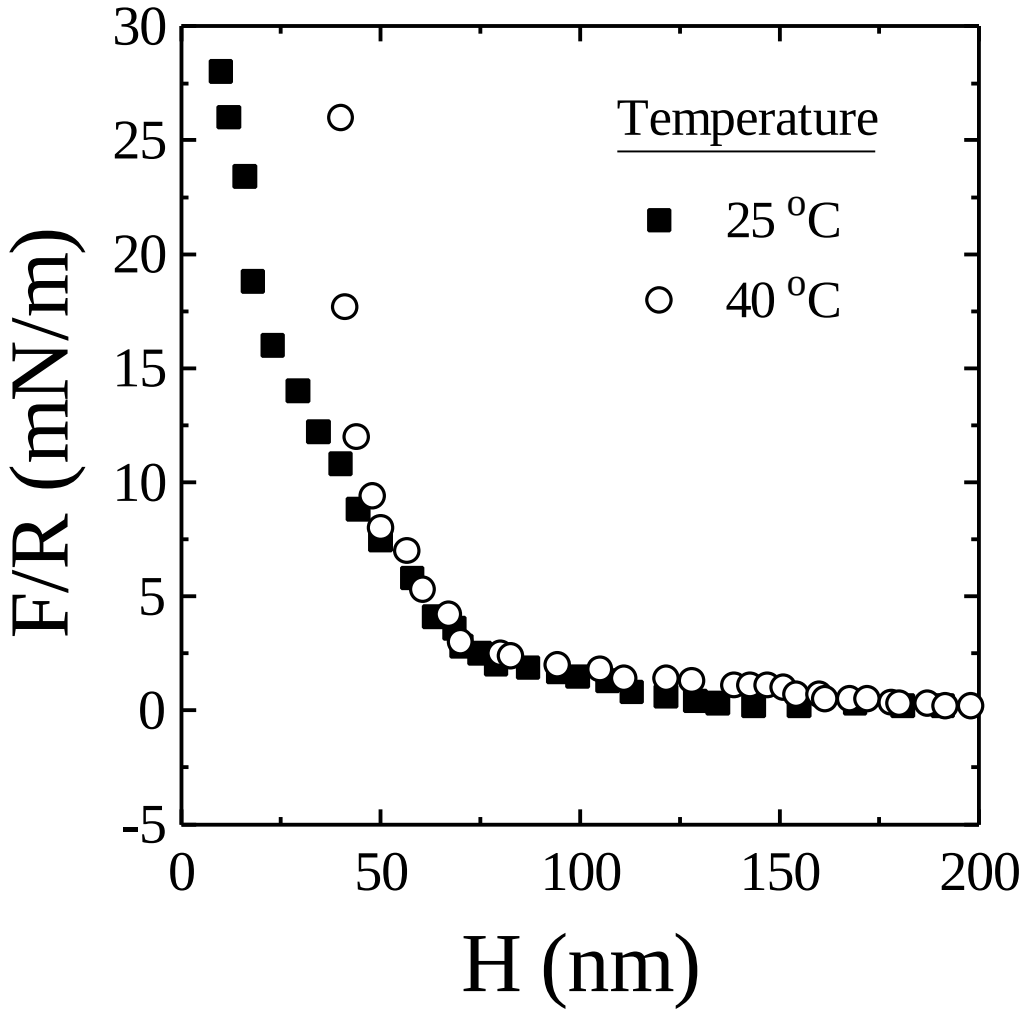

Figure 2.9 Effect of temperature on the asphaltene-coated mica surfaces at pH 5.8.

increase in the solubility of asphaltenes in water at higher temperatures. Polymeric forces depend upon the solubility of the polymer chains in the solvent, repulsive forces being observed in good solvents due to the strong osmotic repulsion when the two polymer layers overlap (10). Upon cooling the system to 25°C, the force curves return to those originally measured at this temperature, suggesting that the temperature behavior is reversible.

The force curves measured between asphaltene-coated mica surfaces support theproposed model that the forces between bitumen-coated mica surfaces are dominated by the asphaltenes exposed on bitumen surface. These forces are undoubtedly of polymeric origin, and are of such a magnitude as to swamp all other forces in the system at short range.

2.3.1 Zeta (Ψ) potential

The ζ-potentials of bitumen-in-water emulsions prepared under different conditions are given in Table 2.1. At pH 5.8 (Nanopure water), the ζ-potential was -70.5 mV. In the presence of NaCl, the negative ζ-potential decreased due to the double layer compression. As the pH was increased to 8.4-8.8, the ζ- potential became more negative, being in the range of -110 to -115 mV. This increase in the negative ζ-potential with increasing pH is consistent with the ψ_0 values obtained from the direct force measurements. The results are also consistent with those reported by Strausz (3), who suggested that the negative charge of bitumen is due to the dissociation of surfactants, e.g., naphthenic acids, with carboxylic groups (11). According to the model proposed in the present work based on the force measurements, the negative charge may be due to the ionization of the functional groups of asphaltene.

Chapter 2: Role of Surface Forces in Tar Sand Processing

Table 2.1 - Zeta (ζ) Potentials of Bitumen in Water at Different pHs.

pH	Electrolytes	Zeta potential (mV)
5.8	H_2O	-70.5
5.8	10^{-1} M NaCl	-48.0
5.8	10^{-2} M NaCl	-66.7
8.4	NaOH	-115
8.5	Borax	-115
8.8	$NaHCO_3$	-110
12.0	NaOH	-115

2.3.2 Induction Time

Figure 2.10 shows the results of the induction time measurements conducted with bitumen-in-toluene droplets in KCl and $MgSO_4$ solutions at pH 5.7. The measurements were conducted at room temperature. The induction time increases with increasing electrolyte concentration, which is opposite of what has been observed with bubble-particle interactions (12). It has been shown that electrostatic repulsion constitutes the major energy barrier against bubble-particle adhesion (12). In the presence of electrolyte, however, the energy barrier can be reduced due to double layer compression, resulting in a decrease in the induction time. Another distinguishing feature of the data shown in Figure 2.10 is that the induction times are in seconds, which are orders of magnitudes larger than for bubble-particle interactions. The induction time data reported in the literature for bubble-particle interactions are usually less than several hundred milli-seconds (12).

That induction time increases with increasing electrolyte concentration suggests that the electrostatic force does not play an important role in determining the stability of the bitumen-in-water suspensions. It appears that the steric force identified in the direct force measurements plays the major role. The large steric forces measured with bitumen and asphaltene-coated mica surfaces provides an explanation for the long induction times. It is not clear, however, why the steric force increases with increasing electrolyte concentration. One possible explanation may be that electrolytes decrease the mobility of the tails of asphaltene molecules by charge neutralization, thereby increasing the steric force and, hence, the induction time. According to the data shown in Figure 2.10, Mg^{2+} ion is more effective than K^{+} ion in

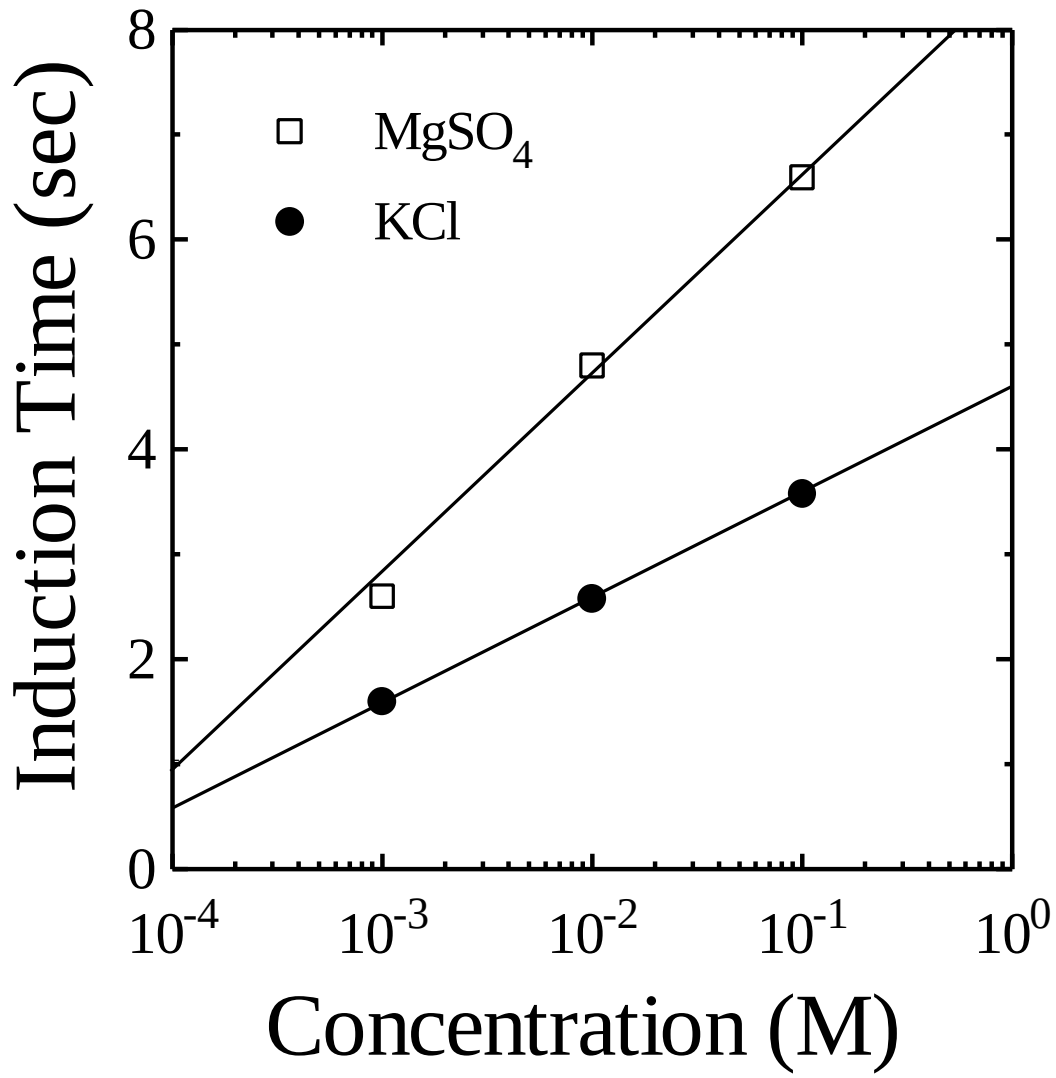

Figure 2.10 Effect of electrolyte concentration on the induction times for the coalescence between bitumen droplets. No efforts were made to control the pH.

increasing the induction time.

Figure 2.11 shows the effect of pH on the induction time. The bitumen droplets were produced by elevating the temperature without using a solvent. It is shown that the induction time increases with pH and temperature. The increase in the induction time with pH may be attributed to the increased solubility of asphaltene due to increased ionization of its polar groups. The induction time increases sharply above pH 9, becoming longer than 5 minutes at pH 10. The sharp increase may indicate that the polar groups of asphaltene are fully ionized above this pH. The increase in induction time with temperature may also be attributed to the increased solubility of asphaltene.

2.4 DISCUSSION

The induction time measurements conducted in the present work showed that the coalescence of bitumen is a very slow process. The kinetics vary depending on the pH, temperature and the type and concentrations of the inorganic electrolytes present in asystem. The slow kinetic may be attributed to the large repulsive steric forces measured using the SFA. As has been suggested, the steric force may be due to the asphaltenes extracted on the surface of bitumen. Since asphaltenes are the more polar of the bitumen fractions, they may be preferentially disposed on the surface, leaving the more hydrophobic fractions, i.e., aromatics, saturates and resins, at the interior. The molecules may be large enough to give repulsive steric forces, particularly when water becomes a good solvent for asphaltene. Steric forces should increase when polymer segments do not interact with each other, and stretch its tails into solution. In poor

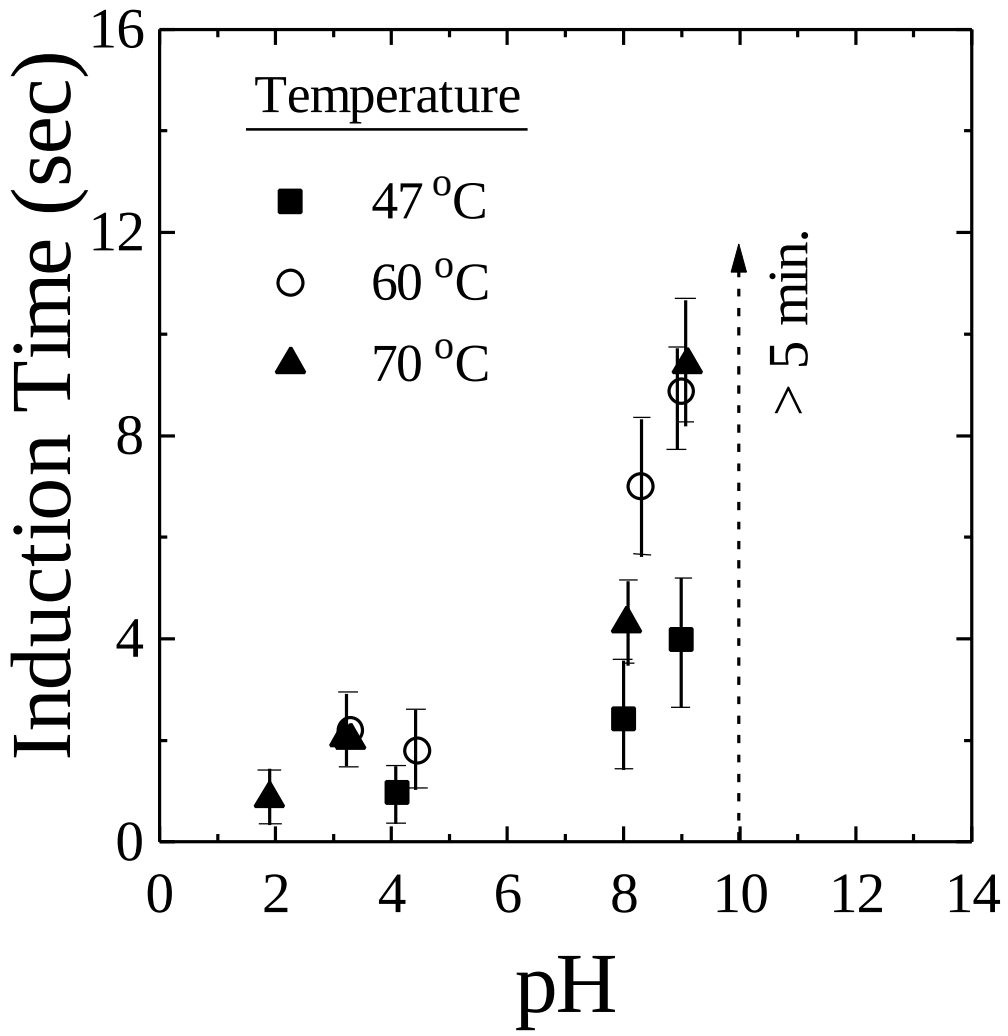

Figure 2.11 Effects of pH on the induction time for the coalescence of bitumen droplets at three different temperatures. At pH 10, the induction time exceeds 5 minutes.

solvents, polymers can give rise to attractive forces (10). It has been shown in the present work that steric force increases with increasing pH (Figure 2.6) and increasing temperature (Figure 2.7), both ofwhich may be attributed to increased solubility of asphaltenes in water.

It is more difficult to explain the effect of salts on the steric force. As shown in Figure 2.7, bitumen-coated mica surfaces exhibit increased steric force at a higher concentration of KCl. Also, the induction time measurements conducted in KCl and $MgSO_4$ solutions show increased induction time for coalescence. A possible explanation may be that the tails of asphaltene become immobilized in the present of a salt. A divalent cation such as Mg^{2+} may be particularly effective in reducing the mobility of the tails. A decrease in mobility would be equivalent to increased packing density of tails on the surface, which should give rise to increased steric repulsion.

There are several evidences for the role of asphaltene as the stabilizer for the bitumen-in-water emulsions. First, the repulsive forces measured with SFA are substantially larger than the double-layer forces which are observed only at longer separation distances beyond the region of steric forces. Second, the repulsive force increases sharply at $H<35$ nm, indicating that a thick adsorption layer ($\approx$15 nm) has been formed on the bitumen surface. The most probable substance that can account for such a thick adsorption layer would be a hydrophilic polymeric substance such as asphaltene. Third, the force measurements conducted with mica surfaces coated with asphaltene extract exhibited the practically the same force curves as those obtained with bitumen-coated mica.

Conventional wisdom is that bitumen-in-oil suspensions are stabilized by surfactants, mostly carboxylates. If it was the surfactants, the thickness of the adsorption layer should not exceed more than 1-2 nm. Furthermore, the repulsive forces should be explainable using the

DLVO theory. One may expect hydration forces, but these are known to be "short-range" forces with decay lengths in the range of 1-2 nm. The thickness of adsorption layer of 15 nm may be large even for asphaltene. One possible explanation would be that more than one layer of asphaltene molecules may deposit on the surface, with the less soluble ones being located closer to the surface. Only the most soluble molecules may be disposed closer to the bitumen/water interface. These molecules would have longer tails with a larger number of ionizable polar groups, which are primarily responsible for the steric force. There are other investigators who suggested asphaltene as the stabilized for oil-in-water emulsions (7-9).

The most important observation made in the present work is that the stability of bitumen-in-water emulsion is stabilized by the surface forces that are substantially larger than double-layer forces. Because of the large stabilizing force, the coalescence is sluggish and the droplet sizes remain small. Since the repulsive steric force increases with pH and temperature, proper control of these variables would be critical for the recovery of bitumen by the hot water process. If the pH exceeds 10, for example, the droplet size may be too small to be recovered by flotation.

Although no force measurement was conducted between bitumen and air bubble, one can speculate the implications of the large steric force on the flotation process. As has been noted, air bubbles are engulfed by bitumen droplets during tumbling, which provides a high degree of turbulence. Under turbulent conditions, the steric force may be more readily overcome by the interacting air bubbles. While a bitumen droplet is subjected to a high degree of turbulence, there may be an instant when the asphaltene layer on the bitumen surface gives its way to an air bubble so that it can be more readily engulfed. The driving force for the engulfment may be the hydrophobic attraction between the air bubble and the hydrophobic inner core of the bitumen

droplet. At Syncrude Edmonton Research Center, an unsuccessful attempt was made to recover bitumen using a pilot-scale flotation column, which may be attributed to the lack of turbulence in the column. On industrial scale, on the other hand, middling fractions are routinely recovered by using mechanically agitated conventional flotation machines. The success of this method may be attributed to the turbulence imparted for the bubble-bitumen interactions. Syncrude is currently in the process of constructing a large-scale tailings flotation cell, which is designed to provide a high degree of turbulence for the bubble-bitumen interaction.

2.5 CONCLUSIONS

A Mark IV surface force analyzer was used to measure the forces between bitumen-coated mica surfaces. The coating was accomplished by spreading bitumen-in-chloroform solutions on a Langmuir-Bloggett trough. The bitumen-coated surfaces exhibit unexpectedly strong repulsive forces at separation distances below approximately 70 nm that cannot be accounted for by the electrostatic forces between charged surfaces. It is suggested that the extraneous repulsive forces are the steric forces created due to the interactions between the tails of asphaltenes exposed on the bitumen surfaces. This view is supported by the force measurements conducted between the mica surfaces coated with asphaltenes extracted from bitumen. It was found that the steric forces increase with increasing pH and temperature, both of which can be attributed to the increased solubilization of bitumen in water. The steric force also increases with increasing electrolyte concentration, which may be explained by the reduced mobility of the tails of asphaltenes due to charge neutralization.

The kinetics of coalescence of bitumen was studied by measuring the induction time. There is an excellent agreement between the kinetic information and the surface force data. In general, the larger the steric repulsion the longer the induction time for the coalescence. It has been found that the induction time increases with increasing pH, temperature and electrolyte concentration. The induction time increases sharply above pH 9, exceeding 5 minutes at pH above 10. The induction times measured between bitumen droplets are orders of magnitudes larger than those measured for the bubble-particle interactions in mineral flotation systems, which may be attributed to the large repulsive steric forces observed in the direct force measurements. The induction time may be reduced significantly, however, when bitumen droplets are subjected to high degree of turbulence during the process of coalescence or of bubble-bitumen interactions.

Chapter 2: Role of Surface Forces in Tar Sand Processing

2.6 REFERENCES

1. Israelachvili, J.N. and Adams, G.E., *J. Chem. Soc. Faraday Trans. I* , **74**, 1978, 975.
2. Israelachvili, J.N., "Thin Film Studies Using Multiple-Beam Interferometry," *J. Colloid Interf. Sci.*, **44**, 1973, 259.
3. Strausz, O.P., *AOSTRA Oil Sands Handbook*, Chapter 3, 35-72.
4. Derjaguin, B.V., Churaev, N.V. and Muller, V.M., "Measurement of Forces Between Two Mica Surfaces in Aqueous Electrolyte Solutions in the Range 0-100nm," *Surface Forces*, Consultants Bureau, J.A. Kitchener, Ed., New York, 1987.
5. Ignasiak, T.M., Kotlyar, L., Samman, N., Montgomery, D.S. and Strausz, O.P., "Preparative Gel Permeation Chromatography of Athabasca Asphaltene and the Relative Polymer-forming Propensity of the Fractions," *Fuel*, **62**, 1983, 363.
6. Cyr, N., McIntyre, D.D., Toth and G., Strausz, O.P., "Hydrocarbon Structural Group Analysis of Athabasca Asphaltene and its g.p.c. Fractions by ^{13}C n.m.r.," *Fuel*, Vol. **66**, 1987, 1709.
7. Issacs, E.E., Huang, H., Babchin, A.J., and Chow, R.S., "Electroacoustic Method for Monitoring the Coalescence of Water-in-Oil Emulsions," *Colloids and Surfaces*, **46**, 1990, 177.
8. Mackay, G.D., McLean, A.Y., Betancourt, O.J., and Johnson, B.D., *J. Institute of Petroleum*, **59**, 1973, 164.
9. Borve, K.G.N., Sjoblom, J. and Stenius, P., "Water-in-crude Oil Emulsions from the Norwegian Continental Shelf," *Colloids and Surfaces*, **63**, 1992, 241.
10. Israelchvili, *Intermolecular and Surface Force*, Second Edition, Academic Press, New York, 1992.

11. *Handbook of Chemistry and Physics*, 64th Edition, CRC Press, Florida, F33.

12. Yoon, R.-H. and Yordan, J.L., "Induction Time Measurements for the Quartz-Amine Flotation System," *J. Colloid Interface Sci.*, **141**, 374 (1991).

13. Yoon, R-H, "Hydrodynamic ans Surface Forces in Bubble-Particle Interactions," in Preceedings of the XVII International Mineral Processing Congress, Dresden, Germany, September 23-28, 17-31, Les Techniques, 1991.

Chapter 2: Role of Surface Forces in Tar Sand Processing

CHAPTER 3

HYDROPHOBIC FORCES IN THIN WATER FILMS STABILIZED BY DODECYLAMMONIUM HYDROCHLORIDE

ABSTRACT

Coalescence of air bubbles in water accompanies negative free energy changes that are larger than those for the coalescence of oil droplets, which suggests that air bubbles are hydrophobic. However, no systematic studies have been made concerning the hydrophobicity of air bubbles. Quantitative information on the hydrophobicity of air bubbles is of paramount importance in flotation studies, as it determines bubble size, froth stability, and bubble-particle interactions, etc.

In determining the hydrophobicity of air bubbles, it was assumed that the equilibrium film thickness between two air bubbles is determined by the balance of three surface forces, namely, electrostatic, dispersion and hydrophobic forces. In the present work, the film thicknesses were measured using the thin film balance (TFB) of Scheludko-Exerowa type in the presence of dodecyl ammonium chloride (RNH_2Cl). The electrostatic forces in thin films were estimated on the basis of the Gibbs potentials corrected for the potential drop due to the specific adsorption of counter ions, while the dispersion forces were determined using the Hamaker constant of $3.7x10^{-20}$ J. The hydrophobic forces estimated in this manner are larger than the van der Waals force, but decrease with increasing surfactant concentration. Knowing that thin aqueous films are stable only at high surfactant concentrations, the hydrophobic force may be the major factor in destabilizing thin aqueous films. The hydrophobic force constants determined from the equilibrium film thicknesses were used to predict the disjoining pressure isotherms using the extended DLVO theory, which includes contributions from the three surface forces considered in the present work. The predicted isotherms were verified by the experimental results obtained using the TFB.

3.1 INTRODUCTION

Thin liquid films play an important role in many industrial and biological systems involving foams, bubbles, emulsions, and lipid membranes. Liquid films are thermodynamically unstable, as the process of film rupture accompanies a decrease in interfacial area, which in turn results in a decrease in free energy. In a horizontal foam film, liquid is drained by Plateau-border suction. When the thickness is thinned to less than approximately 100 nm, the drainage process is controlled by surface forces. The thinnest liquid films are referred to as black films because they reflect virtually no light. Black films of thicknesses in the range of 5 to 20 nm are referred to as common black films (CBF), while those of less than 5 nm are called Newton black films (NBF) (1). A CBF can abruptly transform into an NBF, which consists essentially of a bilayer of amphiphile molecules with almost no free solvent molecules in the film.

Various surfactants are used to increase the stability of thin liquid films. A surfactant increases the potential of the electrical double-layer at the two interfaces facing each other, thereby increasing the positive disjoining pressure and, hence, the film stability. It is known, on the other hand, that thin liquid films are destabilized by the attractive van der Waals pressure. Thus, the DLVO theory is commonly used to predict the stability of CBFs with varying degrees of success. In general, the theory has been useful at relatively high surfactant concentrations. Kolarov, *et al.* (2), showed that the disjoining pressure isotherms obtained in the presence of non-ionic surfactants and in an uncharged phospholipid can be predicted by the DLVO theory; however, the pressures measured in the presence of ionic surfactants are considerably larger than predicted (3). More recently, Bergeron, *et al.* (4), measured disjoining pressure isotherms with octyl β-glucoside and had results which are in agreement with the theory. As for NBFs, it is generally recognized that non-DLVO forces such as steric and hydration forces are responsible for the extraordinary stability observed in references 3-5.

Chapter 3 Hydrophobic Forces in Thin Water Films Stabilized by Dodecylammonium Hydrochloride

According to the DLVO theory, a liquid film should rupture when the disjoining pressure is zero, *i.e.*, the electrostatic pressure is equal to the van der Waals pressure. However, free films rupture (or transform to Newton black films at high surfactant concentrations) at thicknesses considerably larger than predicted. This discrepancy is generally attributed to the hydrodynamic fluctuations of the interface due to disturbances such as thermal motions, vibration, and dust (6). Evidence for the corrugated surface created by hydrodynamic fluctuations is given by the scattering of the light reflected from the surface of thin liquid films (7). Scheludko (8,9) provided a thermodynamic explanation by considering the increase in free energy due to perturbation of an air-water interface and the decrease in free energy due to an increase in the attractive van der Waals force. If the net free energy change is negative, the hydrodynamic fluctuation will grow spontaneously and eventually lead to film rupture. Many other investigators (10,11) carried out similar analyses to predict critical rupture thicknesses and coalescence times.

Recent advancement in the techniques of directly measuring surface forces showed the existence of hydrophobic forces in thin aqueous films between two macroscopic solid surfaces (12,13). Therefore, it would not be unreasonable to look for evidence of hydrophobic forces in free water films. In the absence of a surfactant, the interfacial energies at the air-water interface are larger than those at the solid-(or liquid) water interfaces for many of the well-known hydrophobic substances such as polytetrafluoroethylene (PTFE), paraffin wax, and hydrocarbon oils, etc. In this regard alone, air bubbles may be considered hydrophobic.

Recently, Tchaliovska, *et al.* (14), measured equilibrium film thicknesses of dodecylammonium chloride (RNH_3Cl) solutions using the thin film balance (TFB) of the type developed by Scheludko (8) and used the data for calculating the double-layer potentials using the DLVO theory. The results showed that the potentials are substantially lower than those calculated on the basis of the adsorption densities of the surfactants at the interface. The authors attributed the discrepancy to an additional attractive force. Pugh and Yoon (15) also conducted similar

experiments with nonionic surfactants and calculated hydrophobic disjoining pressures. The calculation was done using the extended DLVO theory, which considers contributions from hydrophobic forces in addition to those from the van der Waals and electrostatic forces. This theory is useful for explaining the role of non-DLVO forces such as the hydration forces in the coagulation of silica and rutile (16,17) and the hydrophobic forces in the coagulation of coal and methylated silica (18,19) and in the flotation of hydrophobic particles (20).

It is the purpose of the present investigation to study the role of hydrophobic forces in free-water films using the thin film balance (TFB) technique. The results reported in this communication have been obtained using dodecylammonium chloride (RNH_3Cl) solutions, and later communications will report those obtained with sodium dodecylsulfate (RSO_4Na) and inorganic electrolytes.

3.2 EXPERIMENTAL

3.2.1 Material

Dodecylammonium chloride (RNH_2Cl) was obtained from Eastman Kodak Co. and recrystallized from ethanol before use. A Nanopure II water treatment unit was used to obtain deionized water (18 mΩ). ACS grade sodium chloride from Fisher Scientific Co. was roasted at 600°C before use to remove possible organic contaminants. The pH of the surfactant solutions was controlled by ACS grade *HCl* and *NaOH* solutions.

3.2.2 Equilibrium Film Thickness Measurements

Equilibrium thicknesses of free water films were measured using a thin film balance (TFB) of the Scheludko-type (8). Figure 3.1 shows the experimental setup. A horizontal film of an RNH_3Cl solution was formed in the film holder (a cylindrical glass tubing of 2 mm radius) by

applying a positive pressure on the gas phase in contact with the film. The pressure was kept at a desired value by means of an aneroid manostat (Pennwalt), which was connected to a nitrogen gas cylinder as a pressure source. The pressure in the cell was monitored using an inclined manometer with a sensitivity of 0.01 inches of water. A glass container filled with a small amount of the RNH_2Cl solution was placed at the bottom of the cell to prevent evaporation of the film. The TFB cell, which was water-jacketed to maintain the temperature within $\pm 0.1\,^{\circ}C$, was placed on an inverted Zeiss microscope, which in turn was mounted on a vibration-free stone table. The microscopic images of a film obtained using a monochromatic light source were recorded as a function of time by means of an image analyzer (Kontron SEM-IPS) until the film ruptured. The last image was used to determine the equilibrium film thickness. At least ten measurements were taken at a given experimental condition and averaged. A detail of the method used for the calculation of the film thickness measurements with an image analyzer was

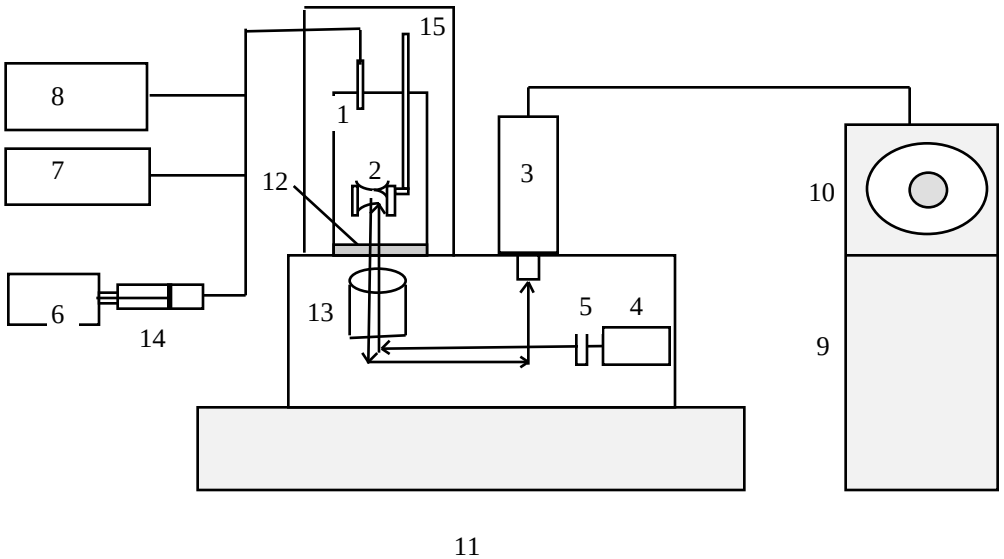

Figure 3.1 The experimental setup used for equilibrium film thickness (H_e) and disjoining pressure (Π) measurements: 1) cell, 2) film holder with foam film, 3) camera, 4) light source, 5) filter, 6) Nanomover, 7) an inclined manometer, 8) aneroid manostat, 9) image analysis system, 10) TV monitor, 11) vibration-free table, 12) working surfactant solution, 13) inverted Zeiss microscope, 14) syringe, 15) isolation box.

given in Appendix 3.1.

For each measurement, the RNH_2Cl solutions were prepared in Nanopure water. All glassware was cleaned initially with chloroform and then rinsed with distilled water. Further cleaning was done by boiling it in concentrated nitric acid solution for 3-4 hours, which was followed by rinsing with Nanopure water and drying with pure nitrogen gas.

3.2.3 Disjoining Pressure Measurements

Disjoining pressure isotherms were obtained using a TFB equipped with a porous film holder made of a sintered glass ring. Mysels and Jones (21) were the first to use the porous holder to measure disjoining pressures, and Exerowa and Scheludko (22) and Bergeron *et al.* (4) made further improvements. Use of porous holders allows one to apply high pressures because the maximum pressures applicable to a film holder are limited by the capillary pressure of the orifice connecting the liquid to the outside. Porous film holders can support pressures of up to several atmospheres (23).

In the present work, a porous holder described by Exorowa and Scheludko (22) was used. The pressure control and the film thickness measurement were conducted in the same manner as described for the equilibrium film thickness measurement.

3.2.4 Coalescence Time Measurement

Figure 3.2 shows the device used in the present work to measure the coalescence time of air bubbles in aqueous solutions. In each experiment, two air-bubbles were formed in an aqueous solution at the ends of capillary tubes (0.5 mm I.D.) by applying a positive pressure. The lower air-bubble was brought to a position directly under the upper air-bubble by means of a micro-mover, which was capable of moving the droplet in x, y, and z directions. The upper air-bubble

was then moved toward the lower air-bubble by means of a Nanomover (Encoder Mike Controller, Model 18011, Oriel Corporation), which was capable of moving the droplet along the z direction at a speed in the range of 1-200 nm/sec. The process was monitored by means of a high-speed video system (Kodak/Spin Physics), which was capable of recording events at a rate of 60-2,000 frames/sec. The measuring cell was immersed in a water bath for temperature control.

All the glassware used for the coalescence time measurements was cleaned in boiling nitric acid solutions for 3-4 hours between experiments. It was then washed with copious amounts of Nanopure water before use. The air-bubble holders were dried with N_2 gas prior to measurements. The coalescence time was measured as the time required for two bubbles to coalesce with each other upon contact. At a given experimental condition, a set of 15-20 measurements was made and averaged.

3.2.5 Surface Tension Measurements

Surface tensions of the RNH_2Cl solutions were measured using the du Nouy ring method in the presence and absence of *NaCl*. The Fisher Tensiomat was calibrated using ethanol solutions of known surface tension (24).

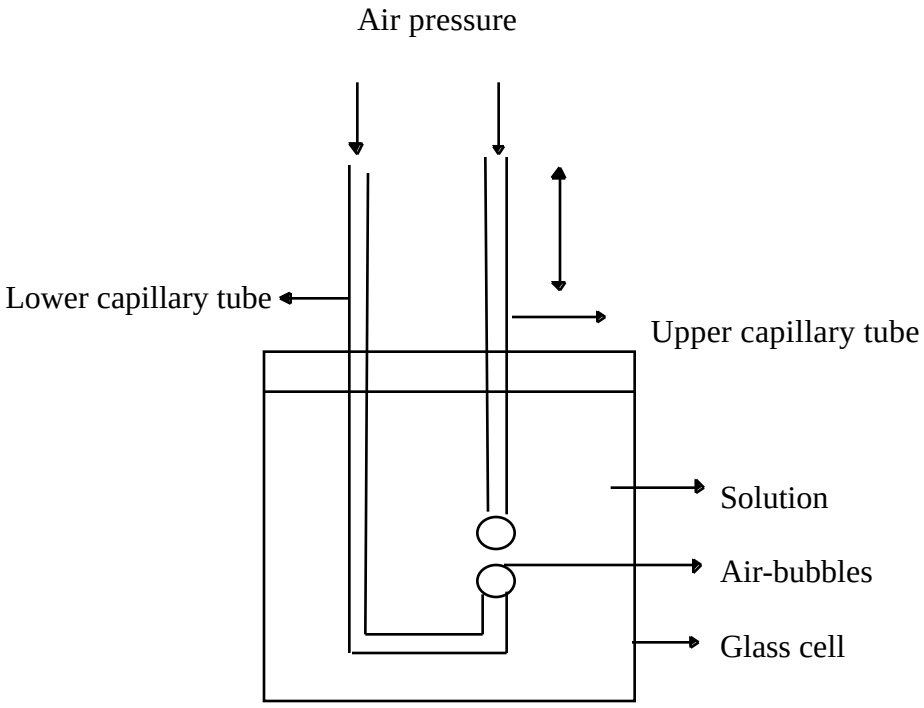

Figure 3.2 A schematic representation of the experimental setup for the coalescence time measurements conducted with two nitrogen bubbles in solution.

3.3 RESULTS AND DISCUSSIONS

3.3.1 Equilibrium Film Thickness

Figure 3.3 shows the equilibrium film thicknesses (H_e) measured as a function of RNH_2Cl concentration (see also Table 3.1). The measurements were conducted without a supporting electrolyte, and the pH was in the range of 5.7-6.0. The data obtained in the present work are superimposed with those reported by Tchaliovska, *et al.* (14). Both sets of the data show that H_e decreases with increasing surfactant concentration, indicating that the adsorption of RNH_3^+ ions at the air-water interface increases the stability of the free film. The increased stability of free water films in the presence of ionic surfactants is generally attributed to the repulsive double-layer forces. The largest film thickness measured in the present work was 169±10 nm at 10^{-5} M. Below this concentration, the film was so unstable that it was not possible to obtain metastable films, i.e., the lifetimes of the films were less than a few seconds. Extrapolation of the measured H_e data to zero concentration gives a value of approximately 170 nm, which is larger than the value of 155 nm for non-ionic surfactants (15).

Figure 3.4 shows the H_e values measured as a function of pH at two different RNH_2Cl concentrations in the absence of a supporting electrolyte. H_e increases considerably with increasing pH, which may be related to the increasing hydrolysis of the RNH_3^+ ions to form soluble neutral amines, RNH_2(aq) with increasing pH. It has been shown that the surface tension of an RNH_3Cl solution decreases steadily as the pH increases from 5.6 to 9.0, and then decreases sharply as the pH increases further to pH 9.5-10.0 (25). The decrease in surface tension may be due to the co-adsorption of the RNH_3^+ and RNH_2 species at the air-water interface, which is

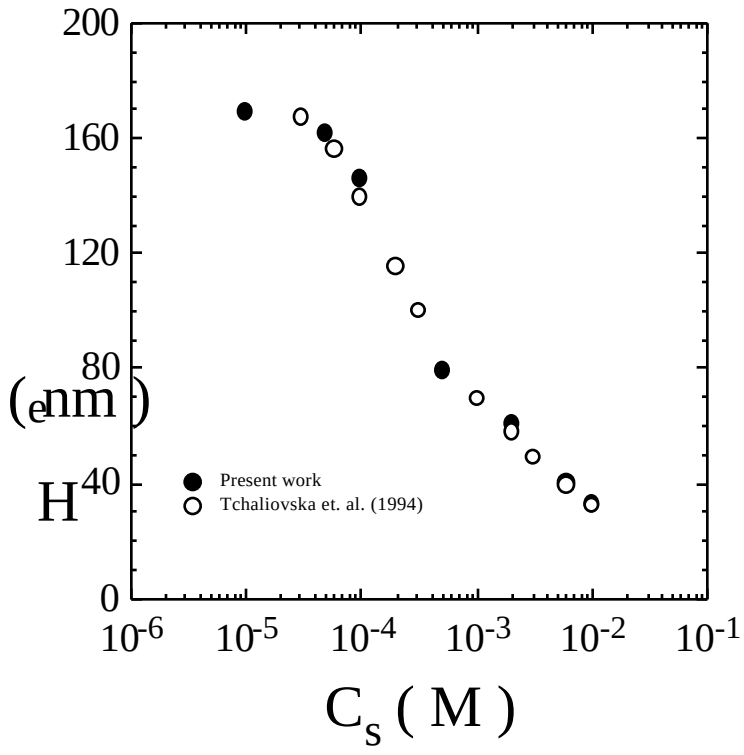

Figure 3.3 Equilibrium film thickness (H_e) as a function of RNH_2Cl concentration (C_s) at pH 5.7-6.0 and at 22±0.1 ^{0}C. The open circles represent the data reported by Tchaliovska, *et al.* (14).

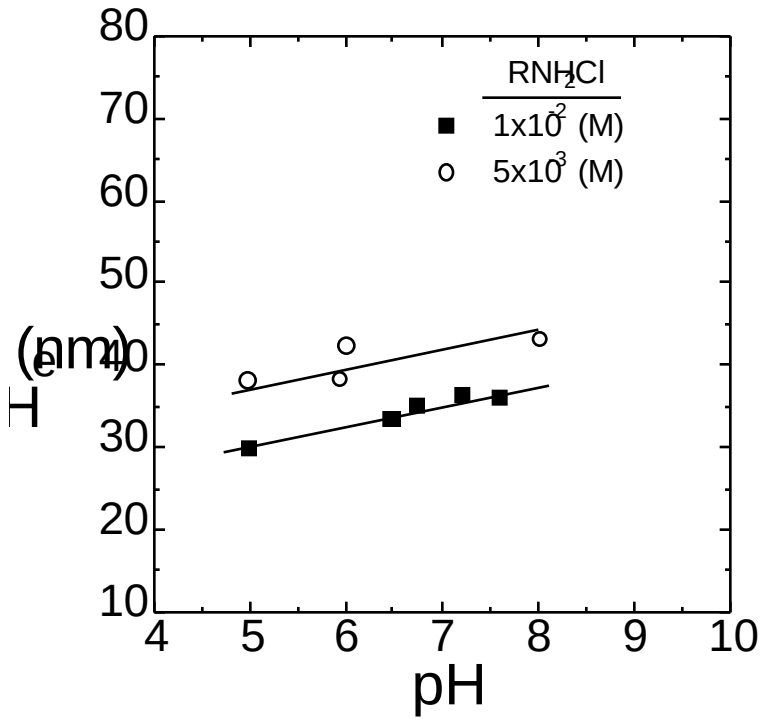

Figure 3.4 Equilibrium film thickness (H_e) as a function of pH in 10^{-2} and 10^{-3} M RNH_2Cl solutions at 22±0.1 ^{0}C.

similar to the mechanisms proposed for the adsorption of the same species on quartz (26) and mica (27) and for the adsorption of iono-molecular species $RNH_2.RNH_3^+$ on the quartz and the air-water interface (25). Obviously, the presence of RNH_2 species at the air-water interface destabilizes the film. Three possible mechanisms may be considered. First, the charge density σ_1 (or the double-layer potential (ψ_1) at the air-water interface) decreases due to the presence of neutral species. Second, the polar head of the neutral surfactant may be less strongly hydrated. It is well known that the higher the charge of a cation, the larger the hydration energy (28). Third, the air-water interface may become more hydrophobic with increasing pH, which may be a consequence of the second mechanism. When the pH was further increased to 9.5-10.0, where the RNH_2 concentration in the solution and, hence, at the air-water interface, reaches a maximum, it was not possible to measure H_e because the film became very unstable.

3.3.2 Coalescence Time

As shown in Figures 3.3 and 3.4, H_e is not a very sensitive measure of film stability at low RNH_3Cl concentrations and high pHs. A more sensitive measure would be the bubble coalescence time. Figure 3.5 shows the results obtained at pH 5.8 and 10.0 by varying the RNH_3Cl concentration. It shows that coalescence time increases, *i.e.*, the film becomes more stable, with increasing surfactant concentration at both pHs. However, the film becomes unstable at the higher pH, which can be attributed to an increase in the concentration of RNH_2 species at the air/water interface. This in turn may result in a decrease in the concentration of RNH_3^+ species and, hence, ψ_1.

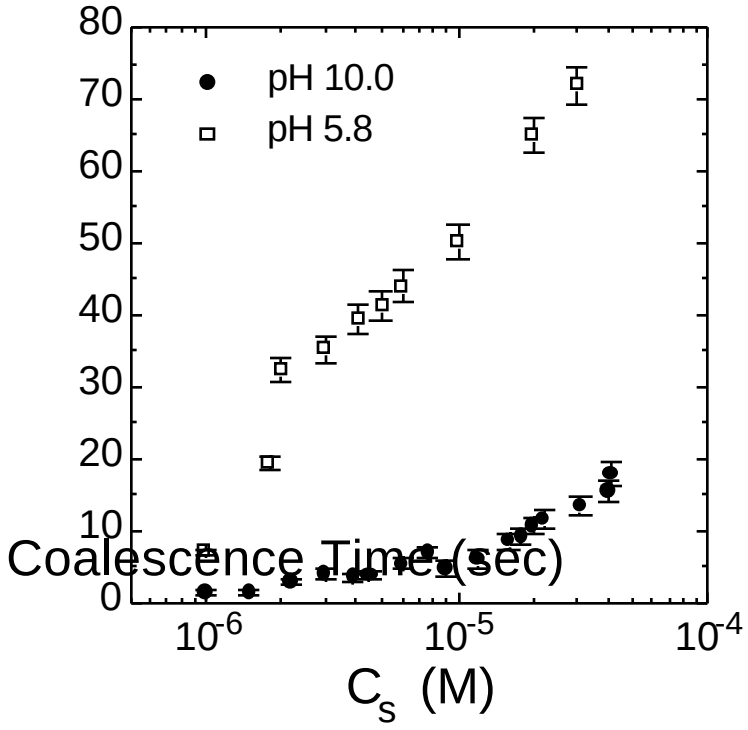

Figure 3.5 Coalescence time for nitrogen bubbles as a function of RNH_2Cl concentration at pH 5.8 and 10.

Figure 3.6 shows the results obtained at various RNH_3Cl concentrations by varying pH. Coalescence time reaches a minimum at pH 9-10, whereas the RNH_2 concentration in the solution reaches a maximum. At a pH above this range, the concentration of soluble RNH_2 species decreases, most probably due to the formation of phase-separated amine, RNH_2(s). Thus, the coalescence time measurements conducted in the present work suggest that the film stability decreases when ψ_1 decreases with decreasing RNH_3Cl concentration and increasing pH. Yoon and Yordan (29) showed, indeed, that the ζ-potential of air bubbles decreases with increasing pH. The poor stability of the foam films at RNH_3Cl concentrations and at higher pHs, particularly in the pH range of 9-10, may also be attributed to the increased hydrophobicity of air bubbles.

3.3.3 Double Layer Potentials

The results presented in the foregoing sections suggest that the stability of thin water films is controlled by the double-layer and hydrophobic forces. However, most of the TFB work (4,22,30) reported in the literature has been interpreted in view of the DLVO theory which considers only the double-layer and van der Waals forces. In a horizontal film at equilibrium in a TFB, the disjoining pressure (Π) is balanced by the capillary pressure (P_c) as follows:

$$\Pi - P_c = 0. \qquad [3.1]$$

For a capillary wall of zero contact angle, P_c is given by

$$P_c = \frac{2\gamma}{r_c} \qquad [3.2]$$

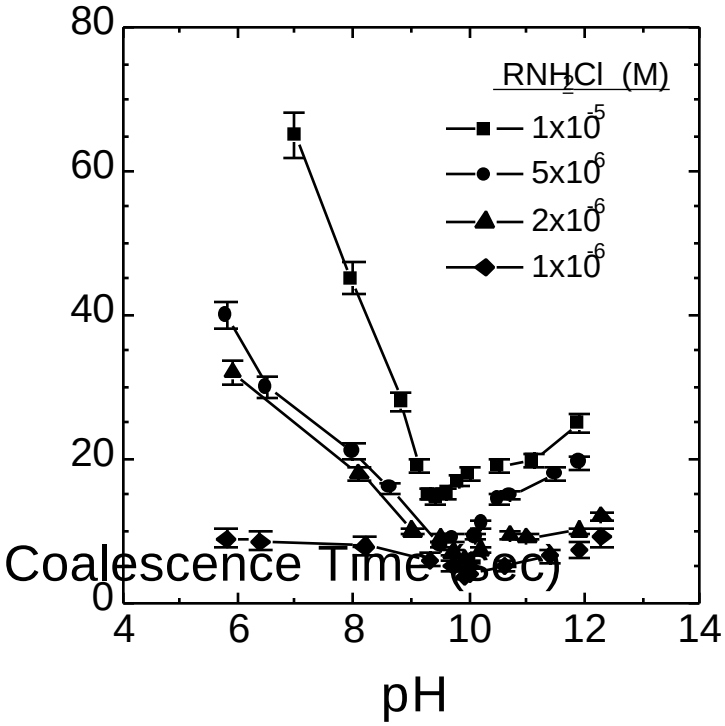

Figure 3.6 Effect of pH on the coalescence time for nitrogen bubbles measured at various RNH_3Cl concentrations.

in which γ is the surface tension of the solution and r_c is the radius of the film holder.

The DLVO theory states that

$$\Pi = \Pi_e + \Pi_d \qquad [3.3]$$

in which Π_d is the component of the disjoining pressure due to the van der Waals force and Π_e is the same due to the double-layer force. In thin film studies, the following expression is commonly used for Π_e:

$$\Pi_e = 64 C_s RT \tanh^2\left(\frac{ze\psi_1'}{4kT}\right)\exp(-\kappa H_e) \qquad [3.4]$$

where C_s is the surfactant concentration, R the gas constant, T the absolute temperature, z the valence of the ionic surfactant stabilizing the film, e the electric charge, ψ_1' the double-layer potential, k the Boltzmann constant, κ^{-1} the Debye length, and H_e the equilibrium film thickness. Π_d, on the other hand, is given by

$$\Pi_d = -\frac{A_{232}}{6\pi H_e^3} \qquad [3.5]$$

where A_{232} is the Hamaker constant for the air **2** in water **3**.

Using Eqs. [3.1]-[3.5], the values of ψ_1' have been calculated from the values of H_e shown in Figure 3.3 and given in Figure 3.7 and Table 3.1. In using Eq. [3.2], the values of γ obtained in the present work were used (see Figure 3.11). At r_c=2 mm, the values of P_e in units of N/m^2 are numerically the same as γ. In calculating Π_e using Eq. [3.4], z=+1 for RNH_3^+ ions, and the Debye lengths were calculated by equating the surfactant concentration as the electrolyte concentration. The values of Π_e were calculated using Eq. [3.5] and the value of $A_{232}=3.7\times10^{-20}$ J (31). As

expected, the values of ψ_1' calculated in this manner increase with increasing surfactant concentration, providing an explanation for increased film stability and, hence, low values of H_e, as shown in Figure 3.3. Note that the ψ_1' versus. C_s curve shows an inflection point at $2x10^{-3}$ M, at which a close-packed monolayer may be formed. As the surfactant concentration is further increased, the double-layer is compressed, causing a decrease in ψ_1'. Note also that the ζ-potentials of air bubbles measured in RNH_3Cl solutions by Okada, *et al.* (32), are substantially lower than the calculated ψ_1' values.

Also shown in Figure 3.7 and Table 3.1 are the values of surface potentials (ψ_o) using the method described by Tchaliovska, *et al.* (14). These investigators calculated the surface charge density σ_o using the following relationship:

$$\sigma_o = e\Gamma_{RNH_3^+} \qquad [3.6]$$

where e is the electronic charge and $\Gamma_{RNH_3^+}$ is the adsorption density of the RNH_3^+ ions at the air-water interface, which can be readily calculated from the surface tension data using the Gibbs adsorption isotherm. From the value of σ_o, they calculated the values of ψ_o using the following relationship:

$$\sigma_o = \sqrt{8kT\varepsilon_o\varepsilon C_s}\,\sinh\left[\frac{e\psi_o}{2kT}\right] \qquad [3.7]$$

where ε_o and ε are the permittivity of vacuum and the dielectric constant of water, respectively. As shown in Figure 3.7, the values of ψ_o calculated in this manner are substantially larger than those of ψ_1' obtained using the classical DLVO theory.

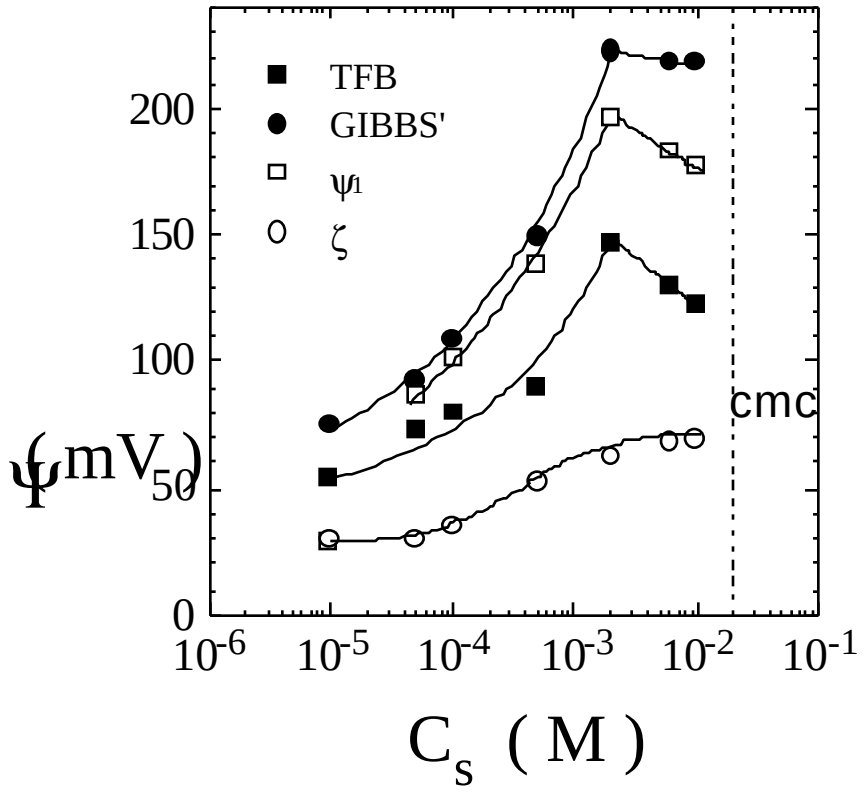

Figure 3.7 The double-layer potentials at the air-water interface as calculated from Gibbs adsorption isotherm (ψ_0), DLVO theory (ψ_1'), Stern model (ψ_1), and ζ potential measurement for air bubbles (ξ) (32).

The difference between ψ_o and ψ_1' can be reduced if the former is corrected for the counter ions, i.e., Cl^- ions that may be considered to form a Stern layer near the polar heads of the RNH_3^+ ions adsorbed at the air-water interface. Figure 3.8 is a schematic representation of the model, which shows that potential decays linearly to ψ_1 at the distance δ away from the charge layer and then decays exponentially into the solution phase. In this case, the charge balance at the interface is given by the following relationship:

$$\sigma_0 + \sigma_1 + \sigma_2 = 0 \qquad [3.8]$$

where σ_0 is the charge density at the center of the polar heads of the surfactant molecules, and σ_1 and σ_2 are the same at the Stern layer and in the diffuse layer, respectively.

Considering the Stern layer as a parallel condenser, one can readily derive the following relationship (33):

$$\sigma_0 = \frac{\varepsilon_1}{4\pi\delta}(\psi_0 - \psi_1) \qquad [3.9]$$

where σ_o is the charge density in the Stern layer and ε_1 is its dielectric constant. It has been shown that ε_1 varies linearly with the counter ion concentration in the Stern layer (34). It has also been shown that (34)

$$\sigma_1 = \frac{zeN_1}{1+\left(\frac{N_A}{V_s n_0}\right)\exp\left(-\frac{ze\psi_1 + \phi}{kT}\right)} \qquad [3.10]$$

where z is the valence of the counter ion, N_1 the number of available adsorption sites per unit area at the interface, N_A the Avogadro's number, V_s the molar volume of the solvent, n_0 the

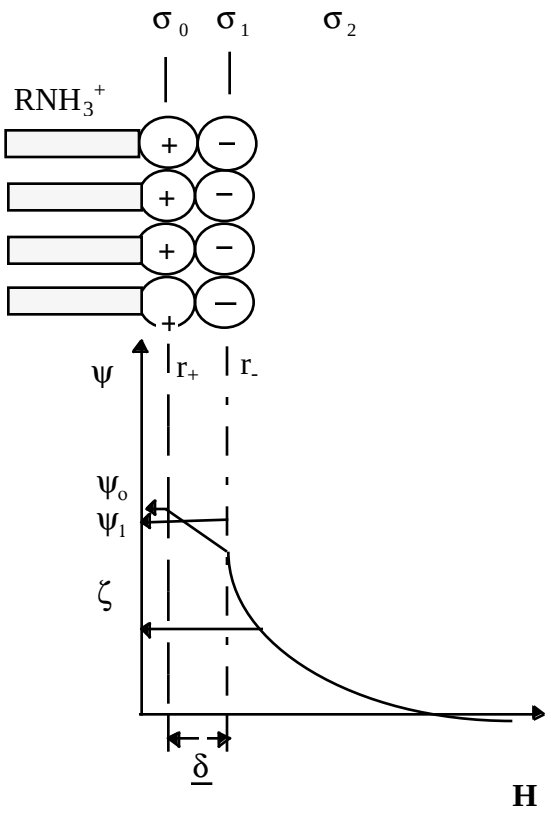

Figure 3.8 Schematic representation of the electrical double layer at the air-water interface in the presence of RNH_3^+ ions. The counter (Cl^-) ions are assumed to form a Stern layer. σ_o, σ_1, and σ_2 represent the surface charge densities at the charge layer, the Stern layer, and the diffuse layer, respectively. δ is the thickness of the Stern layer (4.3 Å). ψ_0, ψ_1, and ζ are the surface potential, Stern potential, and zeta potential, respectively.

Table 3.1 Double layer Potentials in the Thin Films of RNH_3Cl Solutions Calculated Using the Gibbs Isotherm, DLVO Theory, and Stern Model

				Potentials (mV)		
RNH_2Cl (M)	P_c (N/m^2)	κ^{-1} (nm)	H_e (nm)	ψ_0 Gibbs	ψ_1' DLVO	ψ_1 Stern
1.0×10^{-5}	71	96.1	169.2	82	55.0	72
5.0×10^{-5}	69.8	43.0	162.0	93	71.4	87
1.0×10^{-4}	69.5	30.4	141.5	109	79.2	102
5.0×10^{-4}	68	13.6	85.9	150	87.0	138
2.0×10^{-3}	61.7	6.8	58.3	222	143	196
6.0×10^{-3}	46.5	3.9	37.9	218	128	183
1.0×10^{-2}	37	3.0	30.6	218	120	177

number density of the counter ions in solution, and ϕ is the specific adsorption potential for the counter ions. As for σ_2,

$$\sigma_2 = \sqrt{\frac{2n_0 \varepsilon kT}{\pi}} \sinh\left(-\frac{ze\psi_1}{2kT}\right) \qquad [3.11]$$

where ε is the dielectric constant of the medium. Assuming that ϕ=0, δ is the sum of the radius of the polar head of the RNH_3^+ ions (2.8 Å) (27) and of Cl^- (1.91 Å) (24), and that z=-1, Eqs. [3.9]-[3.11] can be used to calculate ψ_1. The results are given in Figure 3.7 and Table 3.2. Also shown in this table are the values of σ_0, σ_1, and σ_2, and the area per charge on the surface and at the Stern plane. The values of ψ_1 calculated in this manner are considerably lower than ψ_o; however, they are still substantially higher than the values of ψ_1' calculated using the DLVO theory.

The discrepancy between the values of ψ_1' and ψ_1 may be accounted for by the hydrophobic force. The first attempt to consider hydrophobic forces for interpreting TFB data was made by Pugh and Yoon (15), who used the ζ potentials for ψ_1 to determine the contributions from the hydrophobic force to Π. These authors used the single-exponential force law to represent the hydrophobic force.

3.3.4 Hydrophobic Force

Recognizing that hydrophobic force may be a factor in determining the stability of thin water films, the DLVO theory (Eq. [3.3]) may be extended to include contributions from the hydrophobic force (Π_h) as follows:

Table 3.2 Double-layer Potentials, Area per Charge, and Charge Densities at the Air-Water Interface in the Thin Films of RNH_3Cl Solutions

RNH_2Cl	Potential (mV)		Charge per Area (nm^2)		Charge Density ($\mu C/cm^2$)		
(M)	ψ_1'	ψ_1	Charge Plane	Stern Plane	σ_0	σ_1 ($x10^3$)	σ_2
$1.0x10^{-5}$	82	72	183.0	230.0	0.02	0.01	0.02
$5.0x10^{-5}$	93	87	65.0	73.5	0.14	0.06	0.14
$1.0x10^{-4}$	109	102	33.3	38.2	0.22	0.12	0.21
$5.0x10^{-4}$	150	138	6.62	8.43	0.67	0.57	0.67
$2.0x10^{-3}$	222	196	0.81	1.35	1.92	2.29	1.91
$6.0x10^{-3}$	218	183	0.50	1.00	3.11	6.87	3.10
$1.0x10^{-2}$	218	177	0.39	0.88	3.87	11.5	3.86

$$\Pi = \Pi_e + \Pi_d + \Pi_h. \qquad [3.12]$$

The hydrophobic pressure may be most conveniently represented by a power law

$$\Pi_h = -\frac{K_{232}}{6\pi H^3} \qquad [3.13]$$

where H is the distance separating the two air-water interfaces in a thin film and K_{232} is a constant. Eq. [3.13] is of the same form as Eq. [3.5]; therefore, K_{232} can be compared directly with the Hamaker constant A_{232}.

From Eqs. [3.1] and [3.12], one obtains the following relationship:

$$\Pi_e + \Pi_d + \Pi_h - P_c = 0. \qquad [3.14]$$

Substituting Eq. [3.2], [3.4], [3.5], and [3.13] into [3.14],

$$64 C_s RT \tanh^2\left(\frac{ze\psi_1'}{4kT}\right)\exp(-\kappa H_e) - \frac{A_{232}}{6\pi H_e^3} - \frac{K_{232}}{6\pi H_e^3} - \frac{2\gamma}{r_c} = 0. \qquad [3.15]$$

In the present work, Eq. [3.15] has been used to calculate K_{232} values from the experimental values of H_e (given in Figure 3.3), γ, r_c (=2 mm), A_{232} (=3.7x10^{-20} J), and the ψ_1 values obtained using the Stern model for ψ_1'. Table 3.3 shows the results of the calculation obtained at various RNH_3Cl concentrations. It shows that K_{232} decreases with increasing surfactant concentration, indicating that the air-water interface becomes less hydrophobic. It is interesting that K_{232} becomes negative, indicating that the non-DLVO force is repulsive at concentrations above 2x10^{-3} M. The repulsive force may be due to the hydrated water molecules associated with the polar heads of the surfactant molecules. Because of the strong repulsive

Table 3.3 The Values of K_{232} Calculated Using the Extended DLVO Theory from the Equilibrium Thicknesses of the RNH_3Cl Solutions

RNH_2Cl (M)	H_e (nm)	K_{232} (J)
$1.0x10^{-5}$	169.2	$3.10 x10^{-18}$
$5.0x10^{-5}$	162.0	$1.97 x10^{-18}$
$1.0x10^{-4}$	141.5	$9.00 x10^{-19}$
$5.0x10^{-4}$	85.9	$4.54 x10^{-19}$
$2.0x10^{-3}$	58.3	$-1.15 x10^{-20}$
$6.0x10^{-3}$	37.9	$-4.52 x10^{-20}$
$1.0x10^{-2}$	30.6	$-4.91 x10^{-20}$

hydration force, the films formed at high-surfactant concentrations were stable for 20-30 minutes.

In Figure 3.9, only the positive values of K_{232} have been plotted versus concentration. Also shown in this figure, for comparison, are the K_{232} values calculated based on the H_e values reported by Tchaliovska, *et al*. (14). It is shown that K_{232} decreases steadily with increasing concentration. This may be attributed to the increasing population of the polar heads of the RNH_3^+ ions at the interface, which are strongly hydrated and, hence, should dampen the hydrophobicity.

As has been shown in Figure 3.6, air bubbles are most unstable at pH 9-10 in RNH_3Cl solutions. This may be explained by the co-adsorption of the RNH_3^+ and RNH_2 species, as has already been discussed briefly in the foregoing section. Since the neutral species would be less strongly hydrated than the charged species, the dampening of the hydrophobic force by the cationic surfactant should be reduced. The increased hydrophobicity coupled with the reduced double layer potential minimizes the coalescence time at the narrow pH range where the concentration of the RNH_2 species reaches a maximum.

An important message from the results shown in Figure 3.9 is that air bubbles are inherently hydrophobic, which is consistent with the fact that the interfacial tension at the air-water interface is among the highest of any material known to date. An extrapolation of the K_{232} versus C_s curve shown in Figure 3.9 suggests that, in the absence of a surfactant, the value of K_{232} for air bubbles is in the neighborhood of 10^{-17} J, which is approximately 270 times larger than the

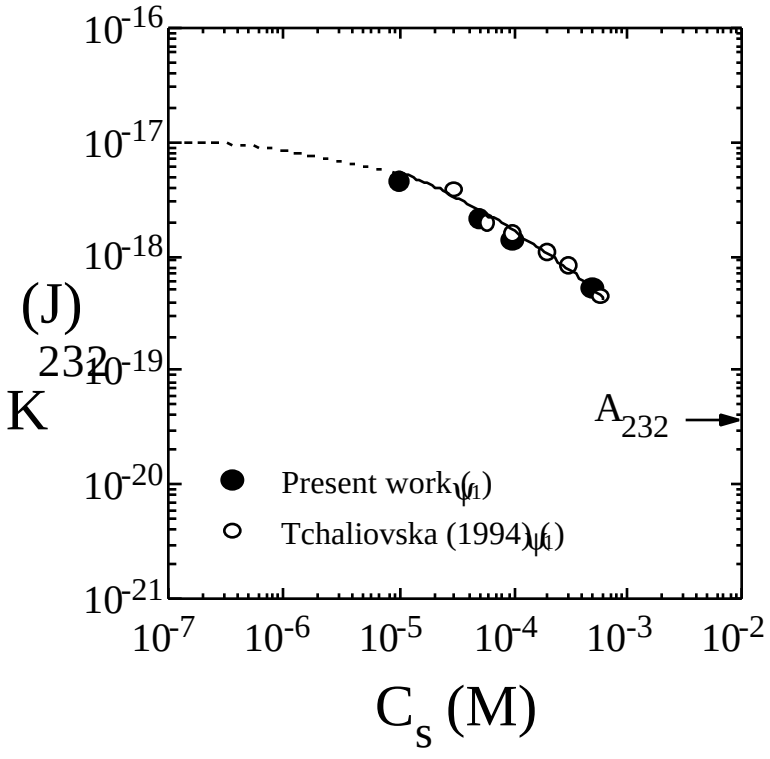

Figure 3.9 The vales of K_{232} of Eq. [3.13] for the foam films in the presence of RNH_3Cl as calculated using the extended DLVO theory. Only the positive values of K_{232} parameters are plotted. The open circles represent the K_{232} values calculated using the film thickness data reported by Tchaliovska, *et al.*(14).

Hamaker constant. The strong hydrophobic force is dampened by the hydrated polar heads of the surfactant molecules which are brought to the interface as part of the surfactant molecules. An increase in the adsorption density at the interface should result in a decrease in the hydrophobic force. As the surfactant concentration continues to increase, the hydrophobic force diminishes to the level of A_{232} before the hydration force becomes discernible at $2\text{x}10^{-3}$ M RNH_3Cl (see Table 3.3). It appears, therefore, that one can use the classical DLVO theory only at a relatively narrow range of concentrations where neither hydration nor hydrophobic force is significant. Similarly, Churaev and Derjaguin (35) noted that the DLVO theory can be used only for weak hydrophobic colloids whose contact angles are in the range of 20-45°. At higher contact angles, the extended DLVO theory, which considers contributions from the hydrophobic force must be used.

The appearance of the hydration force at high RNH_3Cl concentrations may be related to the stability of the Newton black films. The stability of these films is generally attributed to the hydration force (36), for which the negative K_{232} values obtained in the present work may provide evidence. As is well known (37), hydration forces are observed at relatively short ranges; therefore, the foam films stabilized by hydration forces have small film thicknesses.

3.3.5 Disjoining Pressure Isotherm

The K_{232} values obtained from the H_e measurement may be used to predict disjoining pressure isotherms. In the present work, a Π versus. H curve was obtained using a porous tube TFB of the Exorowa and Scheludko type (22). The isotherm was obtained at 22°C using a 10^{-3} M RNH_3Cl solution, as shown in Figure 3.10. The measurements were conducted in the presence of 10^{-4} M *NaCl*, which was helpful in stabilizing the film.

Figure 3.11 shows the surface tension data obtained at different *NaCl* concentrations. The effect of the salt addition is more pronounced at higher salt concentrations.

The experimental results are compared with the theoretical isotherms obtained using the classical and extended DLVO theories. Both isotherms were obtained with ψ_1=152 mV and A_{232}=3.7x10^{-20} J, but the latter has an additional attractive term, *i.e.*, a hydrophobic force whose magnitude is represented by K_{232}=6x10^{-19} J. This value is slightly larger than the value of K_{232}=4x10^{-19} that can be read off the K_{232} versus. C_s curve shown in Figure 3.9. Nevertheless, the extended DLVO theory fits the experiment better than the classical DLVO theory, suggesting that hydrophobic force plays a part in determining the stability of water films. Although the difference between the two theoretical isotherms is relatively small at large film thicknesses (H>30 nm), the difference becomes more significant at smaller film thicknesses as shown in Figure 3.10b. The difference would have been larger had the isotherm been obtained at a lower surfactant concentration. However, the disjoining pressure measurement is very difficult at lower concentrations because the films are unstable due to the hydrophobic force. Figure 3.10b also shows the contributions from all the surface forces considered in the present work. One can see that even at a relatively high concentration of 10^{-4} M RNH_3Cl, the hydrophobic force is stronger than the van der Waals force. Theoretically, the film should rupture when Π becomes zero. The classical and extended DLVO theories predict that the film should rupture at H=2.5 and 8 nm, respectively. However, the rupture actually occurs at H=29 nm. This large

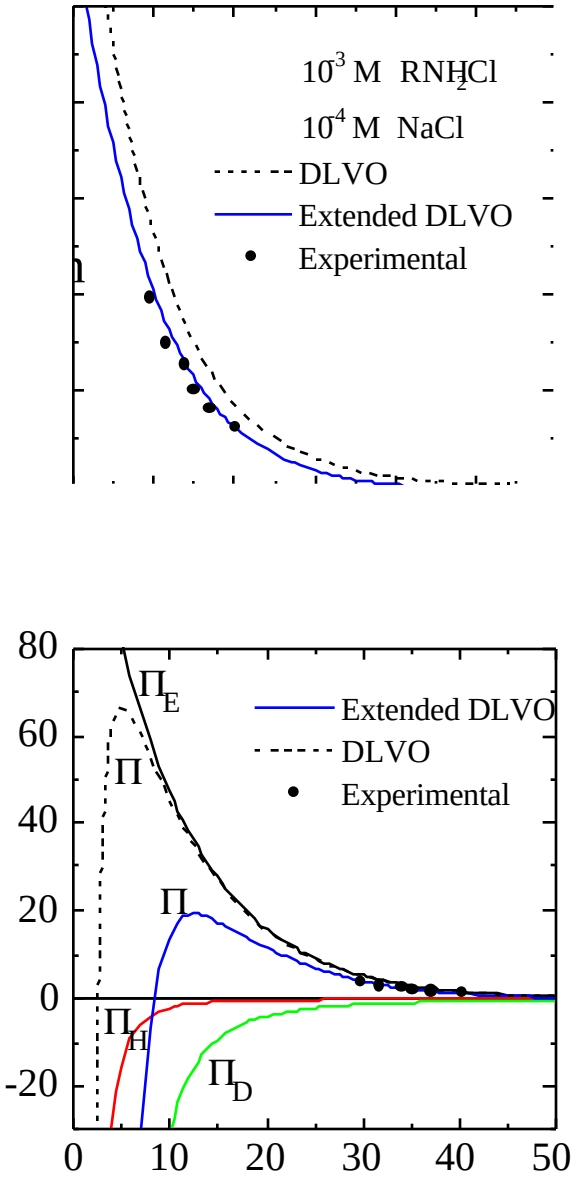

Figure 3.10 Comparison of the disjoining pressures measured using a thin-film balance in the presence of 10^{-3} M *RNH_2Cl* and 10^{-4} M *NaCl* at pH 5.7 with the DLVO and extended DLVO theories. The theoretical isotherms were obtained with ψ_1=152 mV, P_c=63 N/m^2, and K_{232}=6x10^{-19} J. The figure on the bottom (b) shows the electrostatic (Π_e), van der Waals (Π_d), and hydrophobic (Π_h) pressures.

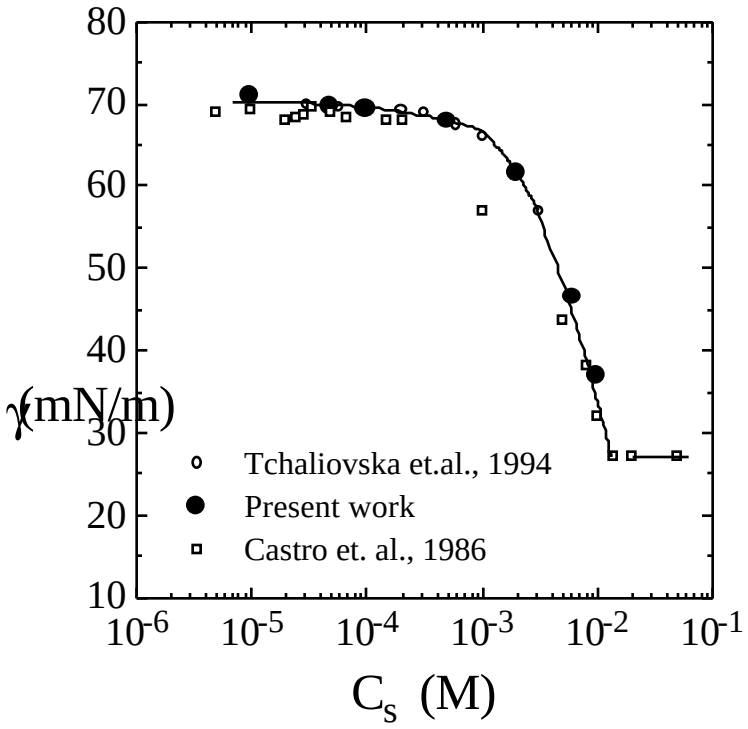

Figure 3.11 The surface tensions measured as a function of RNH_2Cl concentration in the absence and presence of *NaCl.*

discrepancy may be attributed to the hydrodynamic fluctuation of the interface, which will be further discussed in the next section.

3.3.6 Hydrodynamic Effect

When a thin film is subjected to a mechanical perturbation of a given wavelength, its free energy is increased due to an increase in the surface area. On the other hand, the perturbation can bring the local film thicknesses within the range of the attractive van der Waals force, resulting in a decrease in free energy. If the free energy change is net-negative, the perturbation will grow spontaneously and the film will eventually rupture. This hydrodynamic fluctuation model was first proposed by Scheludko (8), who derived this relationship:

$$h_{cr} = \left(\frac{A_{232}\pi}{32K^2\gamma} \right)^{05} \qquad [3.16]$$

where h_{cr} is the critical rupture thickness, K is the wave number of the perturbation, and γ is the surface tension. Vrij (38) and Vrij and Overbeek (7) further developed the model to predict coalescence time. Ruckenstein and Jain (39) also derived an expression for coalescence time using the hydrodynamic fluctuation model, while Donners and Vrij (40) considered both hydrodynamic fluctuation and film drainage in conjunction with the van der Waals force. Other investigators (41-42) considered only the drainage of liquid films using the Reynolds lubrication theory and the van der Waals force.

Most of the hydrodynamic models developed to date considered only the van der Waals force as the destabilizing surface force. Based on the results presented in the foregoing paragraphs, it may be reasonable to consider the hydrophobic force as an additional destabilizing force. In this case, one may substitute A_{232} of Eq. [3.16] with $A_{232}+K_{232}$, which may lead to a better fit with the experiment.

Thus, there are three destabilizing forces for thin liquid films. These include the van der Waals-dispersion force, hydrophobic force, and hydrodynamic force. The DLVO theory considers only the dispersion force, while the extended DLVO theory considers both the dispersion and hydrophobic forces. Inclusion of the hydrophobic force in the hydrodynamic models may prove to be useful.

3.4 CONCLUSIONS

Equilibrium thicknesses of foam films were measured in the presence of dodecylammonium chloride (RNH_3Cl) using a thin film balance (TFB). The results showed that the free liquid film is stabilized by the repulsive electrostatic force, which increases with increasing surfactant concentration. However, the double-layer potentials calculated using the DLVO theory are considerably lower than those calculated from the adsorption densities of the surfactant, even after the corrections for the counter-ion adsorption in the Stern layer. This discrepancy can be attributed to the hydrophobic force not considered in the DLVO theory. Therefore, an extended DLVO theory was used to estimate contributions from the hydrophobic forces to the destabilization of thin liquid films. The hydrophobic forces were represented by a power law which is in the same form as that for the van der Waals force, so that its constant K_{232} can be compared directly with the Hamaker constant A_{232}. The results showed that the air-water interface is most hydrophobic in the absence of surfactants, the value of K_{232} being in the neighborhood of 10^{-17}. As the surfactant concentration increases, K_{232} decreases steadily with increasing concentration of the RNH_3^+ ions at the air-water interface. At $2\text{x}10^{-3}$ M, however, K_{232} becomes negative, indicating that a repulsive hydration force appears at higher surfactant concentrations. The hydration force may be a major stabilizing force in black films. It appears, therefore, that the classical DLVO

theory is applicable to the studies of thin liquid films only at a narrow concentration range where both the hydrophobic and hydration forces are small compared to the van der Waals force.

The extended DLVO theory was also used to fit the disjoining pressure isotherm obtained at 10^{-3} M RNH_2Cl and 10^{-4} M $NaCl$. The experimental results can be fitted to this theory with K_{232}=6x10^{-19} J. Consideration of the hydrophobic force predicts critical film thicknesses substantially larger than predicted by the classical DLVO theory but smaller when measured experimentally. This discrepancy may be attributed to the hydrodynamic forces operating in film thinning processes.

3.5 REFERENCES

1. Exerowa, D., *Kolloid-Zeit*, **232** , 703(1969)
2. Kolarov, T., Cohen, R., Exerowa, D., *Colloids Surf.*, **42**, 49(1989)
3. Exerowa, D., Kolarov, T., and Kristov, KHR., *Colloids Surf.*, **22**, 171(1987)
4. Bergeron, V., Waltermo, R., and Cleasson, P.M., *Langmuir*, **12**, 1336(1996).
5. Joye, J. L. and Miller, C. A. *Langmuir*, **8**, 3083(1992).
6. Kitchener, J. A., *Recent Progress in Surface Science* , **1**, Chap. 2, Academic Press, New York, (1964).
7. Vrij, A. and Overbeek, J. T., *J. American Chemical Society*, **90**, 3074(1968).
8. Scheludko, A., *Proc. Kon. Ned. Akad. Wetensch,* **B65**, 76 (1962).
9. Scheludko, A., *Adv. Colloid Interface Sci*. **1**, 391 (1967).
10. Vrij, A., *J. Colloid Sci*., **19**, 1(1964).
11. Ruckenstein, E. and Jain, R.K., *J. Chem Soc. Trans., 2*, **70**, 132(1974).
12. Israelachvili, J. N. and Pashley, R. M., *Nature*, **300**, 341(1982).
13. Rabinovich, Ya.I., and Yoon, R.-H., *Langmuir*, **10**, 1909(1994).
14. Tchaliovska, S., Manev, E. Radoev, B. Eriksson, J. C. and Claesson, P. M., *J. Colloid Interface Sci*., **168**, 190(1994).
15. Pugh, R. J., and Yoon, R.-H., *J. Colloid Interface Sci*., **163**, 169(1994).
16. Yotsumoto, H. and Yoon, R. H., *J. Colloid Interface Sci*., **157**, 426(1993).
17. Yotsumoto, H. and Yoon, R. H., *J. Colloid Interface Sci*., **157**, 434(1993).

Chapter 3 Hydrophobic Forces in Thin Water Films Stabilized by Dodecylammonium Hydrochloride

18. Xu, Z. and Yoon, R. H., *J. Colloid Interface Sci*., **132**, 532(1989).

19. Xu, Z. and Yoon, R. H., *J. Colloid Interface Sci*., **134**, 427(1990).

20. Yoon, R. H. and Mao, L., *J. Colloid Interface Sci*., **181**, 613(1996).

21. Mysels, K. J. and Jones, M.N., *Discuss. Faraday Soc.*, **42**, 42(1966).

22. Exerowa, D. and Scheludko, A., *Comp. Rend. Bulg. Acad. Sci*., **24**, 47(1971).

23. Kruglyakov, P.M., *Free Films, Foams, and Emulsions*, Chapter 11, 767-827,

24. *CRC Handbook of Chemistry and Physics*, 66th edition, CRC Press, Inc. Boca Raton, Florida.

25. Somasundaran, P., *Int. J. Miner. Prosess.*, **3**, 5(1976).

26. Fuerstenau, D. W., *Transactions AIME*, **208**, 1365(1957).

27. Yoon, R.-H., and Ravishankar, S. A., *J. Colloid Interface Sci.*, **166**, 215(1994).

28. Noyes, R. M., *J. Am. Chem. Soc.*, **86**, 971(1964).

29. Yoon, R.-H. and Yordan, J. L, *J. Colloid Interface Sci*., **113**, 2(1986).

30. Exerowa, D., *Kolloid-Zeit*, **232**, 703-710 (1969).

31. Israelachvili, J. N., "*Intermolecular and Surface Forces*," Academic Press (1985).

32. Okada, K., Akagi, Y., Kogure, M., and Yoshioka, N., *Candian J. Chem. Eng.*, **68**, 393(1990).

33. Stern, O., *Z. Elektrochem.*, **30**, 508(1924).

34. Webb, J. T., Bhatnagar, P.D., and Williams, D.G., *J. Colloid Interface Sci.*, **43**, 346(1974).

35. Churaev, N. V. and Derjaguin, B. V., *J. Colloid Interface Sci*., **103**, 542(1985).

Chapter 3 Hydrophobic Forces in Thin Water Films Stabilized by Dodecylammonium Hydrochloride

36. Jones, M. N., Mysels, K. J., and Sholten, P. C., *Trans. Faraday Soc*., **61**, 583(1966).

37. Pashley, R. M., *J. Colloid Interface Sci*., **83**, 531(1981).

38. Vrij, A., *Discussions Faraday Soc*., **42**, 23(1966).

39. Ruckenstein, E. and Jain, R.K., *J. Chem Soc. Trans.*, *2*, **70**, 132(1974).

40. Donners, W. A. B. and Vrij, A., *Colloid Poly. Sci.*, **256**, 804(1978).

41. Malhotra, A. K. and Wasan, D. T., *Chem. Eng. Commun*., **55**, 95(1987).

42. Li, D., *J. Colloid Interface Sci*., **163**, 108(1994), **181**, 34(1996).

Chapter 3 Hydrophobic Forces in Thin Water Films Stabilized by Dodecylammonium Hydrochloride

APPENDIX 3.1

Chapter 3 Hydrophobic Forces in Thin Water Films Stabilized by Dodecylammonium Hydrochloride

The thickness (H) of the film was obtained from the reflectance (R) of the interference. The relationship between R and H is given by the Raleigh equation:

$$R = \frac{A^2 + B^2 + 2ABCos\theta}{1 + A^2B^2 + 2ABCos\theta} \qquad [A3.1]$$

where

$$A = \frac{n_1 - n_0}{n_1 + n_0} \qquad [A3.2]$$

$$B = \frac{n_0 - n_1}{n_0 + n_1} \qquad [A3.3)]$$

$$\theta = \frac{4\pi n_0 H}{\lambda} \qquad [A3.4]$$

in which λ is the wavelength of the incident light and n_0 (= 1.331) and n_1 (=1.000) are the reflective indices of the solution and gas (air) phases (35, 36). The relationship between reflectance and film thickness for the air-water-air system calculated with the above equations using two different wavelengths of monochromatic light (600 and 533 nm) is presented in Figure A3.1. Since the IPS can only measure the gray level intensity of the digitized image, the reflectance (R) of the interference pattern cannot be measured directly. Therefore, a calibration procedure was necessary. This was accomplished by measuring the gray level intensity of the calibration standard of known reflectance (R). The calibration curve obtained is shown in Figure A3.2, which provides a means of obtaining the reflectance of the interference pattern by simply

measuring the gray level intensity. Reproducibility of the measurements was better than ± 2%. The film radius was measured from the image and ranged from 0.2 ± 0.02 mm. In order to obtain reproducible results, the radius of the film was controlled by manipulating the applied pressure into the cell for each experiment.

Chapter 3 Hydrophobic Forces in Thin Water Films Stabilized by Dodecylammonium Hydrochloride

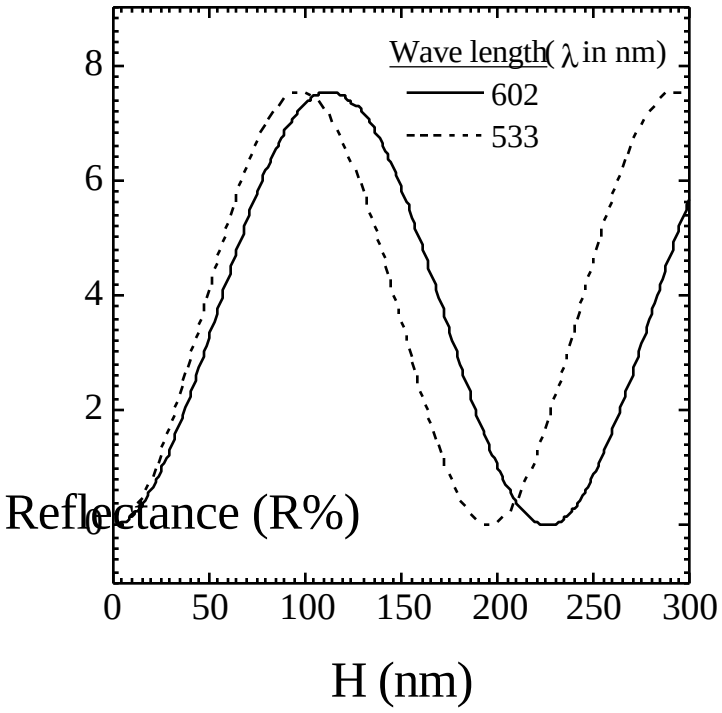

Figure A3.1 Theoretical relationship between reflectance R and film thickness (H) for the air-water-air system and monochromatic light with λ =600 and 533 nm.

Chapter 3 Hydrophobic Forces in Thin Water Films Stabilized by Dodecylammonium Hydrochloride

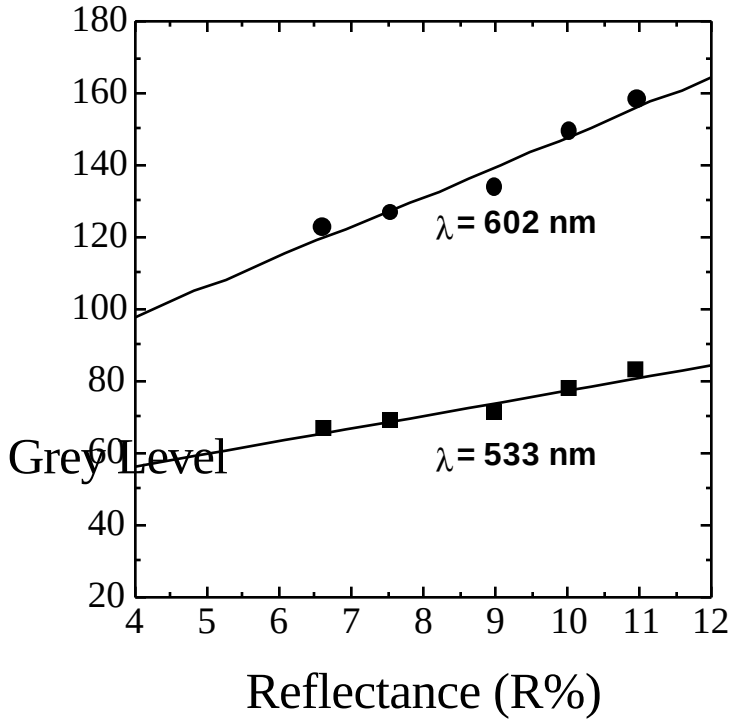

Figure A3.2 Reflectance % versus gray level for monochromatic light with λ =602 and 533 nm.

CHAPTER 4

HYDROPHOBIC FORCES IN THIN WATER FILMS STABILIZED BY SODIUM DODECYL SULFATE

ABSTRACT

Thin film balance (TFB) was used to measure the equilibrium film thickness of free water films drawn from various concentrations of sodium dodecyl sulfate (*SDS*). The results were analyzed using extended DLVO theory to determine the contributions from electrostatic, van der Waals, hydrophobic and hydration forces. Results suggest that hydrophobic force is the major destabilizing factor in free water films, and that its contribution increases with decreasing surfactant concentration. The hydrophobic force term included in the extended DLVO calculation was represented by a power law (of the same form as the van der Waals force). Using equilibrium film thickness, the force parameter (K_{232},) of the power law is estimated to be in the order of 10^{-17} when the data are extrapolated to a zero concentration of *SDS*. The disjoining pressure isotherm was also measured with free water films drawn from a solution containing 10^{-4} M of *SDS* and $4x10^{-4}$ M of *NaCl* at pH 5.7-6.0 and 22±0.1 ^{0}C. The hydrophobicity parameter (K_{232}) of $2.19x10^{-19}$ J was included to fit data to the theoretical disjoining pressure isotherm using the Stern potential, ψ_1 =140 mV and capillary pressure, P_c =66 N/m^2. In the present work, it is shown that the hydrophobicity (K_{232}) of the air bubbles in pure water is the same in the presence of either anionic (sodium dodecyl sulfate) or cationic (dodecyl ammonium chloride) surfactants.

4.1 INTRODUCTION

The role of thin liquid films has been recognized in many industries, including the petroleum, mining, chemical, and biological industries, which use systems involving bubbles, droplets, foams, emulsions and lipid membranes. These films are thermodynamically unstable and the rupture of the films occurs when the free energy decreases. The liquid in the film drains out because of the pressure differences in the film and the Plateau-border and the film thins. When the film thickness reaches less than 100 nm , this drainage process is basically controlled by the surface force. Further reduction in the film thickness will result in either common black films (CBFs) (5-20 nm) or Newton black films (NBFs) (less than 5 nm) (1).

The DLVO theory has been used to predict the stability of the thin liquid films (CBFs). This theory has two components of disjoining pressure; namely, electrical double-layer pressure and van der Waals pressure. The former is a positive disjoining pressure and stabilizes the thin liquid films. The stability of the films increases since the potential of the electrical double layer at the interfaces increases with increasing surfactant concentration. The latter is the negative pressure which destabilizes the films. Even though the theory has been successfully used for the non-ionic surfactants at relatively high concentrations (2, 4), the extraordinary stability of thin water films (NBFs) (3-5) observed in the presence of ionic surfactants was predicted with non-DLVO forces such as steric and hydration forces.

A number of theories such as hydrodynamic fluctuation (6-9), hole formation (10), and hydrophobic interaction (11-13) have been proposed to explain the phenomenon of film rupture. Recently, among these theories, the hydrophobic force in thin aqueous films has been studied extensively. The thin film balance (TFB) has been used to measure equilibrium film thicknesses of

anionic and non-ionic surfactants to estimate the potential at the air-water interface using the DLVO theory. The potentials have also been calculated using Gibbs adsorption isotherm based on the surface tension measurements. It was found that there was a discrepancy between these estimated potentials at the interface. Then it was attributed to the additional attractive hydrophobic force. The first attempt has been made by Pugh and Yoon (12) to calculate the hydrophobic disjoining pressure in thin aqueous films using similar experiments with nonionic surfactants. The authors used the extended DLVO theory which includes the contribution from hydrophobic forces in addition to the electrostatic and van der Waals forces. Recently, the hydrophobic force in thin water films of dodecylammonium chloride was measured and a disjoining pressure isotherm was obtained using a thin film balance (TFB) (13). The magnitude of the hydrophobicity of the air bubbles in pure water was estimated to be about $K_{232} = 10^{-17}$ J, which is 260 times larger than the Hamaker constant ($A_{232} = 3.7 \times 10^{-20}$ J).

As a continuing investigation, the role of hydrophobic force in free water films is studied in the present work using the thin film balance (TFB) technique. The results reported in this communication have been obtained using sodium dodecyl sulfate (*SDS*) solutions and compared with the results reported for dodecylammonium chloride (RNH_2Cl) solutions in Chapter 3 and the previous communication (13).

4.2 EXPERIMENTAL

4.2.1 Materials

Kodak electrophoresis grade (>99% purity) sodium dodecyl sulfate (*SDS*) was used as such without further treatment. *SDS* shows signs of degradation of purity as the solutions age

over a period of days (14). The slow hydrolysis reaction causes this degradation, which occurs in the *SDS* solution at alkaline conditions, producing dodecanol as an impurity. Therefore all solutions were prepared with conductivity water, which is prepared by passing double-distilled water through a Nanopure II water treatment unit and aging it a minimum of one day prior to use. Reagent grade sodium chloride (*NaCl*) was obtained from Fisher Scientific Co., roasted at 600^{o}C to remove possible organic impurities, and stored in pre-cleaned glass containers until use.

4.2.2 Procedure

The equilibrium thickness of free water films was measured using a thin film balance (TFB), known as the Scheludko-Exerowa-type (8, 9), in conjunction with an image analysis system which analyzes the intensity of the monochromatic light reflecting from the thin water film. A detailed experimental procedure and experimental setup were given in Chapter 3 and reference 13.

A disjoining pressure isotherm was obtained using a TFB equipped with a porous film holder made of a sintered glass ring. In the present work, a porous holder described by Exerowa and Scheludko (15) was used, and a detailed description of apparatus and experimental procedures was also given in Chapter 3 and reference 13.

Surface tension of the *SDS* solutions was measured using the du Nouy ring method. The Fisher Tensiomat was calibrated using ethanol solutions of known surface tension.

4.3 RESULTS AND DISCUSSIONS

4.3.1 Equilibrium Film Thickness

Figure 4.1 shows the equilibrium film thickness (H_e) measured as a function of *SDS* concentration (see also Table 4.1). The measurements were conducted without a supporting electrolyte, and the pH was in the range of 5.7-6.0 at 22 ± 0.1°C. The data obtained in the present study are superimposed with those reported by Bergeron, et al. (16) and Lyklema and Mysels (17). In their studies, the data were obtained at high *SDS* concentrations. Both sets of data show that H_e decreases with increasing surfactant concentration, indicating that the adsorption of SD^- ions at the air-water interface increases the stability of the free film. The increased stability of the free water films in the presence of ionic surfactants is generally attributed to the repulsive double-layer forces. The largest film thickness measured in the present study was 164±10 nm at $5x10^{-5}$ M. The film thickness measured at 10^{-6} M was 159±10 nm, which is slightly lower than the largest film thickness. The reduced film thickness with decreasing surfactant concentration attributed to the dimpling of the films at low surfactant concentrations. Below 10^{-6} M, the films were so unstable that it was not possible to obtain metastable films, i.e., the lifetime of the films was less then a second. Extrapolation of the measured H_e data to zero concentration gave a value of approximately 170 nm, which is similar to the results of RNH_2Cl (13) and larger than the value of 155 nm for non-ionic surfactants (12). The equilibrium thicknesses drawn from the SDS solutions film measured using the TFB by Exerowa, et al. (18), are also shown in Figure 4.1 and Table 4.2. Their results were in the presence of $4x10^{-4}$ M *NaCl*. As seen in Figure 4.1, the equilibrium film thicknesses decrease markedly at low surfactant concentrations (10^{-6} - 10^{-4} M) upon the addition of electrolytes.

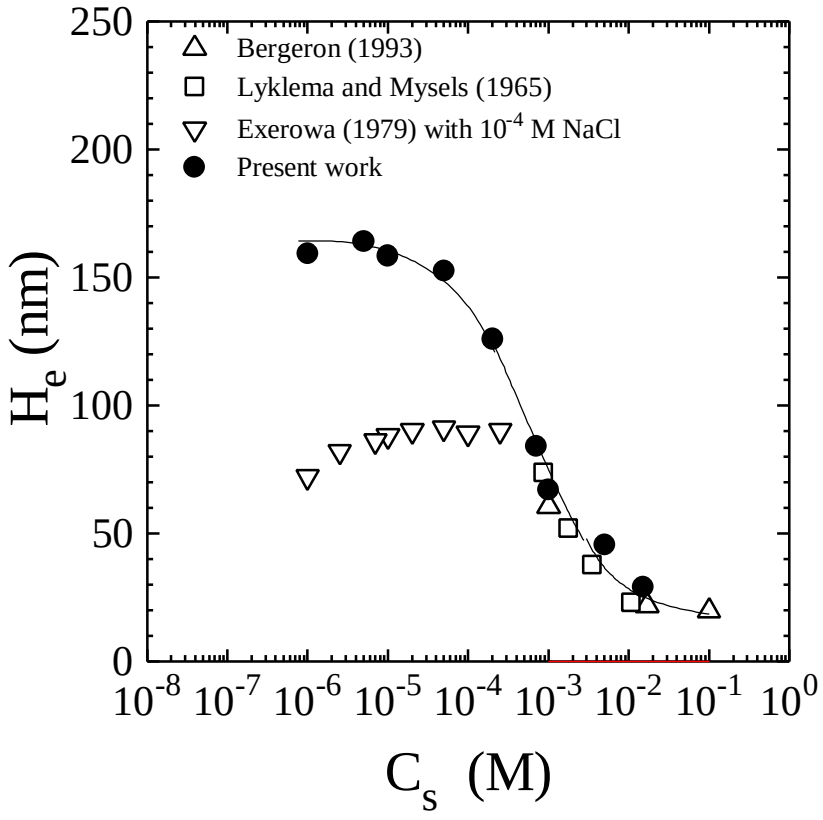

Figure 4.1 Equilibrium film thickness as a function of SDS concentrations at pH 5.7-6.0 and 22±0.1 ^{0}C. The results obtained for the same surfactant system by Bergeron (16), Lyklema and Mysels (17), and Exerowa (10) are also represented.

Table 4.1 Result of equilibrium film thickness measurements conducted with thin film balance (TFB) with sodium dodecyl sulfate (SDS) solution at pH 5.7-6.0.

SDS (M)	P_c (mN/m^2)	$1/\kappa$ (nm)	H_e (nm)	Potentials (mV) ψ_0 Gibbs	Potentials (mV) ψ_1 Stern
$1.0x10^{-6}$	72.2	304.0	159.7	41.0	41.0
$5.0x10^{-6}$	72.0	136.0	164.0	72.0	72.0
$1.0x10^{-5}$	71.5	96.1	158.5	88.0	88.0
$5.0x10^{-5}$	71.0	43.0	152.6	129.0	117.0
$1.0x10^{-4}$	70.6	30.4	125.1	147.0	132.0
$5.0x10^{-4}$	67.0	13.6	86.3	188.0	156.0
$1.3x10^{-3}$	63.0	8.43	68.1	206.0	162.0
$4.0x10^{-3}$	48.3	4.81	44.6	223.0	165.0
$1.5x10^{-2}$	36.0	2.48	25.2	241.0	157.0

The film thickness reduces from about 160 nm for the films of salt-free solutions to 72-90 nm for that of salt solutions. This indicates that the stability of thin water films increases substantially in the presence of inorganic electrolytes. There are two reasons for the reduction of the film thickness. First, the addition of electrolytes increases the stability of films due to the increased viscosity of liquid in the film, causing slow drainage of the water in the film. Second, the adsorption density of SD^- ions (Γ_{SD^-}) at the air-solution interface in the salt solution is higher than that of SD^- ions in the salt-free solution. This reduces the surface tension of the solution, thus increasing the repulsive electrostatic double-layer force. As supporting evidence, Tajima (19) reported that the surface tension of a solution was reduced from 70 dynes/cm to 50 dynes/cm with the addition of 0.115 M of *NaCl* at low-surfactant concentrations.

4.3.2 Double-Layer Potential

In Chapter 3 and reference 13, it was shown that the stability of thin water films is basically controlled by the double-layer and hydrophobic forces. However, the DLVO theory which considers only the double-layer and van der Waals forces, has been used to interpret most of the TFB work (2,10,18) reported in the literature. In a horizontal film at equilibrium in a TFB, the disjoining pressure (Π) is balanced by the capillary pressure (P_c) (Eqs. [3.1] and [3.2] in Chapter 3). Then the DLVO theory has been expressed by the following relationship:

$$\Pi = \Pi_e + \Pi_d \qquad [4.1]$$

in which Π_d is the van der Waals force and Π_e is the double-layer force as the components of the disjoining pressure. In thin film studies, Eqs [3.1]-[3.5] in Chapter 3 have been generally

Table 4.2 Results of Exerowa (1979) for the equilibrium film thickness measurements with sodium dodecyl sulfate (SDS) in the presence of $4x10^{-4}$ M NaCl at pH 5.7.

			Potentials (mV)		
SDS	P_c	H_e	ψ_0	ψ_1'	ψ_1
(M)	(mN/m^2)	(nm)	Gibbs	DLVO	Stern
$1.0x10^{-6}$	72	72	70	45	70
$2.5x10^{-6}$	71	82	70	65	70
$7.0x10^{-6}$	71	86	70	70	70
$1.0x10^{-5}$	69	88	81	76	78
$2.0x10^{-5}$	68	90	94	80	90
$5.0x10^{-5}$	67	91	130	80	121
$1.0x10^{-4}$	66	89	148	79	130
$2.5x10^{-4}$	66	90	169	80	140

combined to obtain the following equation which is identical to Eq. [3.6]:

$$64C_s RT \tanh^2\left(\frac{zey_1'}{4kT}\right)\exp(-kH_e) - \frac{A_{22}}{6pH_e^3} - \frac{2g}{r_c} = 0. \qquad [4.2]$$

Using Eq.[4.2], the value of y_1' has been calculated since it is the only unknown. The results were given in Figure 4.2 and Table 4.1. In these calculations, the values of H_e shown in Figure 4.1 and Table 4.1 and that of g obtained in the present work (see Figure 4.6 and Table 4.1) were used. The valence is equal to -1 for SD^- ions while the surfactant concentration was equated to the electrolyte concentration in order to calculate the Debye length. The Hamaker constant was $A_{232} = 3.7\text{x}10^{-20}$ J (22). As seen in the case of dodecylammonium chloride (13), the values of y_1' calculated in this manner increase with increasing surfactant concentration, providing an explanation for increased film stability and, hence, the low values of H_e, as shown in Figure 4.2. Note that they_1' approaches a constant value at $2\text{x}10^{-3}$ M, at which a close-packed monolayer may be formed. Note also that the zeta potentials of the air bubbles measured in *SDS* solutions by Tajima, *et al.* (19), which are comparable with the results reported by Yordan and Yoon (23), are substantially lower than the calculated y_1' values.

Also shown in Figure 4.2 and Table 4.1 are the values of surface potentials (y_0) using the method described in Chapter 3 and reference 13. The surface charge density (s_0) and then the values of y_0 can be calculated using the Eqs. [3.6] and [3.7] in Chapter 3. As shown in Figure 4.2, the values of y_o calculated in this manner are substantially larger than those of y_1' obtained using the classical DLVO theory.

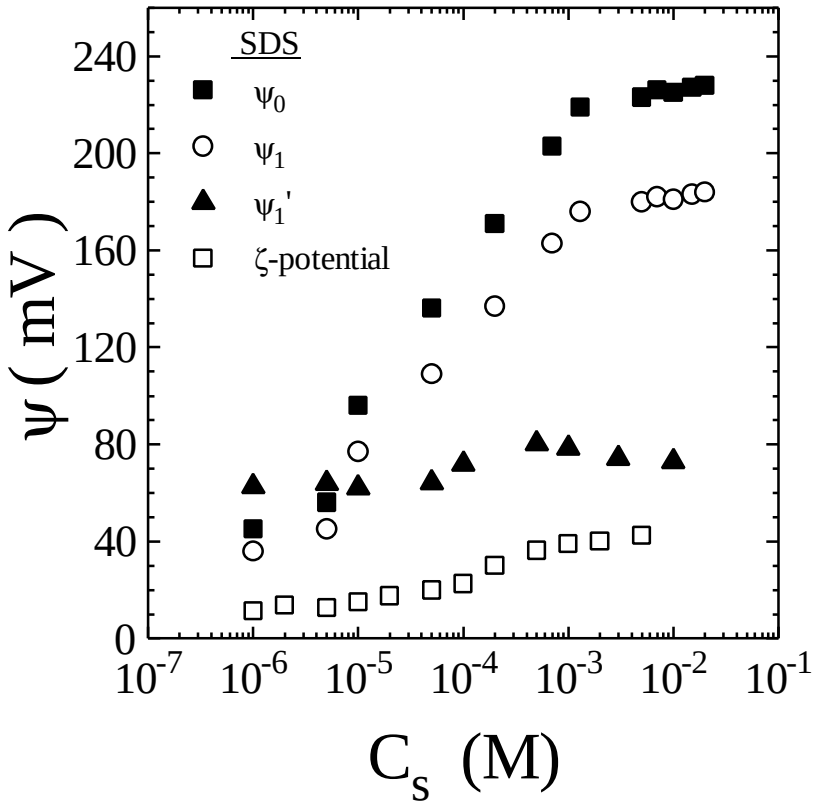

Figure 4.2 The double-layer potentials at the air-water interface as calculated from the Gibbs adsorption isotherm (y_0), DLVO theory (y_1'), Stern model (y_1), and zeta-potential measurement for air bubbles (ζ) (19).

The difference between y_o and y_1' can be reduced if the former is corrected for the counter ions, i.e., Na^+ ions, that may be considered to form a Stern layer near the polar heads of the SD^- ions adsorbed at the air-water interface. Figure 4.3 is a schematic representation of the Stern potential model for the adsorbed layer of SD^- ions at the air-water interface. Similar to the model given for the case of RNH_2Cl solutions, the potential decays linearly to y_1 at the distance δ away from the charge layer and then decays exponentially into the solution phase. In this case, the charge balance at the interface, which was used to calculate the Stern potential (y_1), is given by Eqs. [3.8] through [3.11] in Chapter 3. The results are also given in Figure 4.2 and Table 4.1. The values of y_1 calculated in this manner are considerably lower than y_o; however, they are still substantially higher than the values of y_1' calculated using the classical DLVO theory.

The discrepancy between the values of y_1' and y_1, which is observed in the case of RNH_2Cl solutions, may be accounted for by the hydrophobic force. A power law (Eq.[3.5]) was also used successfully to represent the contribution of the hydrophobic force for the case of *SDS* solutions.

4.3.3 Hydrophobic Force

In Chapter 3 and reference 13, it was shown that the hydrophobic force must include in determining the instability of thin water films of surfactants at low concentrations. So the extended DLVO theory, which includes contributions from the hydrophobic force (Π_h) (Eq. [3.13]) was represented by the following relationship which is identical to Eq. [3.15]:

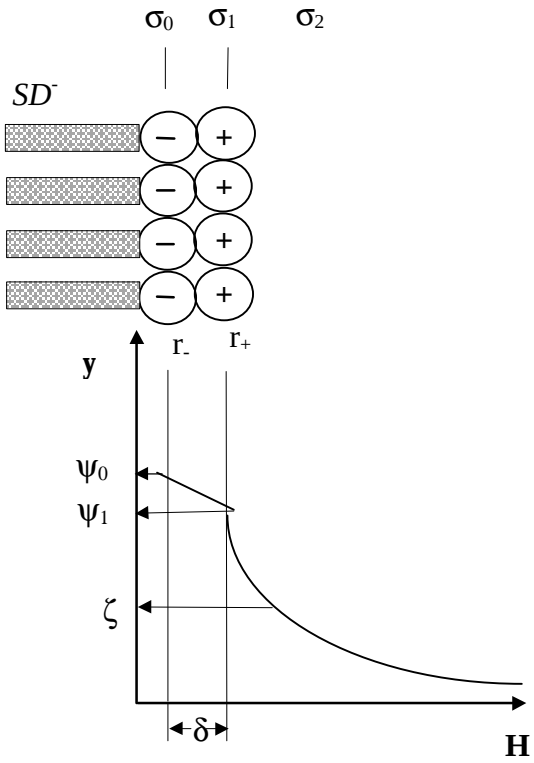

Figure 4.3 Schematic representation of the potential-distance profile in which negatively charged SD^- molecules at the air-water interface and positively charged counter ions Na^+ are shown. Surface charge densities of charge layer, Stern layer, and diffuse layer are σ_0, σ_1, and σ_2, respectively. δ is the thickness of the Stern layer ($\delta = r_+ + r_- = 2.97$ Å). ψ_0, ψ_1, and ζ are the surface potential, Stern potential, and zeta potential in this system, respectively.

$$64C_s RT \tanh^2\left(\frac{zey_1'}{4kT}\right)\exp(-kH_e) - \frac{A_{232}}{6pH_e^3} - \frac{K_{232}}{6pH_e^3} - \frac{2g}{r_c} = 0 . \qquad [4.3]$$

Then K_{232} values were calculated using the known values of H_e (given in Figure 4.1), that of the surface tension of solutions (γ, given in Figure 4.6 and Table 4.1), r_c (=2 mm), A_{232} (=3.7x10^{-20} J), and that of the y_1 obtained using the Stern model. Table 4.3 and Figure 4.4 show the results of the calculation obtained at various *SDS* concentrations. They show that K_{232} decreases with increasing surfactant concentration, indicating that the air-water interface becomes less hydrophobic. It is interesting that K_{232} becomes negative, as in the case of RNH_2Cl (13), indicating that the non-DLVO force is repulsive at concentrations above 1.3x10^{-3} M *SDS*. The repulsive force may be due to the hydrated water molecules associated with the polar heads of the surfactant molecules. Because of the strong repulsive hydration force, the films formed at high surfactant concentrations were stable for 30-60 minutes.

The data obtained in the present work are superimposed with those reported in our previous chapter for the dodecylammonium chloride solutions in Figure 4.4, which shows only the positive values of K_{232} plotted versus concentration. It is interesting to note that the data interface in a similar manner. It is shown that K_{232} values decrease steadily with increasing concentration. This may be attributed to the increasing population of the polar heads of either SD^- or RNH_3^+ ions at the interface, which are strongly hydrated and, hence, should dampen the hydrophobicity.

The results reported by Exerowa, et al. (18), (see H_e in Figure 4.1 and Table 4.2) and in Eq. [4.3] were also used to calculate the values of K_{232} for the free films of *SDS* solutions

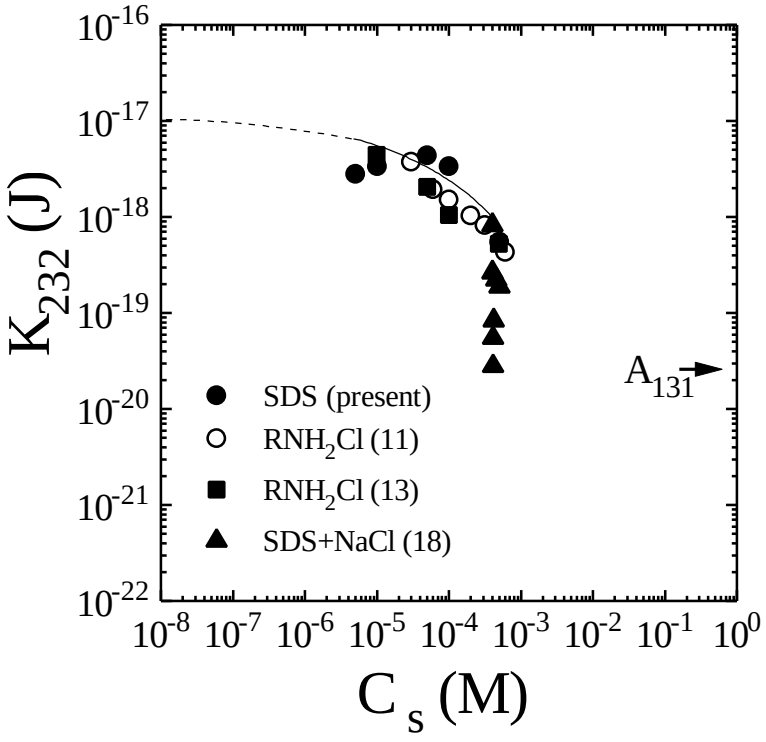

Figure 4.4 The calculated K_{232} values using the extended DLVO theory and the Stern potential (ψ_1) as a function of RNH_2Cl and *SDS* concentrations.

Table 4.3 The Values of K_{232} Calculated Using the Extended DLVO Theory from the Equilibrium Thickness of the SDS Solutions

SDS (M)	H_e (nm)	K_{232} (J)
$1.0x10^{-6}$	159.7	-
$5.0x10^{-6}$	164.0	$1.20x10^{-18}$
$1.0x10^{-5}$	158.5	$4.35x10^{-18}$
$5.0x10^{-5}$	152.6	$5.35x10^{-18}$
$1.0x10^{-4}$	125.1	$4.40x10^{-18}$
$5.0x10^{-4}$	86.3	$5.42x10^{-19}$
$1.3x10^{-3}$	68.1	$-4.80x10^{-20}$
$4.0x10^{-3}$	44.6	$-3.30x10^{-20}$
$1.5x10^{-2}$	25.2	$-2.50x10^{-20}$

containing $4x10^{-4}$ M *NaCl*. The total concentrations of *SDS* and *NaCl* were used to calculate the Debye length, but the results shown in Figure 4.4 were plotted as K_{232} versus C_s as a function of only the SDS concentration. It shows that in the presence of an inorganic electrolyte, K_{232} values are much lower than in the case of salt-free solutions and decrease much more sharply; hence, the hydrophobicity of the air-water interface.

As concluded in Chapter 3 and reference 13, Figure 4.4 gives the important message that air bubbles are inherently hydrophobic, which is consistent with the fact that the interfacial tension at the air-water interface is among the highest of any material known to date. An extrapolation of the K_{232} versus C_s curves for the three different cases shown in Figure 4.4 suggests that the value of K_{232} for air bubbles in the surfactant-free (pure) water is about 10^{-17} J, which is approximately 270 times larger than the Hamaker constant. The strong hydrophobic force is dampened by the hydrated polar heads of the surfactant molecules at the air-water interface. Any increase in the adsorption density of molecules by increasing surfactant and/or inorganic electrolyte concentration should result in a decrease in the hydrophobic force. As the concentration continues to increase, the hydrophobic force diminishes to the level of A_{232} before the hydration force becomes discernible at $2x10^{-3}$ M RNH_2Cl (13), $1.3x10^{-3}$ M SDS, and $2.5x10^{-4}$ M *SDS*. Therefore, it appears that the classical DLVO theory can be valid only at a narrow range of concentrations where neither the hydrophobic nor hydration force is significant. Similarly, it has been noted that the DLVO theory is applicable for the weak hydrophobic solids ($q = 20 - 45^0$). At higher contact angles, use of the extended DLVO theory, which includes the hydrophobic force, is required.

Chapter 4 Hydrophobic Forces in Thin Water Films Stabilized by Sodium Dodecyl Sulfate

As in the case of RNH_2Cl, appearance of the hydration force at high *SDS* concentrations may also be related to the stability of the NBFs. The stability of these films is generally attributed to the hydration force (27) for which the negative K_{232} values obtained in the present work may provide other evidence. As is well known (28), hydration forces are observed only at relatively short ranges; therefore, the foam films stabilized by hydration forces have small film thicknesses.

4.3.4 Disjoining Pressure Isotherms

The K_{232} values obtained from the H_e measurements are used to predict disjoining pressure isotherms. In the present study, a porous tube TFB, such as the one used by Exerowa and Scheludko (15), was used to obtain the disjoining pressure isotherm (Π vs. H curve). The isotherm was obtained at 22 ^{o}C using a 10^{-4} M *SDS* solution in the presence of $4x10^{-4}$ M *NaCl*, as shown in Figure 4.5, since the addition of salt improved the stability of the film.

The experimental results were compared with the theoretical isotherms obtained using the classical and extended DLVO theories. Both isotherms were obtained with $y_1 = 140$ mV and $A_{232} = 3.7x10^{-20}$ J, but the latter has a hydrophobic force whose magnitude is represented by $K_{232}=5.5x10^{-19}$ J. As clearly seen, the extended DLVO theory fits the experiment better than the classical DLVO theory, suggesting that hydrophobic force plays a part in determining the stability of water films. Remembering that, for the thin films of RNH_2Cl solutions (10^{-3} M and $y_1 = 152$ mV), K_{232} was $6x10^{-19}$ J to fit the data (13). Although the difference between the two theoretical isotherms is relatively small at large film thicknesses (H>55 nm for *SDS* and H>29 nm for RNH_2Cl), the difference becomes more significant at smaller film thicknesses, as shown in Figure

4.5b and 3. B, respectively. The difference would have been larger had the isotherm been obtained at a lower surfactant concentration. However, the disjoining pressure measurement is very difficult at lower concentrations because the films are unstable due to the hydrophobic force. Figure 4.5b also shows the contributions from all of the surface forces considered in the present work. It can be seen that even at a relatively high concentration of 10^{-4} M *SDS*, the hydrophobic force is stronger than the van der Waals force. Theoretically, the film should rupture when Π becomes zero. The classical and extended DLVO theories predict that the film should rupture at H=2.5 and 8 nm, respectively. However, the rupture actually occurs at H=55 nm which was H=29 nm for the films drawn from the RNH_2Cl solutions (13). This is strong evidence that this large discrepancy may be attributed to the hydrodynamic fluctuation of the interface.

As discussed in the previous chapter, a mechanical perturbation in a thin water film can cause a local film thickness fluctuation which results in a free energy change in the film. If this change is net-negative, the perturbation will grow spontaneously and the film will eventually rupture. In modeling the coalescence of bubbles and/or droplets and the rupture of liquid films, both hydrodynamic fluctuation and film drainage were considered in conjunction with only the van der Waals force(29-31). Based on the results obtained in previous (13) and present investigations, the hydrophobic force may be considered as an additional destabilizing force. Substitution of the Hamaker constant and hydrophobicity constant (A_{232}+K_{232}) may lead to a better fit with the experiment. Therefore, inclusion of the hydrophobic force as a third component of extended DLVO theory in hydrodynamic models may prove to be useful.

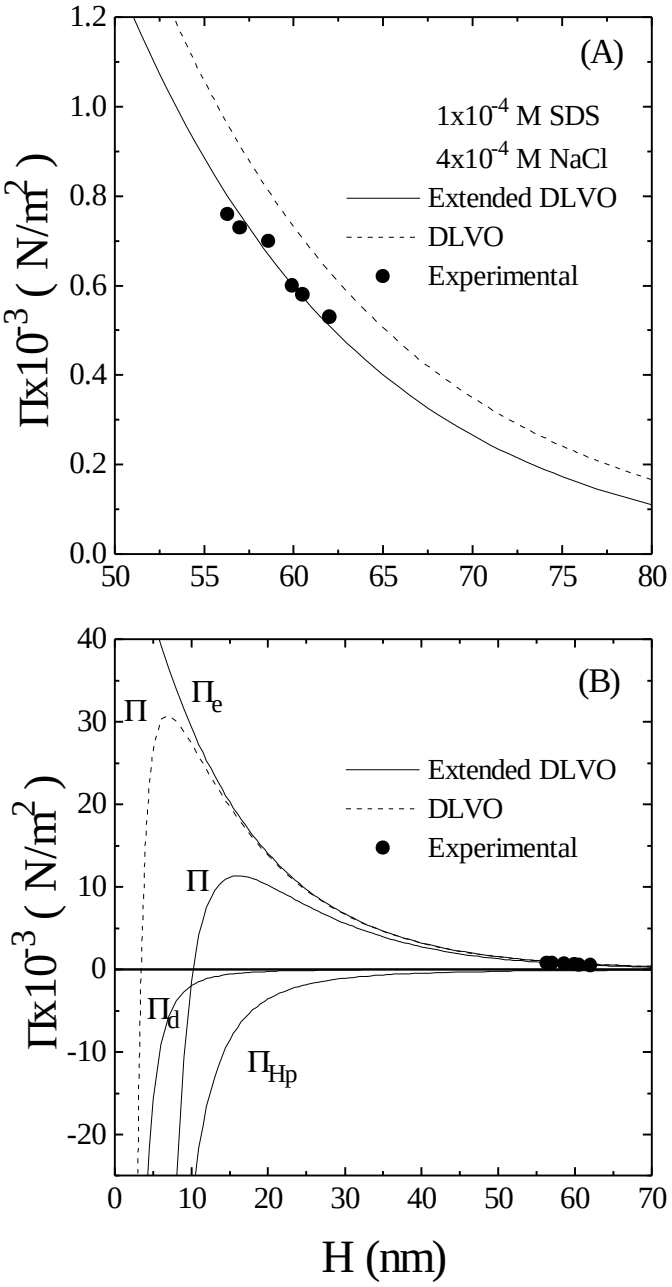

Figure 4.5 Comparison of the disjoining pressures measured using a TFB in the presence of 10^{-4} M *SDS* and $4x10^{-4}$ M *NaCl* at pH 5.7 with the DLVO and extended DLVO theories. The theoretical isotherms were obtained with ψ_1=140 mV, P_c=66 N/m^2, and $K_{232}=5.5x10^{-19}$ J. The figure on the bottom (B) shows the electrostatic (Π_e), van der Waals (Π_d), and hydrophobic pressures (Π_{Hp}).

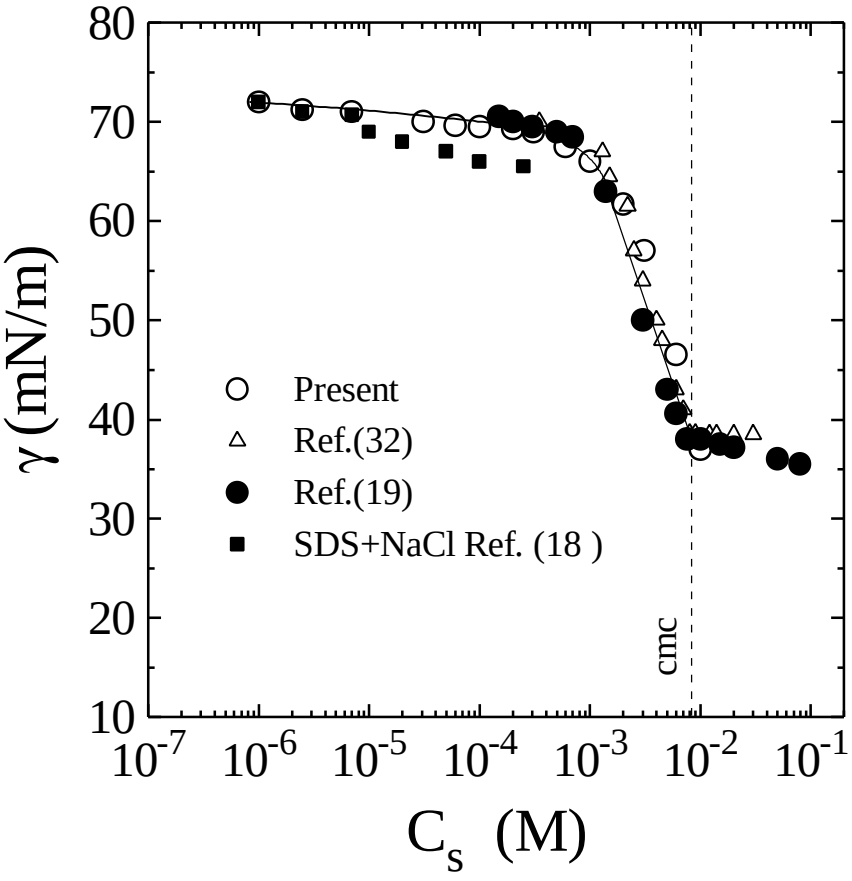

Figure 4.6 The concentration of SDS versus the surface tension of solution at pH 5.7-6.0 and 22±0.1 ^{0}C.

4.4 CONCLUSIONS

The results of equilibrium film thickness measurements obtained using a thin film balance (TFB) in both previous (Chapter 3 and reference 13) and present communications has shown that there are a lot of similarities between the behavior of thin films of RNH_2Cl and *SDS* solutions. Therefore, concerning the hydrophobic forces in free water films, the conclusions were combined and summarized as follows:

The foam film is stabilized by the repulsive electrostatic force. However the interfacial potentials calculated using the DLVO theory are considerably lower than those calculated from the adsorption densities of the surfactant and the Stern model. This discrepancy can be attributed to the hydrophobic forces. Therefore, an extended DLVO theory was used to estimate contribution from the hydrophobic forces to the destabilization of thin liquid films. It was possible to compare the hydrophobicity constant (K_{232}) with the Hamaker constant (A_{232}) by representing the hydrophobic force as a power low. The results obtained for both surfactant systems showed that the air-water interface is most hydrophobic in the surfactant-free (pure) water and the value of K_{232} is about 10^{-17} J. As the surfactant concentration increases, K_{232} decreases with the increasing concentration of the SD^- and RNH_3^+ ions at the air-water interface. However, the values of K_{232} become negative at $2\text{x}10^{-3}$ M RNH_2Cl, $1.3\text{x}10^{-3}$ M *SDS*, and $2.5\text{x}10^{-4}$ M *SDS* concentrations (the last was for the salted solutions). This indicates that a repulsive hydration force appears at high-surfactant concentrations. The hydration force may be a major stabilizing force in CBFs and NBFs. Therefore, it can be concluded that the classical DLVO theory is applicable to the studies of thin liquid films only at a narrow surfactant

concentration range in which hydrophobic and hydration forces are smaller than the van der Waals force.

The extended DLVO theory was also used to fit the disjoining pressure isotherm obtained at 10^{-4} M *SDS* and $4x10^{-4}$ M *NaCl*. The disjoining pressure isotherm obtained experimentally can be fitted to the theory with $K_{232}=5.5x10^{-19}$ J. For the free film of 10^{-3} M RNH_2Cl and 10^{-4} M *NaCl* solution, the same fit was obtained with $K_{232}= 6x10^{-19}$ J. Consideration of the hydrophobic force predicts critical film thicknesses substantially larger than predicted by the classical DLVO theory but smaller than those measured experimentally. This discrepancy may be attributed to the hydrodynamic forces operating in the film thinning processes.

4.5 REFERENCES

1. Exerowa, D., *Kolloid-Zeit*, **232** , 703 (1969)
2. Kolarov, T., Cohen, R., Exerowa, D., *Colloids Surf*., **42**, 49 (1989)
3. Exerowa, D., Kolarov, T., and Kristov, KHR., *Colloids Surf*., **22**, 171 (1987)
4. Bergeron, V., Waltermo, R., and Cleasson, P.M., *Langmuir*, **12**, 1336 (1996).
5. Joye, J. L. and Miller, C. A. *Langmuir*, **8**, 3083 (1992).
6. Kitchener, J. A., *Recent Progress in Surface Science* , **1**, Chap. 2, Academic Press, New York, (1964).
7. Vrij, A. and Overbeek, J. T., *J. American Chemical Society*, **90**, 3074 (1968).
8. Scheludko, A., *Proc. Kon. Ned. Akad. Wetensch*, **B65**, 76 (1962).
9. Scheludko, A., *Adv. Colloid Interface Sci*. **1**, 391 (1967).
10. Exerowa, D., Kashchiev, D., and Platikanov, D., *Adv. Coll. Interface Sci*., 40, 201-256 (1992).
11. Tchaliovska, S., Manev, E., Radoev, B., Eriksson, J. C., and Claesson, P. M., *J. Colloid Interface Sci*., **168**, 190 (1994).
12. Pugh, R. J. and Yoon, R.-H., *J. Colloid Interface Sci*., **163**, 169 (1994).
13. Yoon R.-H and Aksoy, B.S., Submitted *J. Colloid Interface Sci.*, (1996).
14. Jones, M. N., Mysels, K. J., and Sholten, P. C., *Trans. Faraday Soc*., **61**, 583 (1966).
15. Exerowa, D. and Scheludko, A., *Comp. Rend. Bulg. Acad. Sci*., **24**, 47 (1971).
16. Bergeron, V. and Radke, C.J., *Langmuir*, 8, 3020-3026 (1992).
17. Lyklema, J. and Maysels, J., *J. American Chem. Society*, **87**, 2539 (1965).

18. Exerowa, D, Zacharieva, M., Cohen, R., and Platikanov, D., *Colloid and Polymer Sci.*, 257, 1089-1098 (1979).

19. Tajima, K., *Bull. Chem. Soc. Japan*, 44, 7, 1767 (1971).

20. Vrij, A., *J. Colloid Sci.*, **19**, 1 (1964).

21. Ruckenstein, E. and Jain, R.K., *J. Chem Soc. Trans. 2*, **70**, 132 (1974).

22. Israelachvili, J. N., "*Intermolecular and Surface Forces*" Academic Press (1985).

23. Yordan, J. L. and Yoon, R-H., *J. Colloid Interface Sci*., 113, 2 (1986).

24. Stern, O., *Z. Elektrochem.*, **30**, 508 (1924).

25. Webb, J. T., Bhatnagar, P.D., and Williams, D.G., *J. Colloid Interface Sci.*, **43**, 346 (1974).

26. *CRC Handbook of Chemistry and Physics*, 66th edition, CRC Press, Inc. Boca Raton, Florida.

27. Jones, M. N., Mysels, K. J., and Sholten, P. C., *Trans. Faraday Soc*., **61**, 583 (1966).

28. Pashley, R. M., *J. Colloid Interface Sci*., **83**, 531 (1981).

29. Vrij, A., *Discussions Faraday Soc*., **42**, 23 (1966).

30. Ruckenstein, E. and Jain, R.K., *J. Chem Soc. Trans. 2*, **70**, 132 (1974).

31. Donners, W. A. B. and Vrij, A., *Colloid Poly. Sci.*, **256**, 804 (1978).

32. Kubota, K., Hayashi, S., and Inaoka, M., *J.Colloid Interface Sci.*, **95**, 362 (1983).

CHAPTER 5

MODELING OF AIR BUBBLES IN AN AQUEOUS SOLUTION OF IONIC SURFACTANTS USING HYDROPHOBIC SOLID SURFACES

ABSTRACT

In the earlier chapters, it was shown that the hydrophobic force is responsible for the spontaneous rupture of the thin aqueous film, and the air bubble in pure water is hydrophobic and its hydrophobicity is 270 times higher than the dispersion forces. It has been known that the hydrophobicity of the solid surfaces can also be much higher than the dispersion force. Therefore, the hydrophobicity of air-bubble and the solid surfaces should be comparable. It is the objective of this study to simulate the air-water interface using very hydrophobic surfaces (θ>90°). As a first step, the surface of polytetraflouroethelene (*PTFE*) was chosen which is the most hydrophobic surface with an equilibrium contact angle of pure water 110°. Thereafter, the contact angle measurements were conducted using the sessile drop technique with solutions prepared with sodium dodecyl sulfate (0 to 10^{-1} M) and dodecylammonium chloride (0 to 10^{-2} M). This method allows one to observe the changes in contact angle and the hydrophobicity of *PTFE* with the increasing surfactant concentration. As it occurs in the case of air-water interface, the surface will be contaminated with surfactant molecules at the interfaces (solid- liquid, air-liquid) resulting in changes of contact angle.

In addition to the above experiments, the contact angles were also measured on freshly cleaved mica surfaces and hydrophobized mica surfaces. The measurements were conducted with the same surfactants and in the same concentration range above mentioned. The bare mica surfaces exhibit an equilibrium contact angle of pure water of 10° whereas the hydrophobized mica surfaces exhibit that of 45°, 54°, 72°, 97°, and 103°. Therefore, it is possible to estimate the changes in the hydrophobicity of surfaces having different degrees of hydrophobicities in the presence of various surfactant concentration so that comparison can be made between the hydrophobicity of air bubbles and that of solid surfaces.

The results obtained in this study suggest that the hydrophobicity of the of air-water interfaces (pure water) and that of hydrophobic surfaces are comparable, i.e., K_{232} is about 10^{-17} J, which is obtained by extrapolation of data to zero surfactant concentrations, and K_{131} is in the order of 10^{-16} J, which can be determined by the contact angles measured on the surfaces involved. It is certain that hydrophobic force which is much higher than the dispersion force for both systems need to be included when the stability of foam, thin liquid films, and colloids is considered.

Chapter 5 Modeling of Air Bubbles in an Aqueous Solution of Ionic Surfactants Using Hydrophobic Solid Surfaces

5.1 INTRODUCTION

Research concerning the rupture of thin liquid films has been applied in many different industries, including mining, chemical, and mechanical. Some industrial applications of film rupture include foam, emulsions, oil recovery, and detergency. During this research, it was demonstrated that the stability or instability of thin films is related to the disjoining pressure which includes electrostatic, dispersion, and structural components of total disjoining pressure. In the case of foams, the total force per area (disjoining pressure) is generally measured using a single free water film drawn from the bulk solution of surfactants since conducting direct force and film thickness measurements is difficult with foams. As a unique technique, thin film balance (TFB) has been used to measure the disjoining pressure which is then used to calculate the contributions from either electrostatic or dispersion forces. In earlier studies (3, 14, Chapter 3&4) the equilibrium thickness of free water was measured using TFB to estimate the interfacial potential at the air-water interface. For the ionic and nonionic surfactants, the interfacial potentials were also calculated using Gibbs adsorption isotherm based on the data obtained from surface tension measurements. The discrepancies observed between these interfacial potentials were attributed to the hydrophobicity of the air-water interface (8, 21). Based on equilibrium film thickness measurements and disjoining pressure isotherms obtained in the presence of cationic and anionic surfactants, it was shown that air bubbles in pure water are hydrophobic in nature (3, 14, Chapter 3 & 4). Hence, their hydrophobicity causes the spontaneous rupture of thin films between these air bubbles. By applying the extended DLVO theory, the hydrophobicity of the air bubbles in pure water was estimated using a power law at various surfactant concentrations (Chapter 3 & 4).

Chapter 5 Modeling of Air Bubbles in an Aqueous Solution of Ionic Surfactants Using Hydrophobic Solid Surfaces

Then the value of K_{232} for a zero surfactant concentration was found to be about 10^{-17} J, which is much higher than the Hamaker constant (A_{232} = $3.7x10^{-20}$ J). It was also shown that the hydrophobicity of air bubbles diminishes with the addition of a surfactant. In other words, the bubbles becomes more hydrophilic with increasing surfactant concentration. Basically, the air-water interface is contaminated with surfactants due to adsorption of the surfactant molecules at the interface. As a result, the stability of thin water films increases and the rupture of the film does not occur spontaneously. The stability of the thin films appears as an increase in the film lifetime (22, 23) and a decrease in the hydrophobicity of the air-water interface (3, 14, 21).

On the other hand, in the case of wetting or dewetting of either nonpolar or polar solid surfaces with surfactant solutions, the surfactant adsorption on the solid surface and its degree of reversibility are strongly influenced by a large number of variables. This means that the surface properties can be altered from hydrophobic to hydrophilic or the other way around by surfactant adsorption on the solid surface. These variables include (31):

1) Surface polarity (dipole moment, etc.),
2) Surface charge and the nature of the charge-determining ions,
3) Solution pH and ionic strength. This affects both the surface charge and the degree of ionization of an ionic surfactant,
4) The degree of surface hydration,
5) The presence of specific ions, such as Cu^{++} or Ca^{++}, with which chelation complexes or insoluble surface compounds may be formed, e.g., calcium oleate on the surface of calcium carbonate,

Chapter 5 Modeling of Air Bubbles in an Aqueous Solution of Ionic Surfactants Using Hydrophobic Solid Surfaces

6) Type of surfactants (ionic or nonionic) adsorbed on the surfaces.

The contact angle (θ) measured at the three-phase contact (solid-gas-liquid) has been employed as a degree of the hydrophobicity of solid surfaces. Generally speaking, the higher the contact angle the higher the hydrophobicity of the solid surface. On the other hand, for the air-liquid-air systems, there are only two phases: gas and liquid and there is not a single measuring unit, such as contact angle for the solid-gas-liquid systems. Therefore, it is not possible to compare the hydrophobicity of air bubbles (air-water interface) and that of solid surfaces.

However, using a model hydrophobic surface and measuring the contact angles on this model surface with various concentrations of surfactant solutions would be the most realistic approach to overcome this problem. As shown in Chapters 3 and 4, the adsorption of ionic surfactant molecules at the air-water interface reduces the hydrophobicity of the air-water interface. The surface force measurements between the hydrophobic surfaces in the presence of ionic surfactants were shown that the hydrophobic solid surfaces become more hydrophilic as in the case of air-water interface.

The objective of this study is to simulate the air-water interface using polytetraflouroethelene (*PTFE*) having the most hydrophobic surface with an equilibrium contact angle of pure water 110°. In addition, the changes in hydrophobicity of bare mica and hydrophobized mica surfaces with various degree of hydrophobicities will be evaluated by measuring the contact angle of surfactant solution on these surfaces and the surface tension of solutions.

Chapter 5 Modeling of Air Bubbles in an Aqueous Solution of Ionic Surfactants Using Hydrophobic Solid Surfaces

5.2 EXPERIMENTAL

5.2.1 Materials

Two different surfactants were used in this study: cationic dodecylammonium chloride (*RNH_2Cl*) and anionic sodium dodecyl sulfate (*SDS*, purity >99%). The cationic surfactant was supplied by Eastman Kodak Company (recrystallized from ethanol before preparation of a stock solution) and the anionic surfactant by Kodak (used as received without further purification). Since *SDS* shows signs of degradation of purity as the solutions age over a period of days (24-26), all solutions were prepared fresh prior to use with conductivity water (18 μΩ) with pH 5.6, which is prepared by passing double-distilled water through a Nanopure II water treatment unit. The pH adjustment was made with sodium hydroxide (*NaOH*) and hydrochloric acid (*HCl*). The mica specimens used for contact angle measurements were obtained from Unimica Corp., NY. The freshly cleaved mica surfaces were hydrophobized using octadecyltrichlorosilane (*OTS*, 95% purity). The *OTS* molecules were adsorbed on freshly cleaved mica surfaces from HPLC grade cyclohexane as described in the reference to Flinn, *et. al*. (19, 27).

5.2.2 Procedure

5.2.2.1 Contact Angle Measurements

The equilibrium contact angles (θ) were measured using a Rame-Hart Model 100 goniometer. Both the captive bubble and sessile drop techniques were employed to measure contact angles in the *RNH_2Cl* and *SDS* solutions. The captive bubble technique was used only for one series of experiments to compare with the results obtained from the sessile drop techniques.

A Hamilton microliter syringe was used to place a 5 ml drop of solutions or Nanopure water on solid surfaces which included bare mica, hydrophobized mica, and *PTFE*. For the measurements conducted on *PTFE*, the surface was cleaned in boiling nitric acid and rinsed with Nanopure water prior to use. When the hydrophobized mica surfaces were used for contact angle measurements, they were initially washed with copious amounts of ethanol and distilled water, then rinsed with Nanopure water prior to the experiments. Following the cleaning process, the hydrophobicity of all solid surfaces were examined by measuring the contact angle of Nanopure water. If there was any alteration in the degree of hydrophobicity of surfaces, it might have occurred during the cleaning process. No alteration was detected outside the expected range of experimental errors. For the measurements, the solution of dodecylammonium chloride and sodium dodecyl sulfate and the solution pHs were adjusted with *NaOH* and *HCl*. Since the contact angles are time dependent (1-2), the measurements were made after the system reached an equilibrium (until no change was observed in contact angles). To prevent the evaporation of the solution and its contamination from the environment, the measurements were conducted in a covered quartz stainless-steel cell. An average of at least 10 contact angles were measured at different sites on the surfaces for each surfactant concentration and the results were averaged. The measurements were reproducible within $\pm 2^0$.

5.2.2.2 Surface Tension Measurements

The surface tension of the surfactant solutions was measured by using the du Nouy ring method in the absence and presence of *NaCl*. A Fisher Tensiomat, Model 21 (28) was equipped

with an R/r = 53.93 Platinum-Iridium ring, where R is the radius of the ring and r is the radius of the wire. A cylindrical 70x50 mm cell containing 70 ml of solution was used. The ring was cleaned with alcohol and rinsed with Nanopure water, followed by a few seconds of flaming in order to remove hydrocarbon contaminants. The glass cell was cleaned in boiling dilute nitric acid solution for about 2 hours and rinsed with Nanopure water. The calibration was made with alcohol solutions of known surface tensions. The alcohol solutions were prepared by mixing ethyl alcohol and Nanopure water with different volume ratios. At least six solutions were prepared and their surface tension values were obtained from reference (29). The true values of the surface tension were obtained using a correction factor calculated on the R/r value by Zuidema and Waters (30).

5.3 RESULTS AND DISCUSSIONS

5.3.1 Equilibrium Contact Angles for the SDS System

Figure 5.1 shows the equilibrium contact angle (θ) of aqueous solutions on solid surfaces as a function of the *SDS* concentration at pH 5.8. In this figure, three distinct concentration regions, namely Region I, II and III can be observed based on the adsorption mechanism in which the contact angles of solutions on solid surfaces vary. The solid surfaces used in this study are bare mica, hydrophobized mica, and *PTFE* with either $\theta<90°$ or $\theta>90°$. Region (I) is located at low concentrations ($<10^{-4}$ M), much below the critical micelle concentration of *SDS* (cmc = $8.12x10^{-3}$ M); Region (II) is near below cmc; and Region (III) is above cmc. Similar distinct regions were also observed by Bisio, et al. (4), when the contact angles were measured

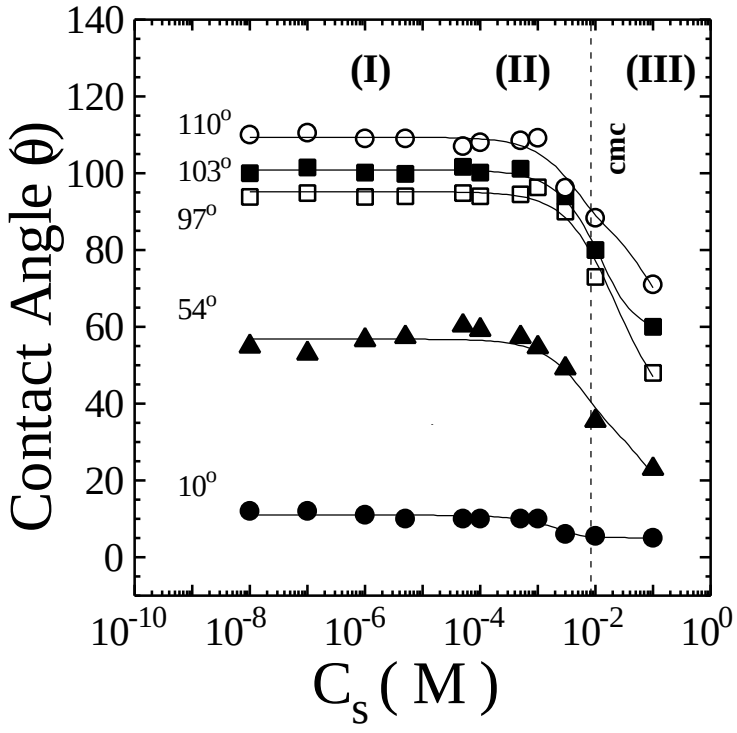

Figure 5.1 Equilibrium contact angle (θ) measured on bare mica (?), hydrophobized mica (? ,? ,□) and *PTFE* surfaces (○) vs. *SDS* concentration.

Chapter 5 Modeling of Air Bubbles in an Aqueous Solution of Ionic Surfactants Using Hydrophobic Solid Surfaces

on the polycarbonate membrane with ionic and nonionic surfactants at pH 3.0. The advancing (θ_a) and receding (θ_r) contact angle measured with pure water were 65° and 28°, respectively.

The contact angles measured on bare mica ($\theta=10^o$ with Nanopure water) basically remain constant in the entire surfactant concentration range studied (in Regions I, II and III). Since the mica surface is classified as a high energy solid surface, pure water with surface tension of 73.8 mN/m and any aqueous solutions of surfactants with surface tension <73.8 mN/m will wet the mica surface showing a very small contact angle. Even thought a small reduction in θ is observed just below cmc, it is not pronounced as much as that of the reduction in contact angles measured on the hydrophobic surfaces. Both mica surface and SD^- ions and/or micelles are negatively charged and the repulsive electrostatic forces between them are dominant. Therefore, no adsorption of SD^- ions and/or micelles takes places on the bare mica surface. This is shown schematically in Figures 5.2.A, 5.2.B, and 5.2.C. Consequently, because of the above reasons, the complete wetting of the bare mica surface is achieved with the SDS solutions throughout the entire concentration range studied.

On the other hand, the equilibrium contact angle measured on the hydrophobized mica surfaces with $10°<\theta< 103°$ and *PTFE* surface with $\theta = 110°$ in the Region (I), does not alter substantially at low surfactant concentrations ($<10^{-3}$ M) and remains in plateau values. The primary reasons for this behavior are: 1) no adsorption of SD^- ions occurs onto uncovered (negatively charged hydrophilic) sites of the mica surface, i.e. mica surfaces with $\theta=54°$ since both mica surface and surfactant ions have the same negative charge, and 2) the adsorption orientation is horizontal to the surfaces since the only driving forces between the hydrophobized

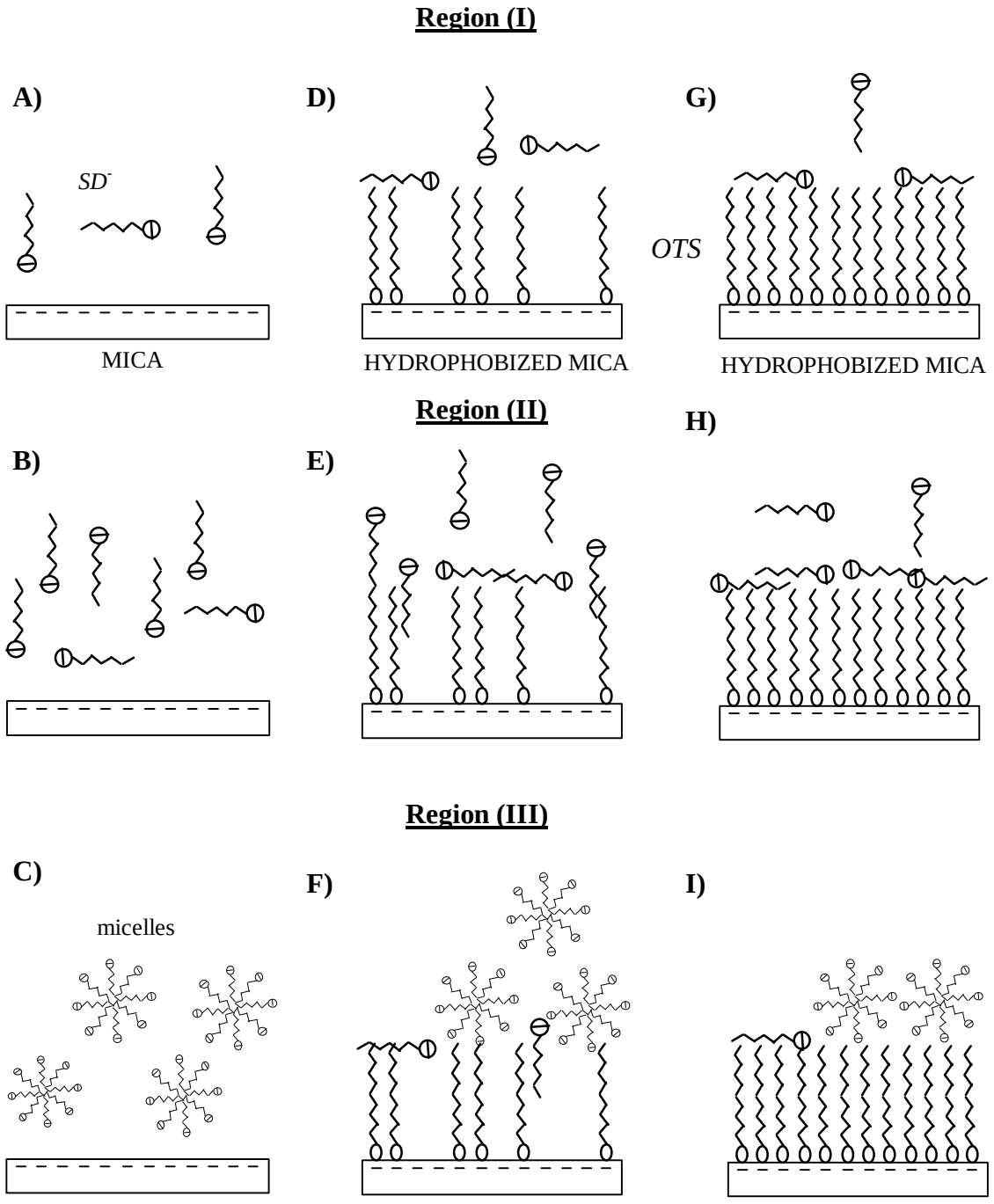

Figure 5.2 : Adsorption orientation of sodium dodecyl sulfate (*SDS*) molecules on the bare mica (A, B, C), hydrophobized mica (D, E, F with $\theta_{eq}<90°$, and G, H, I with $\theta_{eq}>90°$). The mica surfaces were hydrophobized with *OTS* in various degree of hydrophobicities.

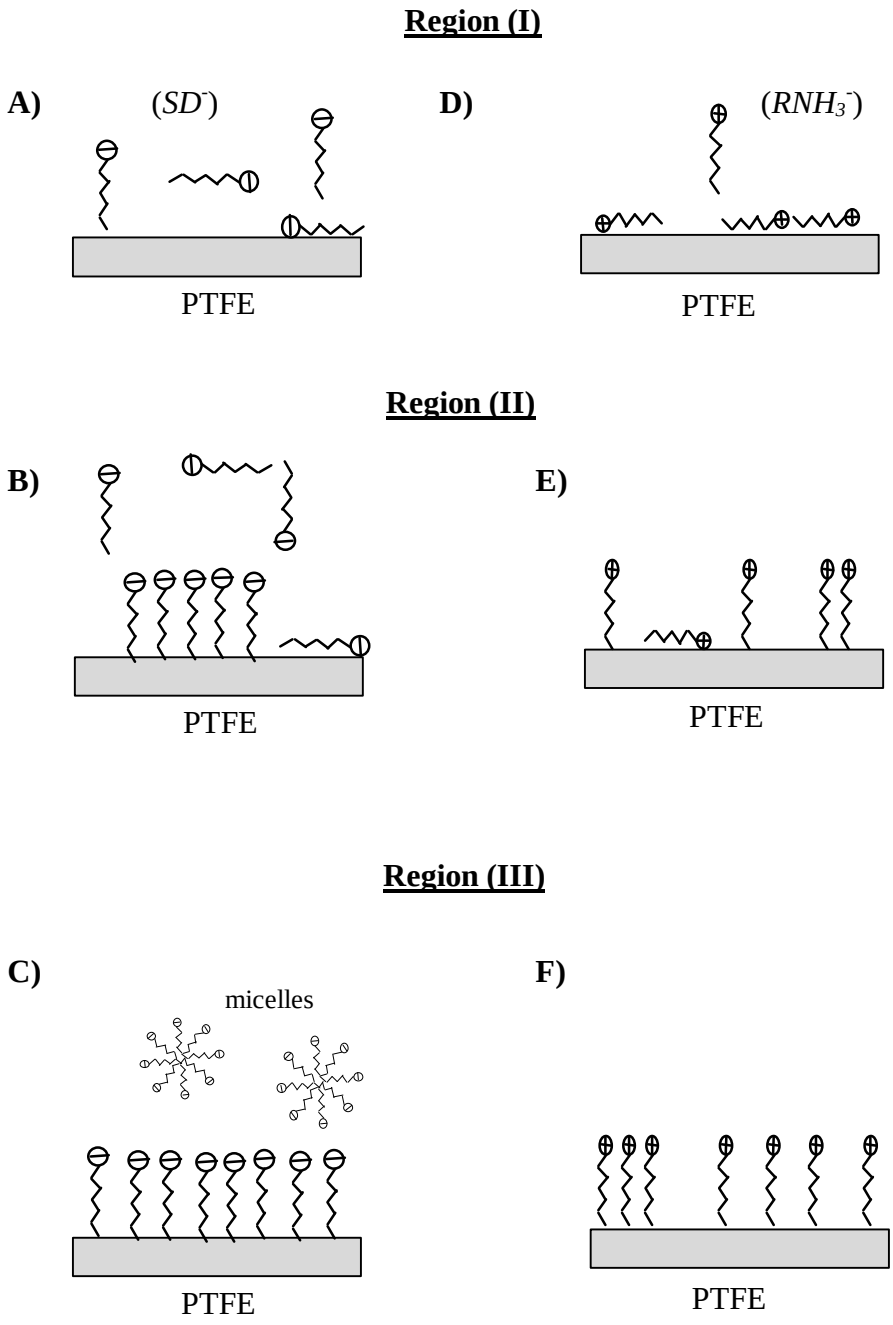

Figure 5.3 : Adsorption orientation of dodecyl ammonium chloride (RNH_2Cl) molecules (A,B,C) and that of sodium dodecyl sulfate (*SDS*) molecules on the *PTFE* (Teflon) on which the contact angle of pure water is 110°.

mica surfaces (*OTS* coated) and hydrocarbon chains of surfactant molecules are the van der Waals and hydrophobic bonding forces. As a result, SD^- ions adsorb on the surfaces due to the molecular interactions and orient themselves horizontally to the surface. The orientation modes are schematically shown in Figures 5.2.D and 5.2.G (on hydrophobized mica surfaces) and Figure 5.3.A (on *PTFE* surface).

At sufficiently high *SDS* concentrations, which are generally just below cmc where the Region (II) starts, the equilibrium contact angle measured on the hydrophobic surfaces with $\theta>10^o$ begins to decline from its constant plateau values. Because the adsorption density and thus the chain-chain interaction (molecular force) between the adsorbed molecules increase (42), the orientation of SD^- ions adsorbed at the solid-solution interface changes from horizontal to vertical and/or tilt position to the surface with the polar heads oriented towards the bulk solution. The orientation of SD^- ions in Region (II) has been termed hemi-micelle formation at hemi-micelle concentration (hmc) (11, 15). Figures 5.2.E and 5.2.H show the orientation of the SD^- molecules on hydrophobized mica surface while Figure 5.3.B shows the orientation of the SD^- molecules on the *PTFE* surface. The hemi-micelles appear to occur due to an increase in interaction of polar heads with the water molecules which contain greater than 8 hydrocarbon chains (11, 15). At the same concentration region, the surface tension of solution (g_{LV}) also begins to decline (Figure 5.4). Hence, these solid surfaces are wetted by the solution with lower surface tension as mention above reason. It can be assumed that the similar hemi-micelle orientation at the solid-solution interface occurs when the molecules adsorb at the air-solution, indicating that both interfaces (solid-solution and air-solution)

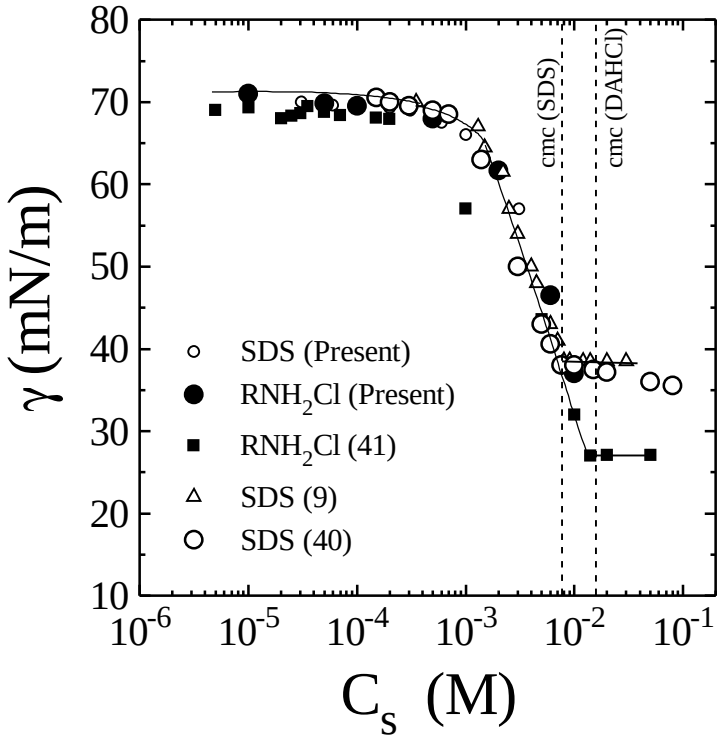

Figure 5.4 Surface tension of solutions as a function of *RNH_2Cl* and *SDS* concentrations at 22 ^{o}C .

become more and more hydrophilic and/or negatively charged with increasing surfactant concentration. As a result, the higher the adsorption density (or the higher the surfactant concentration, $1x10^{-3}$ M $<C_e<$cmc) the lower the contact angle. It is also an evidence that the findings from contact angle measurements agree with the slight increase in the negative zeta potential of the polycarbonate membrane measured in the presence of *SDS* (4). The zeta potential gradually increases to 30 mV when the concentration of *SDS* increases from 10^{-5} to $1.3x10^{-3}$ M (=cmc) in the presence of 10^{-3} M *KCl*.

In Region (III), where the surfactant concentration exceeds cmc, θ decreases about 40° from the plateau values of contact angles measured on all hydrophobic surfaces with θ>90° and the slope of the curve remains fairly constant. For instance, θ measured on the *PTFE* surface decreases from 110° to 70° while θ measured on the hydrophobized mica surface with θ=97° decreases from 97° to about 57° when the concentration increases to 10^{-1} M.

There are two major reasons that the combined effect causes the reduction in contact angles in Region (III). First, at above cmc, the micelles in the solution should not be adsorbed on the hydrophobic surfaces because neither hydrocarbon binding nor electrostatic interactions exist between the micelles and hydrophobic surface. On the other hand, the L-B type of deposition (like hemi-micelles) as proposed in reference 8, may occur at the three-phase contact (solid-air-water) and may induce the interactions between polar heads and water molecules; hence, the surface hydrophobicity. Second, the complete wetting of the solid surfaces can be achieved using solutions whose surface tension are reduced approximately to the critical surface tension (g_C) of solids (14). For instance, the *SDS* solution with g_{LV} =38 mN/m at the cmc wets the surface of

PTFE (θ=70°) more then the Nanopure water (θ=110°), since the g_C of *PTFE* is 18-20 mN/m (28).

As seen in Figure 5.4, the surface tension of *SDS* solutions also declines sharply at 10^{-3} M as a result of the adsorption of surfactant molecules at the air-water interface. As it is well known that the contact angle of a liquid dropped on solid surfaces relates to the interfacial energies of three phases via the Young-Dupre equation,

$$Cosq = \frac{g_{SV} - g_{SL}}{g_{LV}} \qquad [5.1]$$

in which the interfacial tensions are follows: g_{SV} is at solid-vapor, g_{SL} is at solid-liquid, and g_{LV} is at liquid-vapor interface. As clearly seen, when the surface tension of solutions (g_{LV}) decrease with increasing surfactant concentration, an increase occurs in $Cosq$, and hence, a decrease occurs in θ. Therefore, when placed on solid surfaces, these solutions will wet solid surfaces. As a result of these combining effects, θ is reduced, indicating that again the hydrophobicity of the solid surface decreases with increasing surfactant concentration.

In Region (III), for mica at high surfactant concentrations (above cmc), the same reasons given for the case of *PTFE*, such as hemi-micelle formation and the low solution surface tension (38 mN/m), cause reduced contact angles, indicating that the surface is being less hydrophobic.

These results can also be interpreted by determining the quantitative adsorption of molecules at the three interfaces using solution surface tension and contact angle data. A simple method (43) in which two basic relationships, namely Gibbs adsorption:

$$\Gamma^i = -\frac{1}{bRT} * \frac{d\, g_i}{d \ln C} \qquad [5.2]$$

where *i* donates an interface (*sl*, *sv*, or *lv*), Γ is the adsorption density or surface excess of the surface active agent, γ is the interfacial tension, *R* is the gas constant, *T* is the absolute temperature, *C* is the molar concentration of surfactant in the solution, and $1 < b < 2$, and Young-Dupre equations (Equ.5.1) were used. Substituting the Equation 5.1 in Equation 5.2 and rearranging the following equations were obtained for the three interfaces:

$$\Gamma^{sl} = -\frac{1}{bRT} * \frac{d\left(g_{sv} - g_{lv}\cos q\right)}{d\ln C} \qquad [5.3]$$

or in the other form, at constant pressure and temperature,

$$\Gamma^{sl} = -\frac{1}{bRT} * \left(\frac{d\, g_{sv}}{d\ln C} + \frac{g_{lv}\sin q * dq}{d\ln C} - \frac{\cos q * d\, g_{lv}}{d\ln C} \right). \qquad [5.4]$$

Substituting Equation 5.2 in Equation 5.4 yields:

$$\Gamma^{sv} = -\frac{g_{sv}}{bRT} * \frac{d(\cos q)}{d\ln C} + \Gamma^{sl} + \Gamma^{lv} * \cos q \qquad [5.5]$$

Substitution of Equation 5.2 in Equation 5.5 for liquid-vapor (*lv*) yields, after suitable regrouping, an alternative expression for Γ^{sv},

The adsorption density of molecules at the solid-liquid are determined using the following expression:

$$V * (C_1 - C_2) = \Gamma^{sl} * S \qquad [5.6]$$

where V is the volume of the surfactant solution, S is the total surface area of the solids, C_1 and C_2 are the surfactant concentration in the solution before and after the adsorption test, respectively. Using the experimental data obtained in reference 43, the Γ^{sl} values calculated from

Equation 5.6 was platted against surfactant concentration and the relationship was given as follows:

$$\Gamma^{sl} = 6.21x10^{-9} * C^{0.435}$$
$$\Gamma^{sl} = 4.64x10^{-6} * C^{1.19} \quad [5.7]$$

for the low (<10^{-3} M) and high (>10^{-3} M) concentration ranges, respectively.

Using Equations 5.2 for liquid-vapor, 5.5 for solid-vapor and 5.7 for solid-liquid, the adsorption density or surface excess of the SDS were calculated and results were illustrated in Figure 5.5. At low SDS concentrations, the same amount of the SDS molecules are adsorbed at the solid-liquid and solid-vapor interfaces. At high SDS concentrations (>10^{-3} M), the adsorption density at the solid-vapor interface is higher than that at the solid-liquid interface, indicating that the thermodynamic equilibrium requirement ($\Gamma^{sv} > \Gamma^{sl}$) is achieved (43). As a result, the contact angle measured on the PTFE surface decreases sharply at C_s >10^{-3} M, while it remains fairly constant at C_s >10^{-3} M (Figure 5.1). This is a supporting evidence that the reduction in contact angle measured at high concentrations occurs as a result of slow diffusion of SDS molecules from the liquid-vapor interface onto the solid-vapor interface (PTFE) via hydrophobic interaction when a drop of SDS solution is placed on PTFE surfaces.

5.3.2 Equilibrium Contact Angles for the RNH_2Cl System

The equilibrium contact angle (θ) measurements were also conducted on bare, hydrophobized mica and PTFE surfaces using pure water and the solutions prepared in various

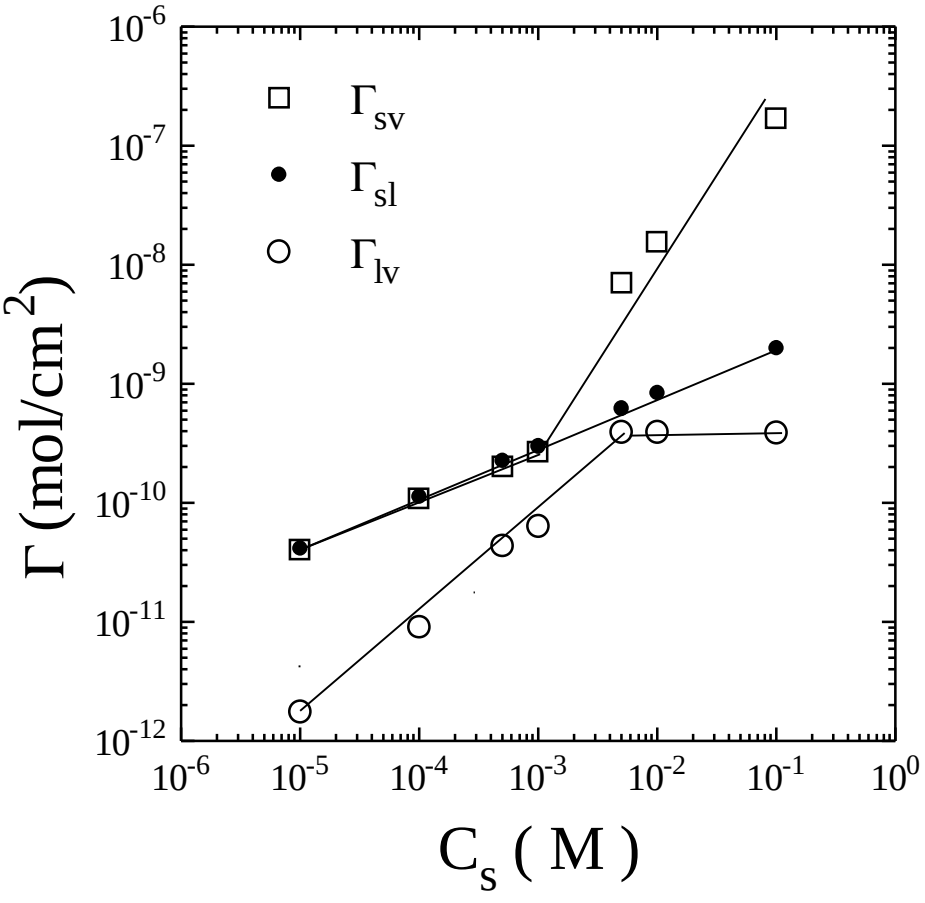

Figure 5.5. The adsorption density of SDS molecules at the three interfaces, solid-liquid, solid-vapor and liquid-vapor, where the solid is PTFE.

concentrations of *RNH_2Cl*. A plot of equilibrium contact angles as a function of concentration at neutral pHs was shown in Figure 5.6. It appeared that there are two major regions in which the differences were observed between the contact angles measured using *SDS* (Figure 5.1) and *RNH_2Cl* solutions (Figure 5.6). First, the Region III shifted towards the Region II and decrease in contact angles for the case of *RNH_2Cl* in Region (II) was more pronounced than that for the case of *SDS*. Second, the contact angles measured on mica ($\theta<90°$) with *RNH_2Cl* solutions were low and increased with increasing concentration in Region (I), unlike in the case of *SDS* system. At concentrations ranging from 10^{-3} to 10^{-2} M, the contact angles for all surfaces decrease more rapidly for *RNH_2Cl* system than the *SDS* system (Figures 5.1 and 5.6). It is interesting to note that the cmc of *RNH_2Cl* was greater by a factor of 1.81 than that of *SDS* (Figure 5.4). At the cmc of *RNH_2Cl* and *SDS*, the lowest surface tensions were 26 mN/m and 38 mN/m, respectively. As a result, the Region (III) was appeared before cmc of *RNH_2Cl*. Even though no measurements were conducted above 10^{-2} M in the present study, the contact angles should be able to measured above cmc. Herder (5, 6) measured the contact angles of *RNH_2Cl* solutions on the *DDOAB*-coated mica surface (θ_a=97° and θ_r=57° with pure water). The advancing (θ_a) and receiving (θ_r) angles were 35° and 19° at $5x10^{-2}$ M *RNH_2Cl*, which is greater than cmc (=$1.47x10^{-2}$ M). The arithmetic and geometric means of the angles are 27° and 28°, respectively. They are much smaller than the equilibrium contact angle of 49° at 10^{-2} M. This indicates that the Region (III) should exist.

This difference in the cmc values suggested that the adsorption densities of both surfactants are not the same at the air-water interface. This variation in the surface tension arises

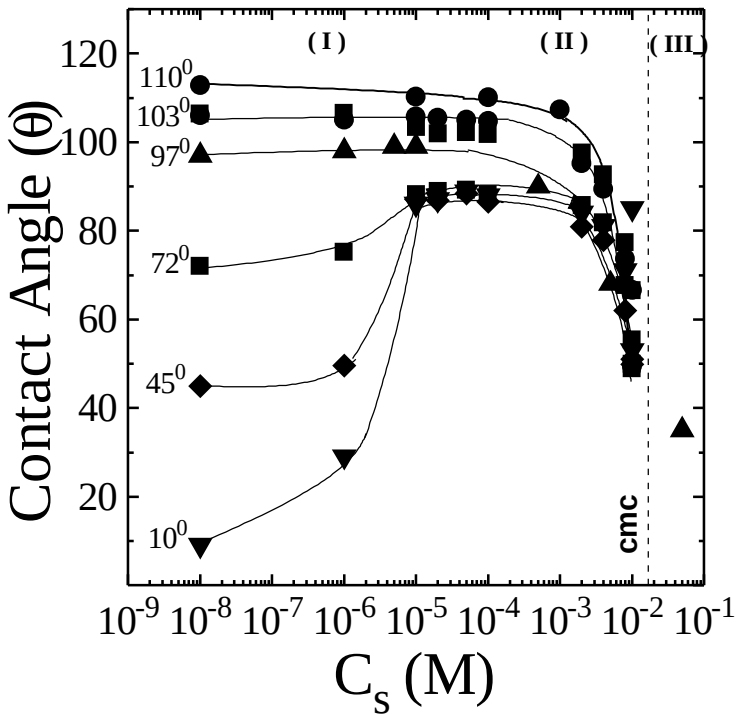

Figure 5.6 Equilibrium contact angle (θ) measured on bare mica(?), hydrophobized mica (? ,? ,♦) and PTFE surfaces (?) vs. RNH_2Cl concentration at 22 °C.

only from the repulsive force among the ionic head groups of the molecules since both surfactants consist of 12 CH groups. The repulsive force among the polar head groups is large enough to overcome the lateral attractive force among the hydrocarbon chains and to make the adsorbed films expand (resulting in a larger area per molecules). The effect of polar head size is larger, therefore, the bigger the polar head groups the larger the area occupied by a molecule at the interface (10). The diameter of the polar head of *SDS* and RNH_2Cl were reported as 0.4 and 0.16 nm, respectively. Therefore, assuming that the air-water interface is similar to the hydrophobic surface-water interface, the adsorption density of RNH_2Cl molecules is also much higher than that of *SDS* molecules. It is well known that the small ions have a higher hydration number, so they are surrounded with more water molecules. Consequently, the hydrophobic surfaces ($\theta>90°$) covered with RNH_2Cl molecules become more hydrophilic than the surfaces covered with *SDS* molecules. Therefore, the sharp reduction in the contact angle occurs before the concentration reaches to the cmc of RNH_2Cl. For instance, the contact angles measured on *PTFE* with RNH_2Cl and *SDS* are 50° and 90° at the concentration of 10^{-2} M, respectively. Above cmc, the differences in the contact angle are much higher, i.e., 70° at 10^{-1} M *SDS* in Figure 5.1 and 27° and 28° at $5x10^{-2}$ M RNH_2Cl (5, 6) in Figure 5.6.

The second and most obvious difference in the contact angles measured on mica ($\theta<90°$) was observed in Region (I). In this region, the adsorption of RNH_3^+ and H^+ ions onto mica occurred due to the electrostatic attraction between positively charged ions and negatively charged sites on the mica surface. The electrostatic attraction force was more dominant than the hydrocarbon-bonding attractive forces for the adsorption process (5, 6, and 8). At low

concentrations, the full coverage of the bare mica and uncovered sites of the hydrophobized mica surface with RNH_3^+ and/or H^+ ions was not completed and adsorption orientation was mostly horizontal to the surface (8) (Figure 5.7.A and D). Besides the electrostatic interaction, the increased packing density of hydrocarbon chains was attributed to the coadsorption of RNH_3^+ and neutral RNH_2 molecules. Therefore, the equilibrium contact angle initially increases to a maximum value of about 87° at about a concentration of 10^{-5} M.

Nishimura, et al. (7) reported that in Region (I) the ζ potential of mica reduces markedly and becomes zero at the so called point-of-charge reversal (pcr=1.6x10^4 M RNH_2Cl) in the presence of 10^{-3} M KCl at pH 3.0. For the same surfactant system, Herder (5, 6) and Yoon and Ravishankar (33) also reported that neutralization occurs at pcr = 10^{-5} M in the absence of inorganic salt at pH 5.5-6.0, which is comparable to the results obtained in this study. The neutralization of the surface charge on mica occurs due to the attractive interaction between hydrocarbon chains of RNH_3^+ ions in addition to the electrostatic interaction between the surface and head groups of surfactant. This causes two dimensional aggregates on the surface, i.e., hemi-micelles at the hemi-micelle concentration (hmc) (15). This situation was shown in Figures 5.7.B and 5.7.E.

It should be noted that charge neutralization occurred at low concentrations. The reason was that, in addition to RNH_3^+ ions, the adsorption of H^+ ions takes part in the neutralization of the surface since, theoretically, the thickness of the RNH_3^+ monolayer is about 0.8 nm while experimentally 0.5-0.6 nm was obtained by Herder (5, 6) using the SFA technique. On the other

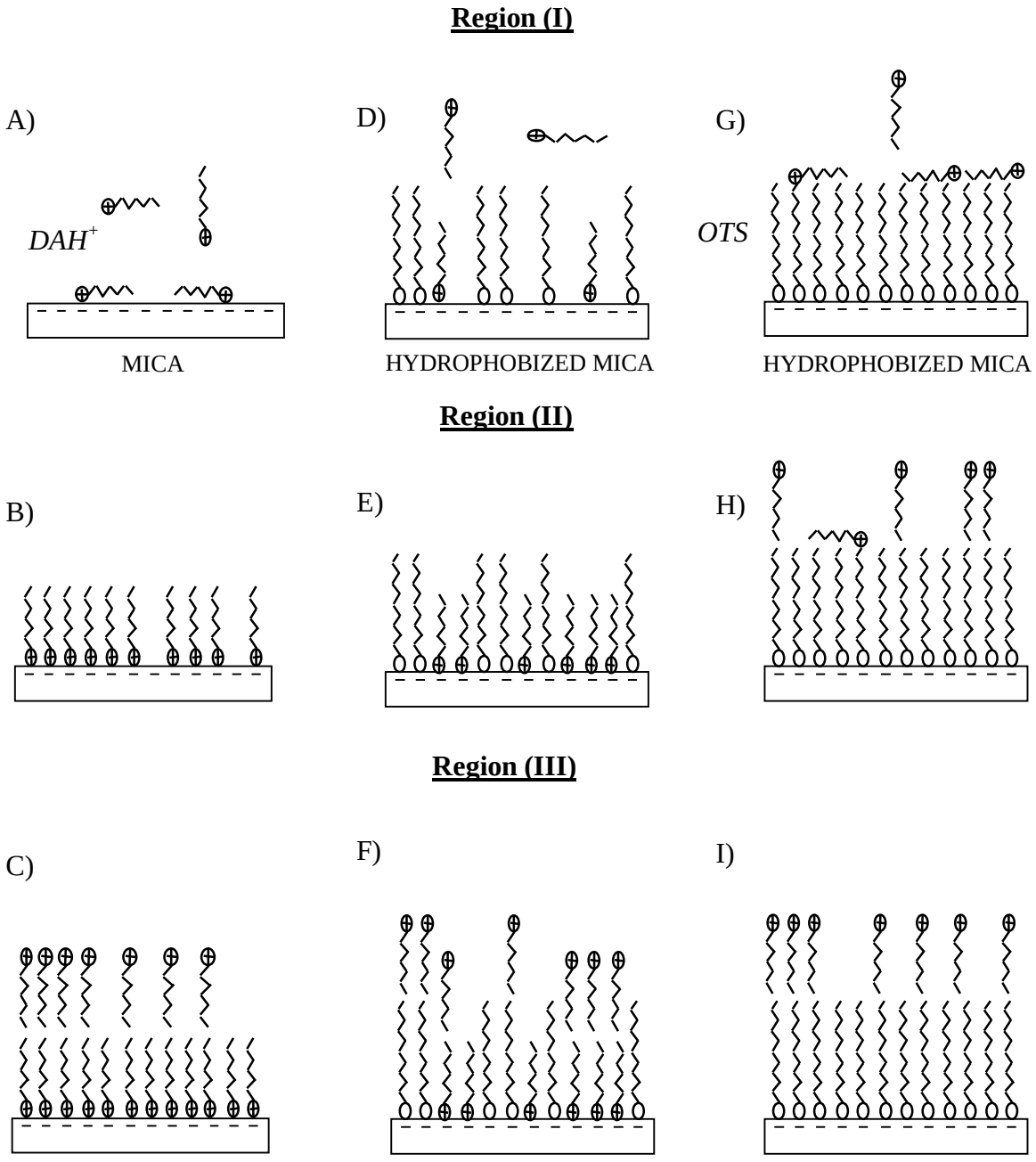

Figure 5.7 : Adsorption orientation of dodecyl ammonium chloride (RNH_2Cl) molecules on the bare mica (A, B, C), hydrophobized mica (D, E, F with $\theta_{eq}<90°$, and G, H, I with $\theta_{eq}>90°$). The mica surfaces were hydrophobized with *OTS* in various degree of hydrophobicities.

hand, the competition in adsorption between RNH_3^+ ions and other cations such as K^+ and H^+ ions, causes a shift of point of charge reversal (pcr) to a higher concentration for mica (7).

In the concentrations above pcr, Region (II), the equilibrium contact angle remained constant at the maximum plateau value of about 87° up to 10^{-3} M (Figure 5.6). These plateau values are comparable to the values reported in reference 5 and 6. In the concentration range 10^{-5} - 10^{-3} M, the advancing and receding contact angles measured on a bare mica surface were 93°-95° and 65°-75°, respectively. The adsorption densities (area/charge) of RNH_3^+ ions on mica were 60 nm^2/molecule at $1x10^{-5}$ M and 6.6 nm^2/molecule at $1x10^{-4}$ M. The surface potentials are +60 mV and +225 mV at the same concentrations, respectively (5, 6). This indicated that the adsorption orientation changes from a horizontal to a vertical and/or tilt position of the close-packed monolayers on a mica surface (16-18).

Finally, because of the condensed layers adsorption, either as a monolayer on *PTFE* or bilayer on bare or hydrophobized mica with θ of 45° and 72°, a marked reduction in the magnitude of the contact angle measured on all these surfaces occurred at a concentration of about 10^{-3} M<C_s>cmc (Figure 5.6). The adsorption mode of RNH_3^+ ions on the *PTFE* surface (Figures 5.3.D, E, and F) and on top of the first monolayer of *OTS* and/or RNH_3^+ ions adsorbed on mica surface (Figures 5.7.G, H, and I) is driven by hydrocarbon-bonding forces. The adsorption density further increases to 0.46 nm^2/molecule and the potential become +220 mV when the concentration reaches $6x10^{-3}$ M (5, 6, 13, 33). Since the polar heads of molecules in the

bilayer were exposed towards the bulk solution, at 10^{-2} M, the contact angle declined to below 50° for all the solid surfaces studied (Figure 5.6).

In the cases of *PTFE* and hydrophobized mica, the changes in θ were very little (from 110° to 107°) when the concentration increases from 0 to 10^{-3} M (Region I). The same reasons given for the *SDS* system would be applied for the RNH_2Cl system; the hydrophobic interaction is dominant between hydrocarbon chains and hydrophobic surfaces (*PTFE* and *OTS*-coated mica). The orientation mode of molecules is horizontal to the surface and adsorption density increases gradually with increasing surfactant concentration (Figures 5.3.D, E, and F).

As in the case of *SDS*, the surface tension of solutions prepared with RNH_2Cl decreases with increasing surfactant concentration. Both adsorption orientation of molecules on solid surfaces and low-surface tension of solutions will cause wetting of the solid surfaces based on Eq.[5.1].

Using Equations 5.2, 5.5, and 5.6, the adsorption density or surface excess of RNH_2Cl molecules at the three interfaces were calculated and result were shown in Figure 5.8. As in the case of SDS adsorption on the PTFE surface, a similar results were obtained for RNH_2Cl adsorption on PTFE surface. This was again a supporting evidence that the reduction in contact angle measured at high concentrations, indicating reduced hydrophobicity, occurs as a result of slow diffusion of RNH_2Cl molecules from the liquid-vapor interface onto the solid-vapor interface (PTFE) via hydrophobic interaction when a drop of RNH_2Cl solution is placed on PTFE surfaces.

5.3.3. Effect of pH on Equilibrium Contact Angles for the RNH_2Cl System

Figures 5.9.A and 5.9.B show the contact angle and surface tension of solutions as a

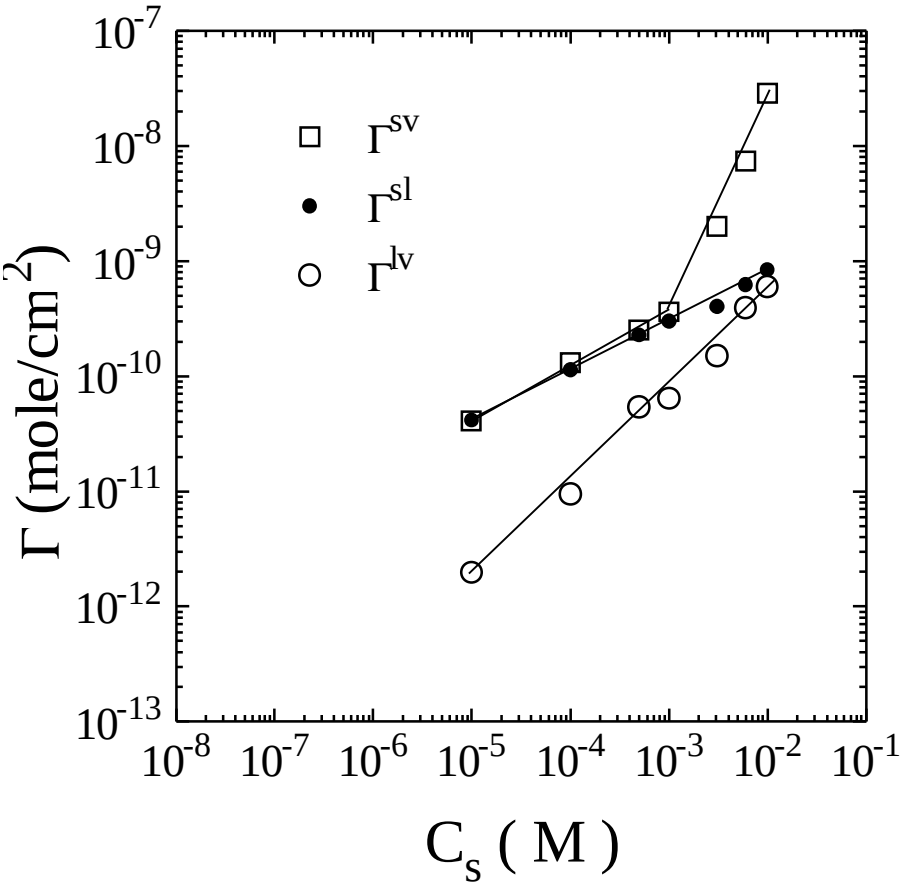

Figure 5.8 The adsorption density of RNH_2Cl molecules at the three interfaces, solid-liquid, solid-vapor and liquid-vapor, where the solid is PTFE.

function of pH at various RNH_2Cl concentrations, respectively. Interestingly, both contact angle and surface tension show similar behavior. In the absence of RNH_2Cl, there are little changes on θ and g_{LV} in the range of pH studied (pH 1 to 12), whereas the marked reduction on both θ and g_{LV} is observed in the presence of RNH_2Cl at high concentrations (C_s>5x10^{-5} M). It is clearly seen that two pH regions in which θ and g_{LV} decrease, are located at pH<3.0 and 9.0-10.0. At high-surfactant concentrations, the reduction in θ and g_{LV} is more pronounced in these two regions. The minimum values of θ measured at alkaline pHs can be explained using the two different mechanisms as suggested for the adsorption of RNH_3^+ and RNH_2 on quartz and mica. The first mechanism, the so called coadsorption of RNH_3^+ ions and neutral RNH_2 molecules, was proposed to explain the abrupt increase in flotation recovery of quartz in the narrow pH range of 9.0-10.5 (11). The concentration of neutral RNH_2 molecules increases due to the hydrolysis of RNH_2Cl molecules at pH close to its pK_a (=10.63) of the RNH_3^+ ions (34). Then the neutral RNH_2 molecules coadsorb in between the RNH_3^+ ions adsorbed on quartz surface (16). This orientation of both species reduces the lateral repulsion between the polar heads of RNH_3^+ ions. The result is an increase in hydrocarbon chain packing density, which in turn increases the hydrophobicity of the surface.

The second alternative mechanism suggested by Somasundaran, et al. (12), is that at pHs close to the pK_a, iono-molecular complexes (RNH_2 . RNH_3^+) are first formed in solutions and then adsorbed onto the surface. Since the iono-molecular complexes represent much longer

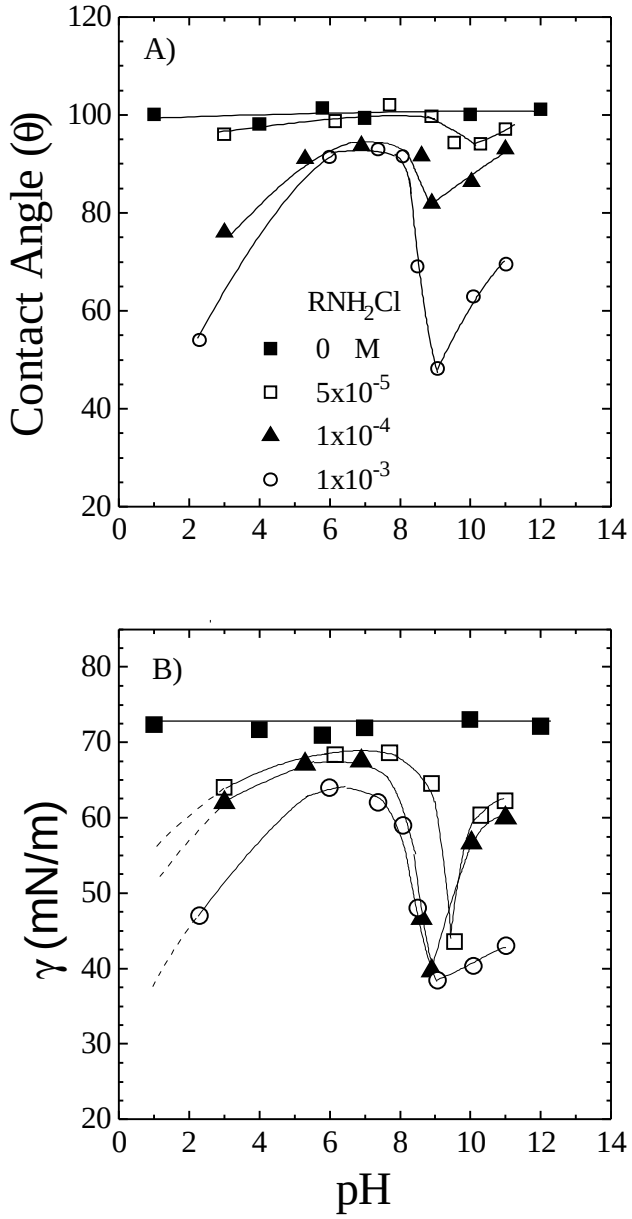

Figure 5.9 The effect of pH on the equilibrium contact angle measured on PTFE (A) and surface tension of solutions (B) prepared various concentrations of *RNH_2Cl*.

chain structures, thermodynamically, their adsorption on the surface would be greater than the RNH_3^+ ions. Both mechanisms cause more adsorption of RNH_3^+ ions on the surface in the presence of neutral RNH_2 molecules.

These mechanisms were also supported by the direct force measurements between mica surfaces in the presence of RNH_2Cl (13, 33). Then it was concluded that since the measurements were conducted at $5x10^{-6}$ M, which is much below pcr (10^{-5} M), there must be sufficient vacant negatively charged sites of mica surfaces on which additional RNH_3^+ ions can adsorb (13, 33).

The adsorption of these two species on hydrophobic and hydrophilic surfaces with either adsorption mechanisms occurs in a similar way. The only difference is the adsorption mode. For adsorption on hydrophobic surfaces, the polar heads of RNH_3^+ ions are oriented towards the bulk solution, while the hydrocarbon chains are oriented towards the bulk solution for adsorption on hydrophilic surfaces. Again, in both mechanisms, the RNH_2 molecules cause greater adsorption of RNH_3^+ ions on the surfaces, therefore, the hydrophobicity of the surface is reduced more at pH 9.0-10.0, which is reflected in the reduced contact angles measured on *PTFE*.

On the other hand, it is expected that these adsorption mechanisms can be used for the adsorption of RNH_2Cl molecules at the air-water interface. Of course, the polar heads of molecules are oriented towards the bulk solution. In Figure 5.9.B, the minimum values of g_{LV} are due to the high affinity of RNH_2 molecules or $RNH_2 \,.\, RNH_3^+$ complexes to the air-water interface at pH 9.0-10.0 (12). Besides these mechanisms, it can be suggested that the combining

effect of the adsorption mode at the hydrophobic surface and reduction in γ based on Eq.[5.1] causes the low hydrophobicity of surfaces and the low contact angle.

Upon addition of *HCl*, g_{LV} decreases and the higher the surfactant concentration the lower the γ measured. This is only observed in the presence of RNH_2Cl. It is well known that the addition of inorganic salts decreases g_{LV} much more rapidly in the presence of surfactants and shifts the critical micelle concentration (cmc) to the lower surfactant concentration (3, 14, Chapter 3&4). Similar effects can be expected in the presence of excess Cl^-. The ionic interactions between RNH_3^+ and Cl^- ions might increase the concentration of neutral RNH_2 molecules in the solution. Therefore, g_{LV} decreases because of the higher affinity of neutral molecules to the air-water interface. The presence of neutral molecules at acidic pHs may also cause higher adsorption of RNH_3^+ ions on the *PTFE* surface. Therefore, the wettability of the *PTFE* surface increases according to Eq.[5.1] and the adsorption mode mentioned earlier.

For comparison purposes, the contact angles measured on bare mica and *PTFE* surfaces at various pHs as a function of RNH_2Cl concentration are combined and shown in Figure 5.8. For bare mica, at both pHs 5.7 and 10.1, the contact angle increases steadily to a maximum value of 87° when the concentration approaches 10^{-5} M. As reported by Yoon and Ravishankar (33) at pH 10.1, bulk precipitation occurs at 10^{-4} M RNH_2Cl; however, the precipitation begins on the surface at $2x10^{-6}$ M, most likely due to the concentration gradient across the solid-liquid interface. The values of θ continuously increase above this concentration until the bulk precipitation is reached (10^{-4} M). These induced contact angles may be attributed to the increase in the hydrophobicity of the uncovered sites of surfaces due to the adsorption mechanisms. The full

coverage of mica surfaces is only completed above the bulk precipitation concentration, then θ drops off rapidly. This indicates that the phase-separated amine has to be hydrophilic. As suggested by Yoon and Ravishankar (33) and Ravishankar (13), the surface and bulk precipitates have the same surface properties; therefore, a reduction in θ should be expected. The patch-wise precipitation (domains) on the surface of mica may cause this unexpected result. On the other hand, at pH 5.7 the contact angle remains fairly constant in the concentration range 10^{-5}-10^{-3} M. This indicates that in the absence of iono-molecular species, the adsorption density of RNH_3^+ ions is low and no bulk precipitates exist at this pH. Above 10^{-3} M, the surface coverage is completed and the bilayer adsorption occurs resulting in a sharp drop.

Figure 5.10 shows the results of contact angles measured on polycarbonate membrane surfaces at pH 3.0 and at various concentrations of RNH_2Cl in the presence of 10^{-3} M *KCl* (7). It is obvious why the flotation of silica and mica is not successful at acidic pHs. The contact angle approaches its maximum value of 57° at concentration $1.6x10^{-4}$ M (=pcr). As mentioned earlier, the competition between RNH_3^+ ions and other cations (K^+ and H^+) causes the shift of the pcr for mica to a higher concentration. In addition to this competition, the concentration of RNH_3^+ ions decreases at acidic pHs because of the excess number of Cl^- ions. Since the contact angle does not exceed 57°, the replacement of the cations on the surface by adsorption of RNH_3^+ and RNH_2 cannot be fully completed at low concentrations as it occurs at pH 5.7. In the same study (7), the results of zeta potential measurements showed that the pcr is $1.6x10^{-4}$ M where the

Chapter 5 Modeling of Air Bubbles in an Aqueous Solution of Ionic Surfactants Using Hydrophobic Solid Surfaces

surface is covered with a monolayer. At low pHs, according to Eq.[5.1], the surfaces wet readily with the solutions having a low surface tension (Figure 5.9.B).

The effect of pH when the contact angles are measured on *PTFE* at pH 5.7 and 9.0-10.0

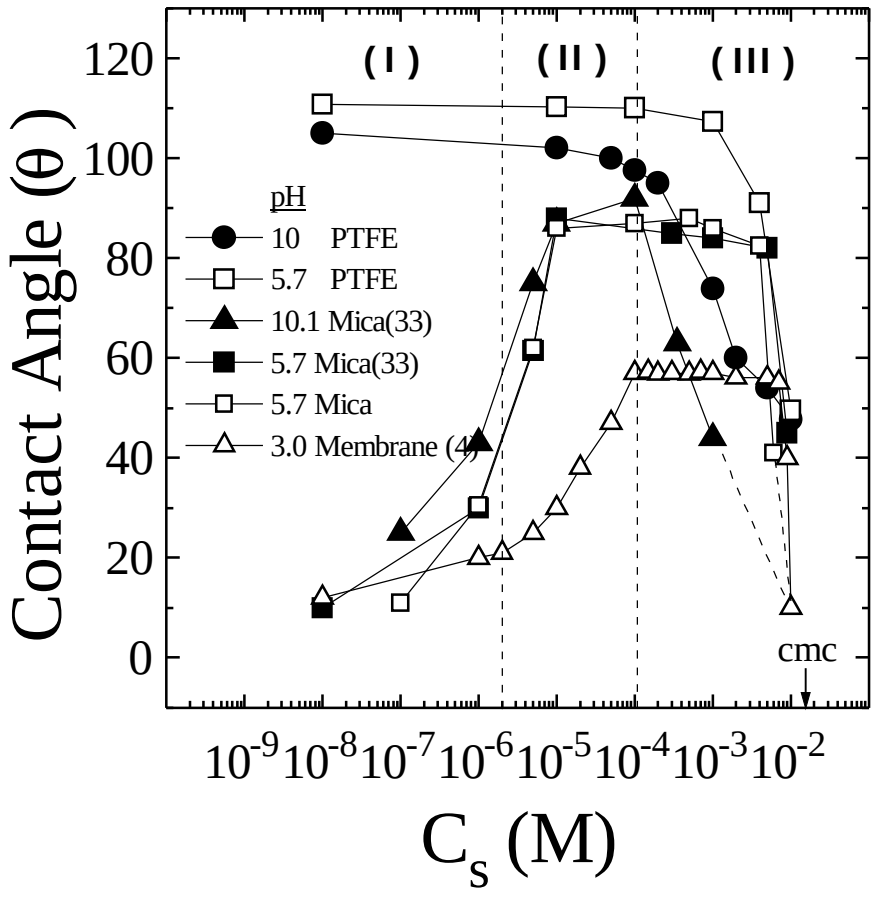

Figure 5.10 Effect of RNH_2Cl concentration and solution pH on the water contact angle measured on PTFE and bare mica at 22 ^{o}C.

is also shown in Figure 5.8. Obviously, at alkaline pHs, the contact angle decreases more rapidly at the concentration of bulk precipitation (10^{-4} M); whereas, at neutral pHs, the reduction in θ begins at about 10^{-3} M (Region III). It seems that the mica and *PTFE* surfaces behave in a similar way so that θ decreases sharply at the same concentration of 10^{-4} M, but at this concentration, the values of θ are slightly different which is in the range of 5°-10°. This difference in θ remains constant above the bulk precipitation concentration. This could be attributed to the fact that the *PTFE* surface is much more hydrophobic than the mica surface coated with a monolayer of RNH_3^+ ions.

5.3.4. Forces Between Hydrophobic Surfaces

The results discussed here about the adsorption of surfactants on solid surfaces has been supported by the studies reported in the literature. Using a Mark IV surface force apparatus (SFA) (5, 6, 13, 33) and an atomic force microscope (AFM), the attractive force between the hydrophobized (*DDOAB*- or *OTS*-coated) mica or silica surfaces was measured in the presence and absence of RNH_2Cl at neutral pHs (19, 35). The force measurements showed that the attractive forces are long-range between hydrophobized surfaces in pure water; whereas, they are short-range between bare mica or silica surfaces in RNH_2Cl solutions. The length, having single or double chains and an adsorption density of molecules are determining factors for being short- or long-range attractive forces. On the other hand, the adsorption of RNH_3^+ ions on the hydrophobized surfaces causes the reduced hydrophobic forces. With increasing concentrations, the monolayer of RNH_3^+ ions on the surface becomes more condensed and the hydrophobic force

can be completely diminished resulting in repulsive electrostatic or hydration forces. Herder (5, 6) observed that the adsorption of a condensed monolayer of RNH_2Cl on *DDOAB*-coated mica surfaces occurs at a concentration of $6x10^{-4}$ M, which is very close to the value of 10^{-3} M where the θ begins to decline. Therefore, it can be suggested that the adsorption mode of RNH_3^+ ions at the hydrophobic surface-water interface and the air-water interface is the same. On the other hand, the adsorption density on the hydrophobic surfaces is much higher than that on the hydrophilic surfaces. There is a limitation for the adsorption of these ions on these surfaces. On hydrophilic surfaces, i.e., mica, each RNH_3^+ ion occupies the center of the oxygen hexagon vacated by the K^+ ion, occupying 0.48 nm^2 on the surface (6). Therefore, RNH_3^+ ions do not form a close-packed monolayer on bare mica at low concentrations. It is known that the cross-sectional area of RNH_3^+ ions ($0.25nm^2$) is almost two times smaller than the area occupied by the K^+ ions (6). Hence, RNH_3^+ ions should adsorb on hydrophobic surfaces (θ>90°) and air-water interfaces more than on hydrophilic surfaces (θ<90°). The calculated area per charge on a hydrophobized mica surface is 60 nm^2 at 10^{-5} M and increases with increasing concentration to 6.6 nm^2 at the concentration of 10^{-4} M (5, 8). Consequently, the repulsion forces due to electrostatic interaction are measured at concentrations greater than 10^{-3} M and this appears as a reduction in θ. As another indication that the adsorption mode of RNH_3^+ ions at the hydrophobic surface-water and air-water interface are the same, the potential at both interfaces shows similarities, i.e., at 10^{-3} M RNH_2Cl, the potential at bare mica and hydrophobized mica surfaces based on surface force measurements is about 150 and 200 mV, respectively (5, 8); whereas the

potential at the air-water interface calculated from the Gibbs adsorption isotherm is about 152 mV (3, 8, Chapter 3).

The hydrophobic interactions as an additional component of the total interaction besides the electrostatic and dispersion components, has been expressed by a single or double exponential or a power law. A general formula for the exponential form is

$$\frac{F}{R} = C_0 \exp\left\{-\frac{H}{D_0}\right\} \qquad [5.8]$$

in which H is the closest distance between two curved surfaces with curvature R. C_0 and D_0 are constant. With soluble surfactants, the decay length (D_0) is usually in the range of 1-2 nm (13, 19, 33).

When the force measurements are conducted with insoluble double-chain surfactants deposited on mica surfaces using the Langmuir-Bloggett technique, the attractive forces are usually described by a double exponential function:

$$\frac{F}{R} = C_1 \exp\left\{-\frac{H}{D_1}\right\} + C_2 \exp\left\{-\frac{H}{D_2}\right\} \qquad [5.9]$$

in which the first term represents the short-range forces, while the second term represents the long-range forces. Forces measured with *DDOAB* (5, 6, 20) and fluorocarbon surfactants (36, 37) on mica surfaces and *OTS* on silica surfaces show that D_1 is in the range of 1-2 nm and D_2 is in the range of 10-26 nm. The decay length (D_0 and D_1) defines the magnitude of this attractive force. The correlation between the parameters and the contact angle shows a very important feature when these decay lengths are plotted as a function of the advancing water contact angle (θ_a) of the surfaces with which the force measurements were conducted (13). The values of D_0

remain in the range of 1-2 nm (6, 13, 25, 33) when the contact angle approaches 90° since the data is obtained with mica surfaces coated with self-assembled monolayers of RNH_2Cl and *CTAB*. Then, it increases sharply above 90°. In this region, the data is obtained with self-assembled mixed monolayers of RNH_2Cl and either dodecanol or octanol (13, 33). This sharp increase in θ may indicate that the packing density of the hydrocarbons and, hence, the degree of ordering also increases sharply at this critical angle. In the region of $\theta \geq 90°$, the data obtained with L-B deposited monolayers of *DDOAB* and fluorocarbons (39-43) on mica and *OTS*-coated silica surfaces (38) are widely scattered, with D_1 values ranging from 10 -26 nm.

Recently, using AFM, Flinn (19) and Rabinovich and Yoon (38) measured the attractive force in pure water and in the presence of RNH_2Cl at pH 5.8 between a silica plate and a glass sphere both hydrophobized with *OTS*. Both studies have shown that hydrophobic force increases with increasing close-packed density of molecules on the surfaces. The measured attractive forces, which were evaluated using the extended DLVO theory with an application of the power law as in the form of van der Waals forces (19, 36-38), were as follows:

$$\frac{F}{R} = -\frac{K_{131}}{H^2} \qquad [5.10]$$

where K_{131} is a single unknown parameter and represents the magnitude of the hydrophobic forces. H is the distance between the surfaces. Using this form of interaction force gives an opportunity to compare the hydrophobic forces with the dispersion forces. The values of K_{131} reported in references 19 and 38 are in the range of 2.8 to 3.5×10^{-16} J, which are nearly four orders of magnitude larger than the Hamaker constant of mica ($A_{131}=2.2 \times 10^{-20}$ J). On the other

hand, the results obtained by Flinn (19) showed that the attractive forces between *OTS*-coated surfaces are lower nearly an order of magnitude in the presence of $4x10^{-5}$ M RNH_2Cl solution at pH 5.8 than the attractive forces measured on *OTS*-coated mica surfaces alone in pure water. Their work also supports the adsorption orientation of molecules at the silica-water interface discussed above.

In the earlier studies (3, 14, Chapter 3 and 4), the hydrophobicity constants (K_{232}) of the air(2)-water(3)-air(2) systems were estimated based on the equilibrium film thickness measurements as a function of RNH_2Cl and *SDS* concentrations, respectively, and are shown in Figure 5.11. The result obtained by extrapolation of data to a zero concentration shows that the K_{232} for pure water is about 10^{-17} J and decreases with increasing surfactant concentration. It is clear that the adsorption of amphiphile molecules at hydrophobic solid-water (5, 6) and air-water interface (3, 14) also causes an increase of the surface and interfacial potentials. All evidence (3, 14, Chapter 3 and 4) indicates that both hydrophobic solid surfaces and air-water interfaces behave in the same manner and show a reduced hydrophobicity with increasing surfactant concentration. It is worth mentioning that for both the air-water interface and the model hydrophobic surfaces, the transition from hydrophobic to hydrophilic nature occurs at about 10^{-3} M of RNH_2Cl (much below cmc) at which a monolayer coverage of surfactant is completed at pH 5.7. Therefore, at these concentrations:

1) High repulsive electrostatic forces appear,

2) The contact angle decreases abruptly,

Chapter 5 Modeling of Air Bubbles in an Aqueous Solution of Ionic Surfactants Using Hydrophobic Solid Surfaces

3) The hydrophobicity constant (K_{232}) changes its sign from negative (attractive) to positive (repulsive),

Chapter 5 Modeling of Air Bubbles in an Aqueous Solution of Ionic Surfactants Using Hydrophobic Solid Surfaces

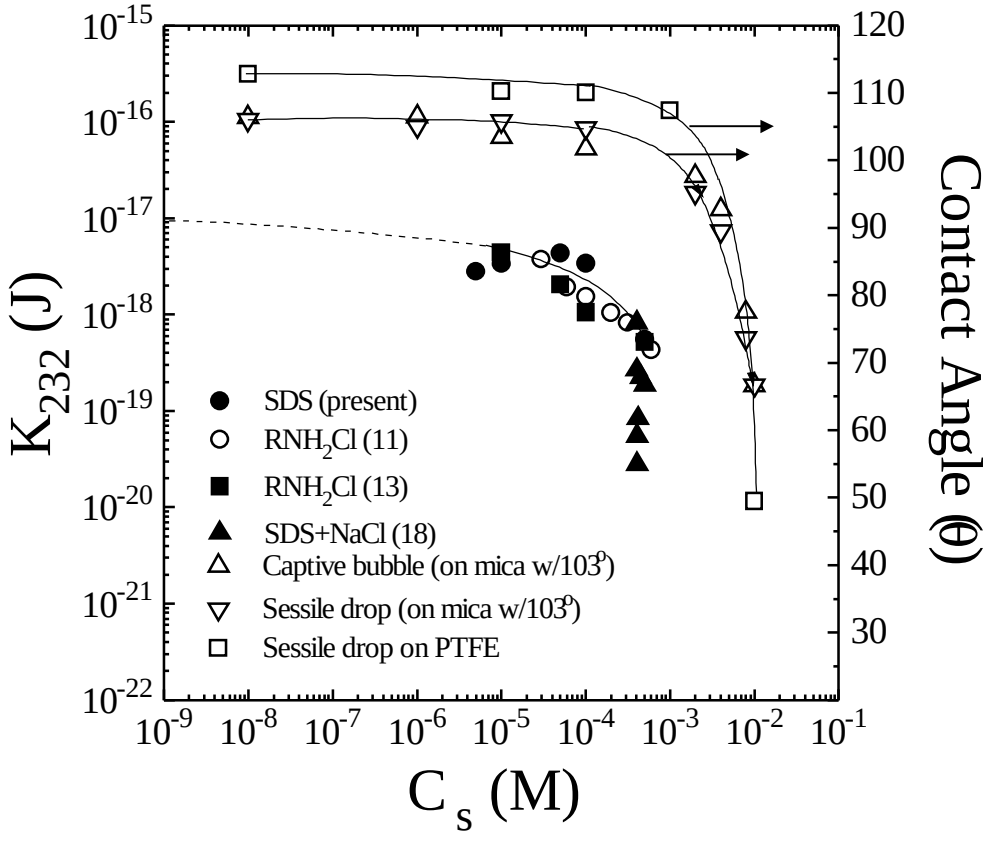

Figure 5.11 The contact angle and the K_{232} values estimated for air/water interface as a function of *RNH_2Cl* concentration at 22 °C.

4) The lifetime of films and film stability increases sharply.

In Figure 5.11, the results of contact angles measured on hydrophobic surfaces also indicated that the relation between K_{232} and θ can be visualized easily. It is interesting to note that either the solid surfaces or the air-water interfaces remains hydrophobic at concentrations lower than 10^{-3} M. The former shows the contact angles higher than 90° while the latter shows the attractive forces (with positive K_{232} values) other than the van der Waals forces.

5.4 CONCLUSIONS

The equilibrium contact angle of Nanopure water, *RNH_2Cl*, and *SDS* solutions was measured on bare mica, hydrophobized mica, and *PTFE* surfaces. When the measurements were conducted on these surfaces, basically three different regions were observed in which theadsorption orientation of the surfactants at the solid-water interface defines and/or alters the surface hydrophobicity. In general, for both surfactants studied in the present work and all hydrophobic surfaces (θ>90°), the contact angle decreases gradually from 110° to about 90° at low surfactant concentrations, indicating that the hydrophobicity of the surfaces decreases. On the other hand, the K_{232} of thin liquid films also decreases, again indicating that the hydrophobicity of the air-water interface decreases. The contact angle drops off sharply below 90°at about 10^{-3} M where the surface potential of hydrophobic surfaces increases and the K_{232} changes its sign from negative to positive, which indicates that the nature of the surface is altered from hydrophobic to hydrophilic. Therefore, these results suggest that the hydrophobicity of air-water interfaces (pure water) and that of hydrophobic surfaces are comparable, i.e., K_{232} is about 10^{-17} J,

which is obtained by extrapolation of data to zero surfactant concentrations, and K_{131} is in the order of 10^{-16} J, which can be determined by either contact angle measurements on the surfaces involved or direct force measurements between the surfaces. It is certain that hydrophobic force which is much higher than the Hamaker constant (A) for both systems needs to be included when the stability of foam, thin liquid films, and colloids is considered.

On the other hand, it was found that the effect of pH on the equilibrium contact angle is pronounced at acidic and alkaline pHs for the RNH_2Cl. The reduced surface tension of the solutions due to the high affinity of iono-molecules (RNH_2 RNH_3^+) to the air-water interface at pH 2.0-3.0 and 9.0-10.0 causes the wetting of the *PTFE* surfaces. The presence of RNH_2 molecules at pH 2.0-3.0 and 9.0-10.0 may also cause more adsorption of RNH_3^+ ions on the *PTFE* surfaces. Therefore, the wettability of *PTFE* surfaces increases according to the Young-Dupre equation and adsorption modes.

It was also shown that the slow adsorption of the molecules at the solid-vapor interface from the liquid-vapor interface was responsible for the reduction of contact angle hence the hydrophobicity of the solid surface.

Chapter 5 Modeling of Air Bubbles in an Aqueous Solution of Ionic Surfactants Using Hydrophobic Solid Surfaces

5.5 REFERENCES

1. Smith, R.W., and Lai, R.W.M., *Trans. AIME* **235**, 413 (1966).

2. Smith, R.W., *Trans. AIME* **226**, 413 (1963).

3. Aksoy, B.S., and Yoon, R.-H., to be submitted J *Colloid Interface Sci*. (1997).

4. Bisio, P.D., Cartledge, J.G., Keeson, W.H., and Radke, C.J., *J. Colloid Interface Sci.* **78**, 225-234 (1980).

5. Herder, P.C., *J. Colloid Interface Sci.* **134**, 336-345 (1990).

6. Herder, P.C., *J. Colloid Interface Sci.* **134**, 346-356 (1990).

7. Nishimura, S., Tateyama, H., and Tsunematsu, K., *J. Colloid Interface Sci.* **159**, 198-204 (1990).

8. Tchhaliovska, S.,Herder, P., Pugh, R., Stanius, P. and Ericson, J.C., *Langmuir*, **6**, 1535-1543 (1990).

9. Kubota, K., Hayashi, S., and Inaoka, M., *J. Colloid Interface Sci.* **95**, 362-369 (1983).

10. Aratono, M., Uryu, S., Hayami, Y., Motomuro, K., and Matuura, R. *J. Colloid Interface Sci.* **98**, 33-38 (1983).

11. Gaudin, A.M., and Fuerstenau, D.W., *Trans AIME*. **202**, 958 (1955).

12. Somasundaran, P., and Ananthapadmanabhan, K.P., *"Solution Chemistry of Surfactants"*, D. Mittal, K.L., **2**, pp 777. Plenum Press, New York (1979).

13. Ravishankar, S., *Ph.D. dissertation*, Virginia Polytechnique and State University, Materials Science (1995).

14. Yoon, R.-H and Aksoy, B.S., to be submitted to *J. Colloid Interface Sci*, (1997).

Chapter 5 Modeling of Air Bubbles in an Aqueous Solution of Ionic Surfactants Using Hydrophobic Solid Surfaces

15. Fuerstenau, D.W., *Trans. AIME*. **208**, 1365 (1957).

16. Delamarche, E., Michel, B., Gerber, Ch., Anselmetti, D., Guntherodt, H.-J., Wolf, H., and Ringsdolf, H., *Langmuir*, **10**, 2869 (1994).

17. Kjaer, K., Als-Nielsen, J., Helm, C.A., Tipperman-Krayer, P., and Mohwald, H., *J. Phys. Chem*. **93**, 3200 (1989).

18. Bain, C.D., and Whithsides, G.M., *Angew. Chem. Int. Engl*. **28**. 506 (1989).

19. Flinn, H.D., *Ph.D. dissertation*, Virginia Polytechnique and State University, Mining and Minerals Engineering, May, 1996.

20. Rutland, M., Waltermo, A., and Claesson, P.M., *Langmuir*, **8**, 176 (1992).

21. Puge, R.J. and Yoon, R.-H., *J. Colloid Interface Sci*., **163**, 169-176 (1994).

22. Exerowa, D., Kolarov, T., and Khristov, KHR., *Colloids Surf*., **22**, 171-185 (1987).

23. Exerowa, D., Zacharieva, M., Cohen, R., and Platikanov, D., *Colloid and Polymer Sci*., **257**, 1089-1098 (1979).

24. Mysel, K.J., *J Phys. Chem*., **68**, 3441 (1964).

25. Kekicheff, P., Christenson, H.K., and Ninham, B.W., *Colloids and Surfaces*, **40**, 31 (1989).

26. Bergeron, V., and Radge, C.J., *Langmuir*, **8**, 3020-3026 (1992).

27. Flinn, D.H., Guzonas, D.A., and Yoon, R.-H., *Colloid and Surfaces, A: Physicochemical and Engineering Aspects*, **87**, 163-176 (1994).

28. Adamson, A.W., *Physical Chemistry of Surfaces, Fifth Edition*, John Wiley& Sons, Inc 1990.

Chapter 5 Modeling of Air Bubbles in an Aqueous Solution of Ionic Surfactants Using Hydrophobic Solid Surfaces

29. CRC Handbook of Chemistry and Physics, 66th edition, CRC Press, Inc. Boca Raton, Florida.

30. Zuidema, H.H., and Waters, G.W., *Ind. Eng. Chem. Anal. Ed.*, **13**, 312 (1941).

31. Surfactants

32. pp 254

33. Yoon, R.-H., and Ravishankar, S.A., *J. Colloid Interface Sci.*, **179**, 391-402 (1996).

34. Somasundaran, P., *Int. J. of Miner. Process*. **3**, 35 (1976).

35. Rabinovich, Ya.I., and Yoon. R.-H., *Colloid and Surfaces A: Physicochem Eng*. Abstract **93**, 263-273 (1994).

36. Claesson, P.M., and Christenson, H.K., *J. Phys. Chem*. **92**, 1650 (1993).

37. Christenson, H.K., Claesson, P.M., Berg, J., and Herder, P.C., *J. Phys. Chem*. **93**, 1472 (1989).

38. Rabonovich, Ya.I., and Yoon, R.-H., *Langmuir*, 10, 1903 (1994).

39. Pashley, R.M., McGuiggan, P.M., Ninham. B.W., and Evans, D.F., *Science* 229, 1088 (1985).

40. Sasaki, T., Hattori, M, Sasaki, J., and Nukina, K., *Bulletin of Chem. Sci. Japan*,**48**, 1397-1403 (1975).

41. Castro, S.H., Vurdela, R.M., and Laskowski, J.S., *Colloid Surfaces*, **21**, 87-100 (1986).

42. Leja, Jan, *Surface Chemistry of Froth Flotation*, Plenum Press, New York and London, 1982.

43. Lin, I.J. and Metzer, A., *J. Colloid Interface Sci.*, **40**, 2, 137-141 (1972).

Chapter 5 Modeling of Air Bubbles in an Aqueous Solution of Ionic Surfactants Using Hydrophobic Solid Surfaces

CHAPTER 6

CONCLUSIONS

The major findings of the present study are summarized as follows:

1) The bitumen-coated mica surfaces exhibited unexpectedly strong repulsive forces at separation distances below approximately 70 nm that cannot be accounted for the electrostatic forces between charged surfaces. It was suggested that the extraneous repulsive forces are the steric forces created due to the interactions between the tails of asphaltenes exposed on the bitumen surfaces. This view was supported by the force measurements conducted between the mica surfaces coated with asphaltenes extracted from bitumen.

2) It was shown that the steric force increases with increasing pH and temperature, both of which can be attributed to the increased solubilization of bitumen in water.

3) It was also shown that the steric force increases with increasing electrolyte concentration, which may be explained by the reduced mobility of the tails of asphaltenes due to charge neutralization.

4) The kinetics of coalescence of bitumen droplets was studied by measuring the induction time. There was a strong correlation between the kinetic information and the surface force data. In general, the larger the steric repulsion the longer the induction time for the

coalescence. It was found that the induction time increases with increasing pH, temperature and electrolyte concentration. The induction time increases sharply above pH 9, exceeding 5 minutes at pH above 10.

5) It was shown that in the presence of cationic (RNH_2Cl) and anionic (SDS) surfactants, the equilibrium thicknesses of thin water films depends on the surfactant concentration and increases with decreasing surfactant concentration. The metastable aqueous films with the thickness of 160-170 nm were obtained from 10^{-5} M RNH_2Cl solutions while the same films were obtained from 10^{-6} M SDS solutions.

6) For both surfactant systems, the free aqueous film was stabilized by the repulsive electrostatic force, which increases with increasing surfactant concentration investigated in the present study. However, the double-layer potentials calculated using the DLVO theory were considerably lower than those calculated from the adsorption densities of the surfactants. This discrepancy was attributed to the hydrophobic forces not considered in the DLVO theory.

7) Using an extended DLVO theory which includes the structural component of the disjoining pressure, as hydrophobic force constant, K_{232}, which is represented with a power law, was estimated about 10^{-17} J for the bubbles interacting in pure water, which is several order of magnitude higher than the Hamaker constant (A_{232} = 3.7 x 10^{-20} J).

Therefore it was concluded that the air-water interface is hydrophobic in the absence of surface active reagents.

8) Addition of inorganic salt (NaCl) markedly reduced the equilibrium thicknesses of thin water films, as a result, the life time and the stability of the films were increased. This effect gave us an opportunity to measure film thicknesses as a function of applied pressure (disjoining pressure isotherm) in the low surfactant and salt concentrations. Therefore it was verified by means of the disjoining pressure isotherms that hydrophobic force is the major factor on the stability of thin aqueous films. Values of the hydrophobic force constant, K_{232}, obtained from the equilibrium film thickness measurements were gave a good fit to the experimental data obtained by the disjoining pressure measurements.

9) The equilibrium film thicknesses exhibited no marked changes when the pH were studied in the range from 5.7 to 9.0 in the presence of RNH_2Cl. However, above this pH, it was impossible to obtained metastable films and rupture occurred spontaneously. On the other hand, there was a good agreement between the kinetic information of bubble coalescence and the equilibrium film thickness measurements. The coalescence time decreases and film thickness increases when the pH of solution reached to 9.0-10.0.

10) The equilibrium contact angles measured on bare mica, hydrophobized mica (OTS-coated), and PTFE surfaces of solutions prepared with RNH_2Cl and SDS were

concentration dependent. In general, the adsorption orientation of surfactant at the solid-water interface defines and/or alters the surface hydrophobicity. The hydrophobicity of hydrophobic surface ($\theta>90^o$) decreases slightly with increasing concentration of both surfactant at low concentrations. On the other hand, the hydrophobicity of mica surface ($\theta<90^o$) increases sharply with increasing cationic surfactant (RNH_2Cl) while the hydrophobicity of same surface does not alter markedly when the contact angles measured with an anionic surfactant (SDS) at low concentrations.

11) The contact angle and surface tension data indicated that at high surfactant concentrations of SDS and RNH_2Cl, both θ and γ_{LV} decrease with increasing concentration. The adsorption orientation of surfactant molecules on solid surface and low surface tension of solutions cause wetting of the solid surfaces based on the Young-Dupre equation.

12) Equilibrium contact angles measured on hydrophobic surface (PTFE) with a cationic surfactant (RNH_2Cl) solution and the surface tension of the solution were also pH dependent. The minimum values of γ_{LV} are due to the high affinity of neutral amine molecules and alkylammonium complex ions to the air-water interface at pH 9.0-10.0. The combining effect of the adsorption orientation of molecules at the hydrophobic surface (PTFE) and reduction in γ_{LV} results in a low hydrophobicity of surfaces and a low contact angle.

Chapter 6 Conclusions

13) The results showed that the hydrophobicity of the air-water interface (pure water) and that of hydrophobic surfaces are comparable, i.e., K_{232} is about 10^{-17} J and K_{131} is in the order of 10^{-16} J. This indicates that the hydrophobic forces are much greater than the Hamaker constant for both systems and need to be included when the stability of foams and colloids is considered.

14) It was showed that either the hydrophobic solid surfaces or the air-water interfaces remains hydrophobic at concentrations lower than 10^{-3} M. However, up to this concentration, the hydrophobicity of both systems diminishes with increasing concentration. At low concentration region, the equilibrium contact angles measured on hydrophobic surfaces are greater than 90^{o}. On the other hand, the sign of hydrophobic constants (K_{232}) calculated using the extended DLVO theory are positive indicating that the interactions in thin aqueous films are attractive (negative).

15) Above 10^{-3} M surfactant concentrations, the hydrophobic force disappears and the positive repulsion forces take place for both systems with the indication of lower contact angles ($\theta<90^{o}$) and negative values of K_{232}, which means that the additional force is repulsive.

Chapter 6 Conclusions

CHAPTER 7

RECOMMENDATIONS FOR FUTURE RESEARCH

Based on the research and results presented in this present study, the following areas of research are recommended:

1) It has been demonstrated that hydrophobicity of air-bubbles in water increases with decreasing anionic and cationic surfactant concentration. The magnitude of the hydrophobic force for air bubbles interacting in pure water, a constant, K_{232}, was estimated approximately 10^{-17} J. The effect of nonionic surfactants such as polyoxyethylenic (POE), decyl methyl sulphoxide (DMS), nonylphenol 20-glycol ether (NP 20), dodecyl 11-ethylene oxide ($C_{12}(EO)_{11}$), etc. should systematically be investigated.

2) The existence of the hydrophobic forces has been determined by direct force measurements between two solid surfaces about 10 years ago. However, the origin of this force is still uncertain. The theories include orientation and rearrangement of water molecules between hydrophobic surfaces, formation of dissolved gas bridges between the surfaces, and the correlation of surfactant domains on the surfaces. It has been clearly shown in the present work that the air-water interface is hydrophobic and it causes the spontaneous rupture of the air bubbles in pure water. The same hydrophobic forces may also be responsible for the spontaneous rupture of the oil droplets in pure water. In this

present study, the experiments were designed to be applied at the air-water interface of the system. Similar experiments should be performed by using another hydrophobic phase such as pure oil-water interface (oil droplets in water). The results of these experiments may then provide an explanation for the origin of the hydrophobic force.

3) The effect of pH, inorganic electrolyte, hydrocarbon chain length, temperature and dissolved gas on the hydrophobic forces for many different interacting interfaces are found in numerous studies. But the results are sometimes inconsistent. Therefore, a series of experiments should be conducted with ionic and nonionic surfactants to systematically explore the influence each of these conditions.

4) Obtaining a disjoining pressure isotherm by TFB technique is difficult. Therefore, other techniques, such as atomic force microscopy (AFM) should be utilized as complementary to TFB.

5) It is well known that the surfactants like industrial chemicals and biological molecules at the surfaces and interfaces play a major role in many industrial processes and their behavior (ordering) is of great interest to scientists seeking to control phenomena which occur at surfaces and interfaces. Some indirect methods, such as surface tension measurements, observation of fluorescent dye molecules at an interface, have been used to obtain information about such behavior. Since this methods have their own unique

problems causing to obtain doubtful information, a new method, so called sum frequency generation (SFG) can be used to obtain a vibrational spectrum of a surfactant at an interface. This technique provides a way to directly observe how amphiphilic molecules orient and assemble at the interface and has possible applications in such important areas as froth flotation, oil recovery, etc.

6) The most difficult part of the experiments encountered in the present study was to obtain a disjoining pressure isotherm using a TFB in the region of low surfactant concentrations in which the hydrophobic forces dominate the stability of the thin aqueous films. This difficulty was overcome by adding a small amount of inorganic salt. The same difficulty may be overcome by using the TFB which has various radius of the film holder. Using a series of these capillary film holders provides different capillary pressures (P_c) applied on the film form in the holder. Therefore the disjoining pressure isotherm (Π versus h) can be obtained for a given surfactant system with carefully measured P_c and the radius of the film holders. This method may correspond to the jump method used for measuring the forces between solid surfaces by a surface force apparatus (SFA). In this technique, when the surface force measurements are performed between the hydrophobic surfaces, different springs with various spring constants are used. Then the force versus jump distance curves are obtained for the system studied. These capillary tubes, film holders with various radius, correspond to the springs of SFA with various spring constants.

Chapter 7 Recomendations for Future Research

VITAE

Bayram Suha Aksoy was born in Ankara, capital city of Turkey. He completed his high school in 1974 and his college degree in Mining Engineering from Hacettepe University in 1979. He worked for the Mineral Research and Exploration Institute of Turkey, Ankara, Turkey as a mining and minerals engineer for seven years. In Fall 1985, he enrolled in a M.Sc. program at Colorado School of Mines, Golden, Colorado. After completion of his M.Sc. degree in May, 1988, he worked for International Process Research Corporation (INTERPRO) Golden, Colorado. He enrolled in a Ph.D. program at University of Toronto, Toronto, Canada in Fall 1988. Then, in Spring 1990, he transferred his Ph.D. program to Virginia Polytechnic Institute and State University, Blacksburg, Virginia.

He has four publications and three additional paper which are to be published. He won a scholarship from ETIBANK AS. Ankara, Turkey, for pursuing his M.Sc. degree. He also won a fellowship from the Department of Mining and Materials Engineering, Virginia Tech, Blacksburg, VA during his Ph.D. study. He has accepted an offer as a Research Associate in the Department of Mining Engineering, at the University of Missouri-Rolla, Rolla, MO and he has been working since November 1996. He is responsible for the coal log pipe line and the coal briquetting projects. He also responsible for four graduate students.

Vitea